**International Scientific-Technical and Production Journal**

# The Paton WELDING JOURNAL

**October 2010 # 10**

English translation of the monthly «Avtomaticheskaya Svarka» (Automatic Welding) journal published in Russian since 1948

***Founders:*** *E.O. Paton Electric Welding Institute of the NAS of Ukraine International Association «Welding»* ***Publisher:*** *International Association «Welding»*



***Address:***
*E.O. Paton Electric Welding Institute,*
*International Association «Welding»,*
*11, Bozhenko str., 03680, Kyiv, Ukraine*
*Tel.: (38044) 287 67 57*
*Fax: (38044) 528 04 86*
*E-mail: journal@paton.kiev.ua*
*http://www.nas.gov.ua/pwj*

State Registration Certificate
KV 4790 of 09.01.2001

***Subscriptions:***
**$324**, 12 issues per year,
postage and packaging included.
Back issues available.



## CONTENTS

# ADEQUACY OF THERMOHYDRODYNAMIC MODEL OF THROUGH PENETRATION IN TIG AND A-TIG WELDING OF NIMONIC-75 NICKEL ALLOY*

**D.V. KOVALENKO**[1], **D.A. PAVLYAK**[2], **V.A. SUDNIK**[2] and **I.V. KOVALENKO**[1]
[1]E.O. Paton Electric Welding Institute, NASU, Kiev, Ukraine
[2]Tula State University, Tula, Russian Federation

Results of experiments on weld formation in TIG and A-TIG welding of Nimonic-75 alloy, and results of computer simulation of the effect of convection on «sand glass» shape of weld are presented. The experiments were carried out with and without activating flux PATIG Nim-75-A on 3.15 mm thick plates. Adequacy of the model was evaluated by comparing the sizes of the real and simulated weld sections. The causes of recirculation flows were analyzed. Correlation of the experimental and computation data was revealed.

***Keywords:*** *TIG and A-TIG welding, nickel alloy, penetration, mathematical model, adequacy of mathematical model*

Positive results connected with an abrupt increase of penetration depth at activating flux deposition on the surface of metal to be welded in TIG welding (A-TIG process ) of titanium obtained at the E.O. Paton Electric Welding Institute [1, 2] stimulated investigations on arc column contraction in TIG welding of steels and other materials [3–5].

Study [6] marked the beginning of investigations of convection in welding. This work is devoted to the influence of surfactants on penetration depth. Work [7] provides experimental proof of the postulates of [6] on the key factor in penetration depth, namely, change of the sigh of temperature coefficient of surface tension $d\sigma/dT$ from negative to positive sign. Addition of surfactants lowers surface tension at melting temperature, and values of $d\sigma/dT$ coefficient become positive. However, at temperature increase up to 1900 °C, surface tension reaches values characteristic for pure metal with a maximum at critical temperature, and values of $d\sigma/dT$ coefficient again become negative, as for pure metal.

World's first two-dimensional model of weld pool convection [8], created in 1983, provided theoretical confirmation of the postulates of [6] and showed that Marangoni surface tension forces are predominating, and together with the Lorentz electromagnetic forces they are responsible for appearance of double eddy regions. Later it was established [9] that the sign of thermal concentration dependence of surface tension and its values determine the direction of convective heat transfer under the arc and number of vortices. Simulation of the role of electromagnetic forces in A-TIG welding is carried on, and the nature of the mechanism of this phenomenon still has not been determined. It is established that arc contraction does not affect austenitic steel penetration, but it should be taken into account as an auxiliary factor [10, 11]. It was proved here that electromagnetic convection promotes deep penetration [12] and the centrifugal component of the electromagnetic force is the dominating factor of penetration [13]. Published results are given only for the simplest axisymmetrical case of a stationary heat source of incomplete penetration on a stationary item from austenitic steel.

Technology of A-TIG welding of Nimonic-75 nickel alloy was tried out for the first time at PWI [14]. It is based on application of a short (1.5 mm) arc and activating salt-oxide flux PATIG Nim-75-A, containing metal fluorides and oxides. Fluorides promote arc contraction [5] and influence development of physical processes in it [15, 16]. Fluoride fluxes allow welding titanium sheets of up to 8 mm thickness [17, 18]. A team of scientists led by B.E. Paton [19] developed a theoretical model of arc contraction by fluoride fluxes. For sodium fluoride NaF at welding current $I_w$ = 100 A value of anode spot radius $r_a \approx 1.5$ mm was obtained.

Another nickel alloy Nimonic-263 was welded over a layer of isolated titanium oxides and their mixtures, and the welding process was simulated using PHOENICS program [20]. Calculation results differed from experimental data.

Computer simulation has recently become the main method of scientific investigations. Program code developers and experimenters using such programs, face the following question: how the error of simulation results should be assessed? Computer simulation ends by prediction of the result of welding, and the most important characteristic of the prediction is the confidence level. According to [2] prediction error is a

*Published by the materials of a paper presented at the V International Conference on Mathematical Simulation and Information Technologies in Welding and Related Technologies (May 25–28, 2010, Katsively vil., Crimea, Ukraine).

vector sum of errors of simulation and experiment, allowing for the normal random distribution of data. The significance of the discrepancy between the results of simulation (prediction) and experimental data is determined by statistical criteria, for instance in comparison of dispersions by Fisher criterion [21], or at unknown dispersion (often the case in practice) by Student criterion [22].

The purpose of this work is comparison of experimental shape of the through-penetration weld made on Nimonic-75 alloy by TIG and A-TIG welding with the simulated shape, as well as analysis of the influence of melt convection on weld shape.

**Experimental studies.** These were conducted by automatic gravity welding of butt joints of plates from Nimonic-75 nickel alloy 3.15 mm thick and of 200 × × 20 mm size. Composition of the studied alloy according to [23] is as follows, wt.%: 0.14 C; 0.14 Si; 0.39 Mn; 21.Cr; 3.4 Fe; 0.28 Ti; 0.05 Cu; 0.001 S; 0.008 P; 0.0175 O; Ni being the base.

Nonconsumable tungsten electrode with 2 wt.% Th of 2.1 mm diameter with sharpening angle of 30° and blunting of 0.5–0.8 mm was used. Argon with not more than 0.1 wt.% of impurities was used as shielding gas (10 l/min flow rate), as well as for weld root shielding (2 l/min flow rate). Welding was performed with VSVU-315 welding power source. Experiments were conducted with application of aerosol activating flux (activator) PATIG Nim-75-A and without it at current $I_w$ = 40–240 A, arc length was 1–4 mm, welding speed was $v_w$ = 50–500 mm/min.

In each experiment a uniform layer of activator 80–100 μm thick was applied on the plate surface. During experiments welding current, arc voltage and welding speed were monitored. After welding, macrosections were prepared and measurements of geometrical dimensions of welds and visual assessment of their formation quality were performed.

Figure 1 shows cross-sections of through-penetration welds made on Nimonic-75 alloy at the same (200 mm/min) welding speed at $I_w$ = 100 A (A-TIG welding) and 180 A (TIG welding). As is seen from the Figure, in A-TIG welding process, welding current and heat input can be reduced almost 2 times to achieve through penetration of the weld, compared to TIG welding.

Figure 2 presents macrosections of a weld made by A-TIG welding, which were cut out of different locations on a sample of Nimonic-75 alloy along its length — at the start (Figure 2, *a*), in the middle

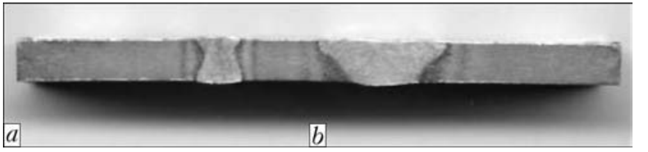


**Figure 1.** Transverse macrosections of through-penetration welds made on Nimonic-75 alloy by A-TIG welding at $I_w$ = 100 A (*a*) and TIG welding at $I_w$ = 180 A (*b*) at the same (200 mm/min) welding speed

(Figure 2, *b*) and at the end (Figure 2, *c*) ($I_w$ = 100 A, arc voltage $U_a$ = 10 V, arc length of 1.5 mm, $v_w$ = = 200 mm/min). The Figure clearly shows the scatter of weld shape and dimensions across its width, which is caused by certain instability of weld formation in through-penetration gravity welding.

**Simulation of welding processes.** Thermohydrodynamic model of though penetration, developed in Tula State University, is based on equations of energy, Navier–Stokes and continuity with the respective boundary conditions allowing for the features of TIG and A-TIG welding. It is used for simulation of the considered processes.

Thremophysical properties of Nimonic-75 alloy are studied only at room temperature [23]. An analog of the above alloy in Russia is KhN55VMTKYu nickel alloy, in the USA — Inconel-718 [24], in Germany — Nicrofer 2520-alloy 75 [25]. Temperature dependencies of thermophysical properties of Inconel-718 and Nicrofer 2520-alloy 75 are known from [24, 25], their comparison with reference points of Nimonic-75 alloy shows good correlation.

*For TIG welding process* the following initial mode parameters were assumed: $I_w$ = 180 A, $U_a$ = 9 V, arc length of 1.5 mm, short arc efficiency of 94 %, $v_w$ = 200 mm/min, temperature coefficient of surface tension of −0.017 N/(cm·K) [24], radii of electric and thermal spots of 5.1 and 6.8 mm, respectively.

Calculated maximum temperature of the weld pool was $T_{max}$ = 1780 °C, calculated weld width — 8.87 mm, experimental value — 10.5 mm, calculated penetration width — 5 mm, experimental value — 0–5 mm. Instability of penetration width in the experiment is attributable to selection of the mode in the region of transition from incomplete ($I_w$ = 170 A) to through ($I_w$ = 180 A) penetration (Figure 3). Assessment of the position of penetration boundary can be determined by the assumed melting temperature of the alloy (liquidus temperature $T_l$ = 1380 °C) or coherence (continuity) temperature $T_c$, at which the liquid phase is absent at boiling temperature of 1367 °C equal to $T_l - (T_l - T_s)/3$, where $T_s$ is the

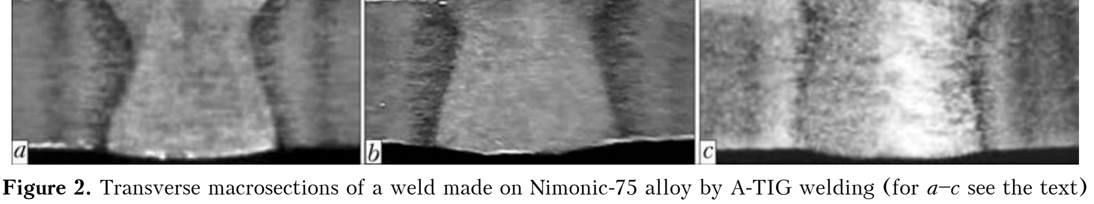


**Figure 2.** Transverse macrosections of a weld made on Nimonic-75 alloy by A-TIG welding (for *a*–*c* see the text)

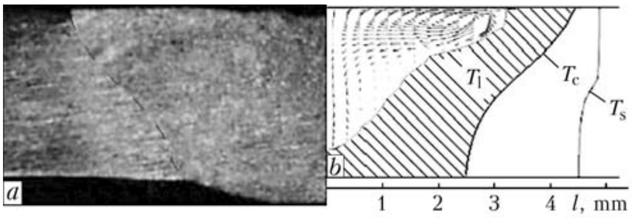


**Figure 3.** Experimental (*a*) and calculated (*b*) section of welds made by TIG welding at $I_w$ = 180 A

solidus temperature [26]. In Figure 3, *b* this region is hatched.

*For A-TIG welding process* the following initial parameters of the mode were assumed: $I_w$ = 100 A, $U_a$ = 10 V, arc length of 1.5 mm, short-arc efficiency of 94 %, $v_w$ = 200 mm/min. Allowing for the features of this process the following was assumed: heat spot radius of 2.2 mm (because of insulating action of activating flux); current spot radius of 0.9 mm (because of arc contraction by fluorine); on the upper surface temperature coefficient of surface tension of +0.01 N/(cm·K) allowing for reverse Marangoni convection; on the lower surface where the conditions were unchanged, temperature coefficient of surface tension was equal to −0.017 N/(cm·K).

Figure 4 shows a three-dimensional view of a plate from Nimonic-75 alloy at simulation of the process of A-TIG welding with non-characteristic for arc welding width and shape of the weld. Maximum weld pool temperature $T_{max}$ = 2700 °C is in good agreement with the current concepts of nonconsumable electrode welding, allowing for the cooling action of the evaporation process, which was taken into account in the model boundary conditions.

Figure 5 gives the results of calculation of weld longitudinal section, made by A-TIG welding ($x$ = = −12 mm), which are indicative of good reproducibility of weld shape in the form of «sand glass». Analysis of the obtained results shows that two eddy regions with Marangoni convection form in a weld pool with two free surfaces. At the lower surface of the weld pool temperature-capillary Marangoni flow has a classical shape — from weld pool center to its edges. Now, on the upper surface the flow pattern is more complicated with elements of both straight (from center to edges of weld pool) and reverse Marangoni convection towards weld pool center. Cross-sectional dimensions of the weld in the form of «sand glass» and their flow patterns are different in different sections. For such patterns three-dimensional volume presentation of the flows is more rational, similar to how it is presented in [26].

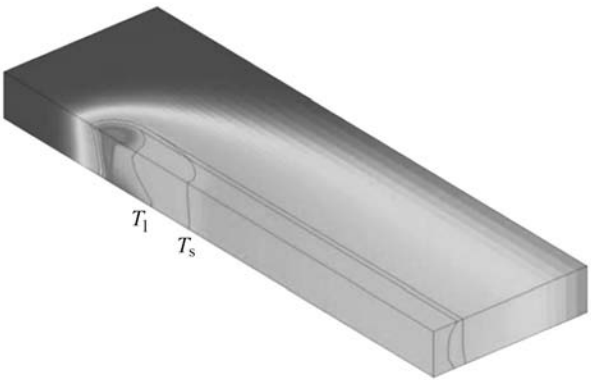


**Figure 4.** Three-dimensional view of a plate from Nimonic-75 alloy at simulation of A-TIG process

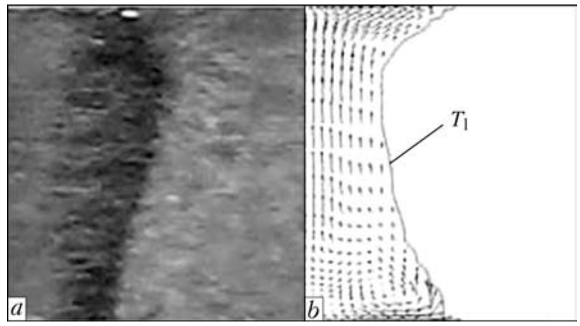


**Figure 5.** Experimental (*a*) and calculated (*b*) section of welds made by A-TIG welding at $I_w$ = 100 A (arrows indicate the direction of liquid metal motion at maximum speed of 0.232 m/s)

Proposed possible mechanism of through penetration in A-TIG welding consists in formation of the following flows of weld pool liquid metal: main flow of heat transfer of over-heated melt across the sheet thickness in the contracted arc zone caused by magnetic forces and determining the width of the weld narrow neck in the form of «sand glass» and two additional fluxes of recirculation boundary flows caused by thermocapillary forces on both the weld pool surfaces, which determine the width of the weld molten zones decreasing to the neck size.

**Adequacy of mathematical model.** This term usually means the degree of correspondence of the same properties of the object and the model. Procedure of assessment of adequacy of computer simulation of the process of A-TIG welding of Nimonic-75 alloy characterized by penetration in the form of «sand glass» (see Figure 5), and TIG welding consisted in statistical processing of experimental results and obtaining an evaluation of mean-root-square deviation $S$ of parameter values (each of weld width dimensions on upper $W$ and lower $B$ sides of the sheet, as well as width $W_n$ and height $H_n$ of «sand glass» neck):

$$S = \sqrt{\frac{1}{n-1}\sum_{j=1}^{n}(y_{exp} - y_{cal})^2},$$

where $n$ is the sample size; $y_{exp}$ and $y_{cal}$ are the experimental and calculated values of the parameter.

Adequacy assessment was performed by Student's statistical criterion

$$t_{m,\,1-\alpha} \geq \frac{y_{exp} - y_{cal}}{S}\sqrt{n},$$

where $t_{m,\,1-\alpha}$ is the tabulated value of $t$-distribution; $\alpha$ is the level of significance equal to 0.05.

Results of experiments and calculations are given in Tables 1 and 2.

**Table 1.** Results of experiments and calculations obtained across the width of welds made by A-TIG and TIG on plate upper $W$ and lower $B$ surfaces

| Welding process | $I_w$, A | $v_w$, mm/min | Weld width, mm | | | | | |
|---|---|---|---|---|---|---|---|---|
| | | | $W_{exp}$ | $W_{cal}$ | $S$ | $B_{exp}$ | $B_{cal}$ | $S$ |
| A-TIG | 100 | 200 | 3.9 | 3.60 | 0.72 | 3.6 | 3.1 | 0.42 |
| | | | 3.8 | | | 4.1 | | |
| | | | 3.3 | | | 3.4 | | |
| | | | Average 3.67 | | | Average 3.7 | | |
| TIG | 180 | 200 | 10.5 | 8.87 | 1.62 | 5.0 | 2.5 | 2.95 |
| | | | 10.0 | | | 4.6 | | |
| | | | 9.0 | | | 3.6 | | |
| | | | Average 9.83 | | | Average 4.4 | | |

*Notes*. 1. Here and in Table 2 Student's criterion $t_{m,\,1-\alpha} = 4.3$. 2. Condition of adequacy is assumed. 3. Indices «exp» and «cal» indicate experimental and model values, respectively.

Suggested hypotheses of coincidence of average values of two sets — experimental and calculates ones, assessed by Student's criterion, are accepted with confidence probability of 0.95.

Thus, experiments on A-TIG welding of plates from Nimonic-75 nickel alloy 3.15 mm thick showed that at complete (through) penetration the weld takes the shape of «sand glass». Simulation by a thermohydrodynamic model of weld pool in A-TIG welding of plates of Nimonic-75 nickel alloy reproduces the shape of complete (through) penetration in the form of «sand glass». Assessment of the accuracy of reproducing cross-sectional dimensions of weld by this model by comparing average experimental and calculated values from Student's criterion showed the adequacy of this model with confidence probability of 0.95. Proposed mechanism of through penetration of A-TIG welding includes the main flow of heat transfer of overheated melt across sheet thickness in the contracted arc zone caused by electromagnetic forces and determining the width of the narrow neck in the form of «sand glass», as well as two additional recirculation boundary flows caused by thermocapillary forces on both surfaces of the weld pool and determining the width of the weld molten zones which are reduced to the size of «sand glass» neck.

**Table 2.** Results of experiments and calculations obtained by width $W_n$ and height $H_n$ of weld neck in the form of «sand glass» at simulation of A-TIG welding process

| $I_w$, A | $v_w$, mm/min | Neck width, mm | | | Neck height, mm | | |
|---|---|---|---|---|---|---|---|
| | | $W_{n\,exp}$ | $W_{n\,cal}$ | $S$ | $H_{n\,exp}$ | $H_{n\,cal}$ | $S$ |
| 100 | 200 | 3.1 | 0.95 | 1.32 | 1.5 | 0.8 | 0.28 |
| | | 3.0 | | | 1.2 | | |
| | | 2.4 | | | 0.9 | | |
| | | Average 2.83 | | | Average 1.2 | | |


1. Gurevich, S.M., Zamkov, V.N., Kushnirenko, N.A. (1965) Increase in effective penetration during argonarc welding. *Avtomatich. Svarka*, **9**, 1–4.
2. Gurevich, S.M., Zamkov, V.N. (1966) Some peculiarities of nonconsumable electrode welding of titanium with application of fluxes. *Ibid.*, **12**, 12–16.
3. Ostrovsky, O.E., Kryukovsky, V.N., Buk, B.B. et al. (1977) Effect of activating fluxes on penetrating capacity of welding arc and energy concentration in anode spot. *Svarochn. Proizvodstvo*, **3**, 3–4.
4. Savitsky, M.M., Leskov, G.I. (1980) Mechanism of effect of electronegative elements on penetrating capacity of arc with tungsten cathode. *Avtomatich. Svarka*, **9**, 17–22.
5. Zamkov, V.N., Prilutsky, V.P. (1987) Distribution of current density in anode spot during welding of titanium. *Ibid.*, **3**, 19–22.
6. Heiple, C.R., Roper, J.R. (1982) Mechanisms for minor element effects on GTA fusion zone geometry. *Welding J.*, 61(**4**), 97–102.
7. Mills, K.S., Keene, B.I., Brooks, R.F. et al. (1984) The surface tension of 304 and 316 type steels and their effects on weld penetration. In: *Proc. of Conf. on Centenary of Metallurgy Teaching* (Glasgow, 1984), 1–11.
8. Oreper, G.M., Eagar, T.W., Szekely, J. (1983) Convection in arc weld pools. *Welding J.*, 62(**11**), 307–312.
9. Zhao, Y. (2006) The study of surface-active element oxygen on flow patterns and penetration in A-TIG welding. *Metallurg. and Mater. Transact. B*, 37(**6**), 485–493.
10. Tanaka, M. (2005) Effect of surface active elements on weld pool formation using TIG arcs. *Welding Int.*, 19 (**11**), 870–876.
11. Zhang, R.H., Fan, D. (2007) Numerical simulation of effects of activating flux on flow patterns and weld penetration in A-TIG welding. *Sci. and Techn. of Welding and Joining*, 12(**1**), 15–23.
12. Wang, Y., Shi, O., Tsai, H.L. (2001) Modelling of the effects of surface-active elements on flow patterns and weld pool penetration. *Metalurg. and Mater. Transact. B*, 32(**2**), 145–161.
13. Yushchenko, K.A., Kovalenko, D.V., Krivtsun, I.V. et al. (2008) Experimental studies and mathematical modelling of metal penetration in TIG and A-TIG stationary arc welding. *IIW Doc. 212-1117–2008*.
14. Yushchenko, K.A., Kovalenko, I.V., Kovalenko, D.V. et al. (2000) A-TIG welding of nickel alloy Nimonic-75. *Svarshchik*, **4**, 26–27.
15. Lucas, W., Howse, D. (1996) Activating flux — increasing the performance and productivity of the TIG and plasma processes. *Welding & Metal Fabrication*, 65(**1**), 11–17.
16. Howse, D., Lucas, W. (2000) Investigation into arc constriction by active fluxes for tungsten inert gas welding. *Sci. and Techn. of Welding and Joining*, 5(**3**), 189–193.
17. Perry, N., Marya, S., Soutif, E. (1999) *New perspectives of flux assisted GTA welding in titanium structures*, 55–62.

18. Leconte, S., Pillard, P., Chaelle, P. et al. (2007) Effect of flux containing fluorides on TIG welding process. *Welding and Joining*, 12(**2**), 120–126.
19. Paton, B.E., Zamkov, V.N., Prilutsky, V.P. et al. (2000) Contraction of the welding arc caused by flux in tungsten-electrode argonarc welding. *The Paton Welding J.*, **1**, 5–11.
20. Xu, Y.L., Dong, Z.B., Wei, Y.H. et al. (2007) Marangoni convection and weld pool shape variation in A-TIG welding process. *Theoretical and Applied Fracture Mechanics*, **48**, 178–186.
21. Sudnik, W., Radaj, D., Erofeev, W. (1998) Validation of computerized simulation of welding processes. In: *Mathematical modelling of weld phenomena 4*. London: IOM Commun., 477–493.
22. Erofeev, V.A., Karpukhin, E.V., Sudnik, V.A. (2001) Computer simulation of nonstationary laser welding. Computer technologies in joining of materials. In: *Proc. of 3rd All-Union Sci.-Techn. Conf.* (Tula, 9–11 October 2001). Tula: TulGU, 111–118.
23. *B5 HR 20–72*: Specification for nickel-chromium-titanium heat-resisting alloy plate, sheet and strip. Great Britain.
24. Sudnik, V.A., Erofeev, V.A., Richter, K.H. et al. (2006) Numerical modelling of the EBW process. In: *Computer techn. in welding and manufacturing*. Kiev: PWI, 295–300.
25. *Nicrofer 2520-alloy 75*: ThissenKrupp VDM Material Data Sheet, 4035.
26. Zhao, C.X., Van Steijn, V., Richardson, L.M. et al. (2007) Unsteady interfacial phenomena during inward weld pool flow with an active surface oxide. *Sci. and Techn. of Welding and Joining*, 14(**2**), 132–140.

# OPTIMAL REDUCTION OF WORKING PRESSURE IN PIPELINES FOR WELDING REPAIR OF THINNING REGIONS

**V.I. MAKHNENKO, V.S. BUT, S.S. KOZLITINA, L.I. DZYUBAK** and **O.I. OLEJNIK**
E.O. Paton Electric Welding Institute, NASU, Kiev, Ukraine

The possibility of using welding to repair defects of corrosion origin in walls of pressurised pipelines is considered. It is shown that the safety of welding operations is affected not only by the overall size of a defect, but also by the shape of a pipe wall thinning. Calculation algorithms are applied to substantiate the possibility of repair of defects by overlaying welding due to optimal reduction of internal pressure in the main line for a period of repair.

***Keywords:*** *main pipeline, welding repair, overlaying welding, sizes of defects, residual thickness of pipe wall, optimal pressure*

Repair of main pipelines by welding without interruption of their operation, i.e. in a pressurised state, is finding now an increasingly wider application, as it allows an optimal reduction of downtime and pollution of the environment. A key point of this technology is safety of repair operations performed on a pressurised pipeline depending on the type of a defect, its shape and size. The most frequent defects in underground main gas pipelines are wall thinning defects of the corrosion origin, which are associated with violation of waterproof insulation. Such defects with overall sizes $s_0 \times c_0 \times a$ (Figure 1), where $s$ is the size of $a$ defect along the pipe axis, and $c$ and $a$ are the sizes of the defect on the circumference and through the wall thickness, respectively, are well studied. Different criteria are available for estimation of the risk of fracture within the zones of such defects depending on their sizes, geometric parameters of a pipeline, its mechanical properties, pressure inside a pipe [1–3], etc. For example, study [1] gives fairly simple relationships based on numerous experimental investigations, which make it possible to judge whether the wall thinning defects in pipelines are permissible or not depending on the above parameters.

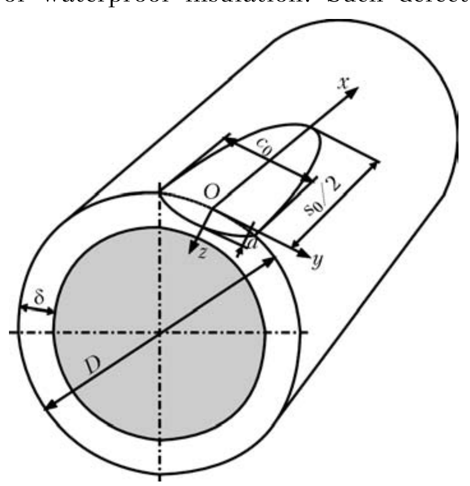


**Figure 1.** Schematic of pipeline with thinning defect in the form of an ellipsoid measuring $s_0 \times c_0 \times a$ before welding

The condition of permissibility of a corrosion thinning defect with sizes $s(t)$ and $c(t)$ at time moment $t$ in a pipeline, according to [3], can be written down as

$$y(t) = \delta - a(t) - [\delta]R_j > 0, \tag{1}$$

where

$$R_j = \delta_{min}/[\delta] \quad (j = s, c); \tag{1a}$$

$\delta_{min}$ is the minimal measured wall thickness within the defect zone ($\delta_{min} = \delta - a$); and $[\delta]$ is the permissible calculated thickness of the pipeline wall without considering the thinning defects, i.e.

$$[\delta] = \frac{PD}{2[\sigma]}, \tag{2}$$

where $P$ is the working pressure in the pipe with external diameter $D$, made from a material with permissible stresses $[\sigma]$ for given conditions; and the following dependencies suggested in [1] for the value of $R_j$ ($j = s, c$):

$$R_s = \begin{cases} 0.2, \text{ if } \lambda = \dfrac{1.285}{\sqrt{D[\delta]}}\, s \le 0.3475, \\ \left[0.9 - \dfrac{0.9}{\sqrt{1 + 0.48\lambda^2}}\right]\left[1.0 - \dfrac{0.9}{\sqrt{1 + 0.48\lambda^2}}\right]^{-1}, \\ \text{ if } \lambda > 0.3475; \end{cases} \tag{3}$$

$$R_c = \begin{cases} 0.2, \text{ if } c/D \le 0.348, \\ \dfrac{10.511(c/D)^2 - 0.7358}{1.0 + 13.838(c/D)^2}, \text{ if } c/D > 0.348. \end{cases}$$

The problems of prediction of safety, allowing for the technological effects within the defect zone (cleaning, overlaying welding), which cause changes in geometric parameters $a(t)$, $s(t)$ and $c(t)$, are often encountered in practice of repair of the detected thinning defects. Of particular importance is the possibility of in-process predicting an increase in defect depth $a(t)$ as a result of cleaning the surface from corrosion (approximately to 1 mm), or as a result of welding heating using the corresponding welding technology [4] (approximately to a depth of penetration of isotherm of about 1000 °C for steel, depending on the position of a heat source in the thinning zone, allowing for variations in sizes $s(t)$ and $c(t)$ due to the regions already welded by time moment $t$).

It is very important at this point to take into account the extra margin for ensuring safety due to a short-time decrease of pressure in a pipeline, causing no substantial violation of the working conditions. That is, it is necessary to quite promptly obtain a compromise estimate of minimal decrease of the pressure in the pipe providing the required safety, i.e. meeting conditions (1). So, this study is dedicated to this issue.

Assume that defect sizes $a(t)$, $s(t)$ and $c(t)$ in a pipeline with geometric parameters $D \times \delta$, made from a material with permissible stresses $[\sigma]$ outside the defect, are set for time moment $t$.

It follows from dependencies (1) through (3) at $y = 0$ that

$$\begin{cases} \lambda(R_s) = \left[0.81\left(\dfrac{1 - R_s}{0.9 - R_s}\right)^2 - 1\right]^{0.5} 1.4434 \text{ at } R_s > 0.2, \\ \lambda(R_s) = 0.3475 \text{ at } R_s \le 0.2; \end{cases} \tag{4}$$

$$s_{\mathrm{cr}}(R_s) = \lambda(R_s)\, \frac{\sqrt{D[\delta]}}{1.285};$$

$$c_{\mathrm{cr}}(R_c) = D\left[\frac{R_c + 0.73589}{10.511 - 13.838R_c}\right]^{0.5} \text{ at } R_c \ge 0.2; \tag{5}$$

$$c_{\mathrm{cr}}(R_c) = 0.348D \text{ at } R_c < 0.2,$$

**Table 1.** Results of calculation of $s_{\mathrm{cr}}$ and $c_{\mathrm{cr}}$ for $P$ = 7.5 MPa

| $\delta_{\min}$, mm | $R_s = R_c$ | $s_{\mathrm{cr}}$, mm | $c_{\mathrm{cr}}$, mm |
|---|---|---|---|
| 3.10 | 0.2 | 40.1 | 494.2 |
| 4.65 | 0.3 | 53.3 | 573.7 |
| 6.20 | 0.4 | 68.0 | 678.8 |
| 7.25 | 0.5 | 83.1 | 835.0 |
| 9.30 | 0.6 | 118.0 | 1104.8 |
| 10.85 | 0.7 | 151.1 | 1874.0 |
| 12.40 | 0.8 | 192.0 | – |
| 13.185 | 0.85 | 417.9 | – |

where $s_{\mathrm{cr}}$ and $c_{\mathrm{cr}}$ are the permissible critical sizes at given $R_s$ and $R_c$.

By using (1a) and (2), we can write down that

$$R_j = \frac{\delta_{\min}}{P}\,\frac{2[\delta]}{D} \quad (j = s, c). \tag{6}$$

It follows from (4) through (6) that

• at $R_j \le 0.2$, permissible sizes $s$ and $c$ for a thinning defect do not depend on the value of $\delta_{\min}$ and are equal to $s = 0.27D\sqrt{P/2[\delta]}$ and $c = 0.348D$, respectively;

• at fixed $\delta_{\min}$, the ultimate values of parameters $R_s$ = 0.9 and $R_c$ = 10.511/13.838, at which $s_{\mathrm{cr}}$ and $c_{\mathrm{cr}} \to \infty$, according to (4) and (5), can be approached

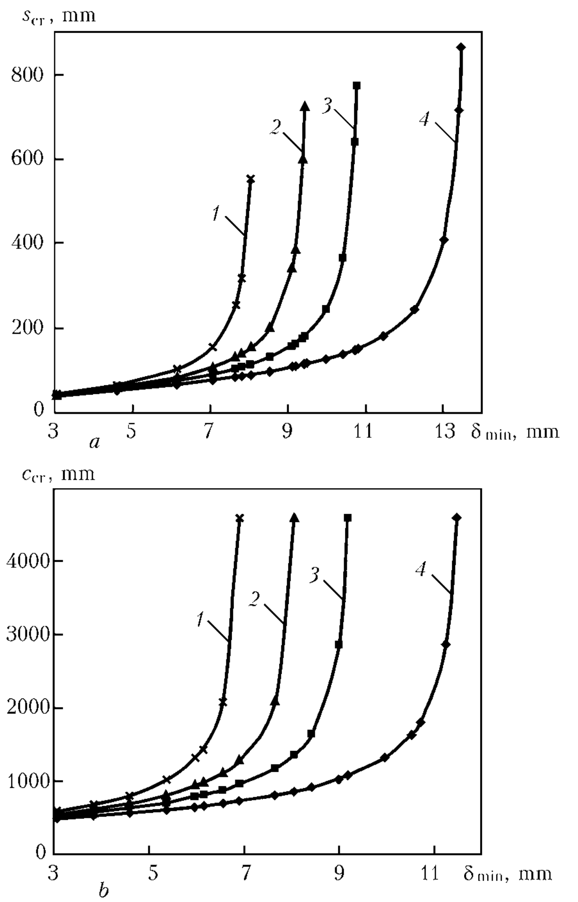


**Figure 2.** Dependence of $s_{\mathrm{cr}}$ ($a$) and $c_{\mathrm{cr}}$ ($b$) on minimal thickness $\delta_{\min}$ of the wall of a pipe measuring ∅ 1420 × 20 mm and $[\sigma]$ = 345 MPa at $P$ = 7.5 MPa: *1* — 0.6$P$; *2* — 0.7$P$; *3* — 0.8$P$; *4* — $P$

**Table 2.** Results of calculation of $s_{cr}$ and $c_{cr}$ for pressures of 0.8$P$ and 0.6$P$

| $\delta_{min}$, mm | 0.8$P$ = 6 MPa | | | 0.6$P$ = 4.5 MPa | | |
|---|---|---|---|---|---|---|
| | $R_s = R_c$ | $s_{cr}$, mm | $c_{cr}$, mm | $R_s = R_c$ | $s_{cr}$, mm | $c_{cr}$, mm |
| 3.10 | 0.250 | 41.7 | 531 | 0.333 | 44.9 | 596 |
| 4.65 | 0.375 | 57.3 | 649 | 0.500 | 66.5 | 833 |
| 6.20 | 0.500 | 76.8 | 833 | 0.667 | 119.5 | 1485 |
| 7.25 | 0.5846 | 94.1 | 1051 | 0.7796 | 192.7 | – |
| 9.30 | 0.750 | 166.6 | – | – | – | – |
| 10.85 | 0.875 | 654.0 | – | – | – | – |

as closely as possible due to decrease in $P$, according to (6); i.e. such thinning defects become «absolutely permissible».

Consider a specific example of a steel pipe ($[\sigma]$ = = 345 MPa, $P$ = 7.5 MPa, $[\delta]_{cal}$ = 15.5 mm) measuring ∅ 1420 × 20 mm. By setting a series of values of $\delta_{min}$ = = 20 − $a(t)$, we obtain a corresponding series of values of $R_s = R_c$ for $P$ = 7.5 MPa (Table 1), on the basis of which we determine $s_{cr}$ and $c_{cr}$ from (4) and (5).

As follows from the data of Table 1 and curves $P$ in Figure 2, $a$, $b$, the value of $c_{cr}$ for the given example at the working pressures is by an order of magnitude higher than $s_{cr}$ over the entire range of $\delta_{min} \geq 3.1$ mm. $s_{cr}$ has rather low values at low $\delta_{min}$. Here a reduction of the working pressure during repair is a relevant measure to ensure safety. This is clearly demonstrated by the data of Table 2 and curves *1* and *3* in Figure 2, $a$, $b$.

It can be seen that at low $\delta_{min}$ close to $0.2[\delta]_{cal}$ = = 3.1 mm the effect of reduction of pressure does not lead to any pronounced variation of values of $s_{cr}$ and $c_{cr}$. However, at $\delta_{min}$ > 6 mm, a 40 % decrease in the working pressure leads to an order of magnitude increase in $s_{cr}$ and $c_{cr}$, which is very important for practical application.

As an example of using such curves, consider the safety of welding repair of a thinning defect with sizes

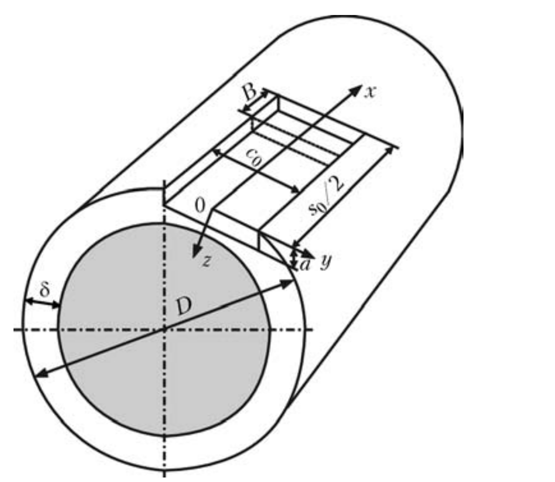


**Figure 3.** Schematic of pipeline with thinning defect of a rectangular shape and size $s_0 \times c_0 \times a$ before welding

$s_0 = s_{cr}$ = 100 mm and $c$ = 40 mm at $\delta_{min}$ = 8.5 mm (Figure 3). Welding is performed from the ends of the defect around a circumference at the parameters that provide penetration of the 1000 °C isotherm to depth $\xi$ = 3 mm (with a certain conservatism) at deposited bead width $B$ = 10 mm. Therefore, within the deposited bead zone the residual conditional wall thickness will be $\delta_{con} = \delta - a(x) - \xi$. If $\delta_{con} > \delta_{min}$ = = $\delta - a_{max}$, ultimate critical size $s_{cr}$ (see Figure 2, $a$) will remain equal to $s_0$, and there will be no need to reduce the pressure.

At the next step of deposition of the bead around a circumference at the other end of the defect at a working pressure, when $s = s_0 - B$ = 90 mm, and according to Figure 2, $a$, $\delta_{min}$ should be not lower than approximately 8 mm. If in this case $\delta_{con}$ is higher than 11 mm, there is no need to reduce the pressure.

In a general form, for welding from the ends we will obtain a change in length $s_n = s_0 - nB$, where $n$ is the pass number. Hence, for length $s$ of the defect, knowing its depth $a(x)$, where $x$ is the coordinate along the axis of the defect in the $n$-th pass, we calculate conditional defect depth $a_{con} = a(x) + \xi$, and then compare difference $\delta - a_{con}$ with the corresponding permissible (see Figure 2, $a$) value of $\delta_{min}$ for $s_n$ at pressure $P$. Based on this comparison, we make a decision on the necessity and degree of reduction of the pressure. For this example, Table 3 gives values of $s_n$, $x_n$, $\delta - a_{con}$ and $\delta_{min}(s_n)$ (see Figure 2, $a$) for $n$ = 1, 2, ... at different pressures in the pipe.

It holds for a defect described by equation

$$a(x) = a_0 \sqrt{1 - \left(\frac{2x}{s_0}\right)^2 \left(\frac{2y}{c_0}\right)^2},$$

where $a_0 = \delta - \delta_{min}$, along the $y$ = 0 axis, that

$$a(x) = (\delta - \delta_{min})\sqrt{1 - \left(\frac{2x}{s_0}\right)^2} \text{ at } -\frac{s_0}{2} < x < \frac{s_0}{2}.$$

The conditional depth of the defect for the $n$-th pass will be

$$a^n_{con} = 11.5\sqrt{1 - \left(\frac{2x_n}{s_0}\right)^2} + 3 \text{ mm}.$$

It can be seen from Table 3 that, for the defect and welding parameters ($\xi$ = 3 mm) under consideration, the process can be quite safely performed at a working pressure of 7.5 MPa.

Consider the most conservative shape of the defect (Figure 3) in the form of

$$a(x, y) = \begin{cases} \delta - \delta_{min} \text{ at } -\frac{s_0}{2} < x < \frac{s_0}{2},\ -\frac{c_0}{2} < y < \frac{c_0}{2}, \\ 0 \text{ at } |x| > \frac{s_0}{2},\ |y| > \frac{c_0}{2}. \end{cases}$$

In this case, at $\delta$ = 20 mm and $\delta_{min}$ = 8.5 mm the defect is at a tolerable limit at $P$ = 7.5 MPa. However,

**Table 3.** Example of calculation of the necessity of reducing the pressure in welding repair of thinning defect with $s_0$ = 100 mm, $c_0$ = = 20 mm and $\delta_{min}$ = 8.5 mm in a pipe measuring ∅ 1420 × 20 mm (see Figure 2)

| $n$ | $s_n$, ,mm | $x_n$, mm | $a^n_{con}$, mm | $\delta - a_{con}$, mm | $\delta_{min}(s_n)$ ($P$ = 7.5 MPa) | $\delta_{min}(s_n)$ ($P$ = 6.0 MPa) | $\delta_{min}(s_n)$ ($P$ = 4.5 MPa) |
|---|---|---|---|---|---|---|---|
| 0 | 100 | 50 | 3.0 | 17.0 | 8.5 | 7.3 | 5.6 |
| 1 | 90 | −50 | 3.0 | 17.0 | 8.0 | 6.6 | 5.1 |
| 2 | 80 | 40 | 9.9 | 10.1 | 6.0 | 6.0 | 4.6 |
| 3 | 70 | −40 | 9.9 | 10.1 | 6.0 | 5.5 | 4.3 |
| 4 | 60 | 30 | 12.2 | 7.8 | 5.1 | 4.5 | 3.9 |
| 5 | 50 | −30 | 12.2 | 7.8 | 4.0 | 3.6 | 3.3 |
| 6 | 40 | 20 | 13.7 | 6.3 | 3.0 | 3.0 | – |
| 7 | 30 | −20 | 13.7 | 6.3 | 3.1 | – | – |

in welding to a depth of $\xi$ = 3 mm, the condition of permissibility from $s$ for $\delta_{min}(s_n)$ = 8.5 − 3.0 = 5.5 mm at $s_0$ = 100 mm can be met only at $P \leq 4.5$ MPa, i.e. this defect can be repaired by welding by reducing the pressure to the said limit (4.5 MPa).

It can be noted in conclusion that for welding repair of thinning defects in main pipelines, depending on the size and shape of thinning, and allowing for decrease in deformation resistance of a material during heating, the safety of operations can be improved by using an appropriate pressure in a pipeline.

It is shown that sizes of a thinning defect are far from always determining the safety of the welding operations. The shape of the thinning defect, in particular the presence of a region with a developed surface area in a zone of the maximal defect depth, has a strong effect on the safety of welding operations associated with removal of the thinning defect. Nevertheless, there is always a level of pressure in the pipe, below which the welding repair of the thinning defect is a safe operation in terms of preservation of integrity of the pipe. It is important that this level should satisfy, at least for a short time, the service conditions of the pipeline. For this, it is expedient to develop the diagrams of permissibility of defects of the type shown in Figure 2 for typical sizes and strength of a material of main pipelines, from which it would not be difficult to determine the optimal level of pressure in the pipeline for the case of typical defects with a developed surface area within the maximal depth zone to ensure the safety of repair under corresponding welding conditions.

1. (2000) *Fitness-for-service*: American Petroleum Institute Recommended Practice 579.
2. *VRD 39-1.10-004–99*: Procedure recommendations on quantitative assessment of state of main gas pipelines with corrosion defects, their ranking by the hazard degree and determination of residual life. Moscow: Gazprom.
3. *RD EO 0571–2006*: Standards for permissibility of thickness of pipeline elements made from carbon steels. Moscow: Rosenergoatom.
4. Makhnenko, V.I., But, V.S., Kozlitina, S.S. et al. (2010) Risk of fracture of pressurized main pipeline with defects of the type of wall thinning during repair. *The Paton Welding J.*, **1**, 7–10.

# PECULIARITIES OF ARC CONTROL BY EXTERNAL MAGNETIC FIELD (Review)

**I.A. RADKEVICH, S.L. ShVAB, V.P. PRILUTSKY** and **S.V. AKHONIN**
E.O. Paton Electric Welding Institute, NASU, Kiev, Ukraine

Theoretical and practical aspects of methods of effect of variable magnetic field on the arc, burning on a tungsten electrode in argon, to control arc position in space are considered. Analysis of effectiveness of application of arc control by variable transverse magnetic field in welding and its influence on weld formation and quality was performed.

***Keywords:*** *argon arc welding, tungsten electrode, weld pool, magnetic field, arc control, vertical welding*

One of the important disadvantages of argon arc is small number of parameters (welding current, welding speed and length of arc gap), significantly influencing the changes of sizes of produced welds (width, depth of penetration and height of bead reinforcement). This disadvantage somewhat limits the fields of application of this welding method. Influence of magnetic field on such arc can widen its application not only in welding, but also in surfacing, as far as possibilities to control sizes of deposited metal and depth of penetration become more efficient and reliable.

The authors made an analysis of theoretical and practical investigations of regularities of movement of arc, burning at tungsten electrode in argon, under influence of magnetic field on it.

Nowadays two principally different approaches towards investigations of arc burning in magnetic field were outlined: micro- and macrokinetic ones. Some researchers consider the electric arc in magnetic field as a conductor (flexible, gaseous, plasma), the movements of which are governed by the laws of electrodynamics [1, 2]. Others suppose that movement of electric arc in magnetic field is the spreading of ionization state at which the energy is transferred from particle to particle, but not the movement of all totality of particles of conductor plasma [3–5]. One can suppose that micro- and macroprocesses which are proceeding in the arc under the effect of magnetic field are closely connected with each other.

The effect of magnetic field in microprocesses is manifested through a peculiar movement of charged particles under the influence of electromagnetic forces, on which such parameters depend as density of current, change of voltage in active spots of the arc, gradient of potential of arc column, etc. The works are known on study of microkinetic phenomena in welding magnetically-controlled arc with a purpose to explain the mechanism of its movement [6, 7].

The phenomena of macroscopic character are revealed in change of shape, sizes and position of arc in the space. Therefore, it is accepted to consider the welding arc in magnetic field as a single whole.

To establish the regularities of arc deviation in transverse magnetic field the arc was considered in the work [1] as a elastic conductor with current in a magnetic field. Here, the welding arc column is smoothly deformed with increase in magnetic field intensity. The cathode spot remains almost immovable, however the anode spot is moved in the direction of action of electrodynamic force.

To control welding arc by transverse magnetic field is extremely difficult in connection with limited capacity of the arc to be elongated without interruption during its deviation by magnetic field. The interruption of the arc occurs not due to its simple elongation, but as a result of break of the anode spot at some critical value of intensity of magnetic field. In the places of transfer from the arc spot to the column with different density of current the intensity of magnetic field is sharply decreased and, consequently, a negative gradient of pressure along the arc column arises which stipulates the stationary flow of plasma flows from active arc spots. The electrodynamic nature of plasma flow creates a field of speeds where the arc nucleus has a movement speed higher by one-two orders than the speed of a flame [8]. Therefore, in movement of arc in magnetic field, different amplitude of deviation of flame and a nucleus should be expected. Such differentiated character of nucleus and flame deviation is observed in the arcs with a tungsten cathode [9] due to high current densities as compared with other cathodes (for example, carbon).

In all arcs with high density of current in anode spot the plasma flow is observed [8]. Under the conventional conditions of axisymmetric location of active spots the flows from anode and cathode are directed towards each other, but cathode flow suppresses the anode one. At a shift of one active spot relatively to another the pattern of interaction of plasma flows, directed perpendicularly to the surfaces of active spots, is changed: the deformation of arc in magnetic field is defined by deformation of two flows directed at an angle. In the area of contact of two plasma flows the intensive forcing out of charged particles from the arc column takes place, which in the opinion of the authors of study [9] is the main reason of abnormal increase in voltage of arc, deformed by the transverse magnetic field. The violation of thermal balance in the place of contact of two flows, stipulated by this phenomenon, causes the interruption of arc.

The highest effect of increase of arc stability in transverse magnetic field is obtained by stabilization of arc by the gas jet [9]. This is explained by the fact that, at first, short arc, especially in the upper part of the column, is deformed as a single whole, and, secondly, the cathode spot is stabilized at the cathode end.

The stability of arc in transverse magnetic field depends on thermal balance at the area of contact of cathode and anode plasma flows. Having provided thermal balance in any way, one can rely on stable burning of deviated arc or on increase in its deviation angle. On such assumption the method of arc stabilization in transverse magnetic field using «guiding wall» [9] (Figure) is based. The walls, manufactured of graphite or copper, are electrically isolated from the anode and cathode and have a guiding profile of a parabolic shape.

This provides maximum value of the anode spot shifting. The stabilizing wall reflects the anode flow $+A$ and directs it towards the cathode flow $C$, which causes preserving of thermal balance in arc column during deviations by 2–2.5 times larger than those at the absence of a guiding wall.

The compression of arc column by a natural magnetic field and its stabilization by a plasma jet imparts it properties of a flexible conductor with current, deviation of which in transverse magnetic field occurs due to action of electrodynamic forces. Therefore, the change of current direction at constant magnetic field or change of direction of transverse magnetic field at direct current should lead to change of direction of arc deviation.

Let us study the behavior of direct current arc in transverse variable magnetic field. The deviation of arc can be defined considering the movement of arc column as oscillation of an elastic conductor of a variable length around a definite point. According to empiric equations the speed of sliding of anode spot depends on amplitude angle of arc deviation, frequency of transverse variable magnetic field and time. At constancy of heat capacity of arc its input energy will change in accordance with the speed of arc movement, which allows controlling heat influence of arc on the base metal. At the areas with a decreased input energy the smaller penetration depth is noticeable.

The welding arc in the variable transverse magnetic field is less stable than in constant one [9]. The less value of critical intensity of magnetic field for the arc in the variable magnetic field is explained by different movement inertia of column and active spots at arc movement. In the moment of change of direction of arc movement the anode spot is stabilized by the plasma flow. The arc column, having high mobility, is tending to shift that leads to remaining the spot behind the column and under certain conditions to arc interruption.

The stabilization of arc by the gas jet leads to increase of its stability in a variable transverse magnetic field. Some effect of improving the arc stability is provided by additional transverse magnetic field, the force lines of which are normal to the lines of variable field. The authors of work [9] explain this by the fact that constant field, acting on the arc column with a constant force, a bit stabilizes the cathode spot. The decrease in amplitude of cathode spot oscillation at the end of electrode under the influence of this force is the reason of increasing the arc stability in the variable magnetic field.

The considered peculiarities of magnetically-controlled arc widen its technological possibilities. As a rule, the depth of penetration is controlled by change of relation between the current value and welding speed. To prevent burn-out of metal at increase of welding current the welding speed is increased that can cause a jumpy movement of an active spot over the surface and, as a consequence, the unsatisfactory weld formation. To prevent burn-out is possible by superposition of constant transverse magnetic field, directed along the weld axis, on the arc. The decrease in penetration depth and some reduction of weld width are observed. The significant change of weld width is attained in welding in transverse magnetic field by adjusting the amplitude of arc oscillation which is directly proportional to magnetic induction in the zone of arc burning [10].

Thus, the application of transverse constant and variable magnetic fields allows welding of metal in different technological variants: with transverse and longitudinal oscillations, angle forwards and backwards, i.e. controlling shape and sizes of welds within wide ranges. Here, the shape of weld pool is changed, which influences the character of weld metal crystallization. The impressive characteristic of change of shape of weld pool is the coefficient of pool shape (relation of weld width to the length of crystallized

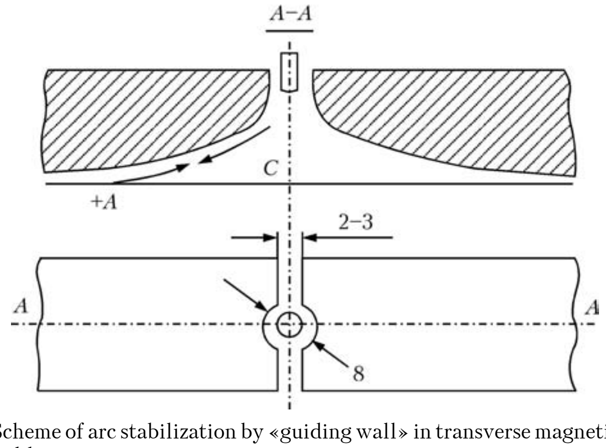

Scheme of arc stabilization by «guiding wall» in transverse magnetic field part). This coefficient grows from 1.1–1.4 (in welding without magnetic control) up to 3.0–3.3 at influence of transverse variable magnetic field with amplitude intensity of 4030 A/m. The influence of transverse magnetic field on the movement of weld pool metal in the process of crystallization opens up the possibilities of change of initial structure of crystallizing metal. The molten metal, located under the arc, is moving during movement of arc over the surface of weld pool under the influence of electromagnetic force. The repeated passing of arc across the weld and movement of molten layer of metal results in change of conditions of crystallization and producing of fine-grain weld structure.

The use of magnetically-controlled arc in welding in vertical plane to increase the quality of welds is of a special interest. Producing horizontal welds the molten metal under the influence of gravity is leaking to the lower edge, thus leading to non-uniform bead formation with an undercut at upper edge and overlap at the lower edge. Sometimes this is the reason of formation of such defects as lack of penetration, which are difficult to remove, especially in multi-pass welding. Under the conditions when input energy and welding speed are limited the unsatisfactory result of welding works is imminent.

With the purpose to solve the above-mentioned problem the authors of study [11] developed a method of welding where electric field in weld pool is subjected to influence of additional electromagnetic field caused by passing the electric current through two filler wires. The generated magnetic field influences the molten metal by electromagnetic force, which is directed upwards, balances the gravity force and contributes to prevention of a bead sagging. Thus, it is possible to control the flow of molten metal and bead shape. The value, which defines the quality of bead formation, can be the relation between the density of magnetic flux and contact angle. With the increase in density of magnetic flux the contact angle is decreased.

The given-above method of welding was tested in making horizontal welds of large-size steel structures. Along with the achieved high rate of deposition (up to 100 g/min) it is necessary to note some complication of welding process, as far as presence of two filler wires creates additional difficulties due to increase of amount of adjustable parameters.

To change the spatial position of arc the application of welding using tungsten electrode in argon by magnetically-controlled arc, which was realized both in automatic narrow-gap welding of titanium [12, 13] and also in manual (mechanized) welding under site conditions, is seemed as more challenging [14].

Thus, application of transverse variable magnetic field in welding widens greatly its technological capabilities, as it allows controlling the distribution of heat energy of arc between welded edges, filler wire and metal of weld pool, changing the conditions of crystallization of weld pool metal and, as a consequence, controlling the shape and sizes of the weld.


1. Bachelis, I.A. (1963) About calculation of welding arc deviation in constant transverse magnetic field. *Svarochn. Proizvodstvo*, **7**, 8–10.
2. Bron, O.B. (1961) *Movement of electric arc in magnetic field*. Moscow; Leningrad: Gosenergoizdat.
3. Gvozdetsky, V.S., Mechev, V.S. (1966) On problem of displacement of electric arc in magnetic field. *Avtomatich. Svarka*, **6**, 38–41.
4. Gvozdetsky, V.S., Mechev, V.S. (1963) Displacement of electric arc in magnetic field. *Ibid*., **10**, 54–62.
5. Mechev, V.S. (1968) Amplitude of electric arc oscillation in variable magnetic field. *Svarochn. Proizvodstvo*, **3**, 9–11.
6. Mechev, V.S., Dudko, D.A. (1967) Magnetically impelled arc welding. *Avtomatich. Svarka*, **1**, 59–63.
7. Mechev, V.S., Dudko, D.A. (1966) Specifics of equipment for magnetically impelled arc welding. *Ibid.*, **10**, 39–44.
8. Finkelnburg, V., Mekker, G. (1961) *Electric arcs and thermal plasma*. Ed. by V.A. Fabricant. Moscow: Inostr. Literatura.
9. Kovalev, I.M., Akulov, A.I. (1965) Stability of welding arc in transverse magnetic field. *Svarochn. Proizvodstvo*, **10**, 6–9.
10. Serdyuk, G.B., Kornienko, A.N. (1963) Welding arc in variable transverse magnetic field. *Avtomatich. Svarka*, **10**, 9–14.
11. Fujita, Yu., Manabe, Yu., Zenitani, S. et al. (2000) Development of two wires TIG welding with electromagnetically controlled molten pool process. *The Paton Welding J.*, **9/10**, 145–148.
12. Paton, B.E., Zamkov, V.N., Prilutsky, V.P. (1996) Narrow-groove welding proves its worth on thick titanium. *Welding J.*, **5**, 37–41.
13. Prilutsky, V.P., Zamkov, V.N., Lapchenko, S.V. et al. (1989) Narrow-gap magnetically controlled arc welding of titanium. *Avtomatich. Svarka*, **3**, 71–73.
14. Zamkov, V.N., Prilutsky, V.P. (2005) Methods for welding titanium alloys. *The Paton Welding J.*, **8**, 41–44.

# FRICTION STIR WELDING OF ALUMINUM ALLOYS OF DIFFERENT ALLOYING SYSTEMS

**A.G. POKLYATSKY, A.A. CHAJKA, I.N. KLOCHKOV** and **M.R. YAVORSKAYA**
E.O. Paton Electric Welding Institute, NASU, Kiev, Ukraine

Comparative analysis of the degree of weakening and level of strength of the 1.8 mm thick TIG- and FS-welded joints on dissimilar high-strength multi-component aluminum alloys AMg6M, 1420, 1201 and 1460 was carried out. Peculiarities of formation of the weld structure in both cases were studied. It is shown that strain hardening of the welds on high-strength multi-component aluminum alloys in friction stir welding provides their higher strength level, compared with that in fusion welding.

**Keywords:** *friction stir welding, TIG welding, high-strength aluminum alloys, composite joints, degree of weakening, tensile strength, structure of welded joint metal*

Aluminum alloys of different alloying systems are widely used in manufacture of welded structures. Different methods of fusion welding based on weld metal crystallization from a weld pool melt are used for obtaining permanent joints. High-temperature heating of a welding zone results in structural and phase transformations in the weld metal itself as well as in the areas adjacent to it. In this connection, strength of weld metal and welded joints on cold-worked and hardenable by heat treatment aluminum alloys does not exceed 70 % of that of the base metal [1, 2] in most cases. Besides, many aluminum alloys are tend to formation of hot cracks in the weld or its fusion zone (FZ) with the base metal in the process of melt crystallization. Such an intergranular fracture is also conditioned by heating of metal up to the melting temperature in the welding zone and occurs in the places of precipitation of low-melting secondary phases [3]. Introduction of filler metal of a specific chemical composition in the weld allows increasing welded joint resistance to hot cracks formation and providing the necessary level of their strength [4].

The necessity to weld dissimilar aluminum alloys arises, however, during development of recent high-efficiency, multifunctional and economy structures in which specific advantages of each material are rationally used. It is natural that a system of metal alloying in the melt becomes significantly complicated during joining of such alloys by fusion welding that develops additional difficulties for selection of composition of the filler wire. The letter, mixing with alloys being welded, promotes obtaining of the weld metal composition providing minimum susceptibility of joints to hot cracking and high level of their mechanical properties [5, 6]. Therefore, if heating of a joint zone up to solidus temperature to be eliminated from a technological process of welding of aluminum alloys, then the conditions can be removed resulting in occurrence of crystallization cracks in the welds, and their strength characteristics are increased.

Friction stir welding (FSW) is an effective method for obtaining solid phase permanent joints without melting of the base metal. A weld in this method of welding is formed as a result of movement in limited area of small amount of plasticized metal heated due to friction to the temperature not higher 75 % of alloy melting temperature [7, 8].

The aim of the present paper is to evaluate degree of weakening, peculiarities of structure and level of strength of FS- and automatic TIG-welded joints on dissimilar thin sheet aluminum alloy.

High-strength aluminum alloys AMg6 (Al–Mg–Mn) and 1201 (Al–Cu–Mn) as well as lithium-containing alloys 1420 (Al–Mg–Li) and 1460 (Al–Cu–Li), having increased specific strength, and widely applied in manufacture of elements of aircrafts, were used in the investigations. 1.8 mm thick sheets were TIG-welded with 20 m/h speed on MW-450 unit («Fronius», Austria) at 130–150 A current applying SvAMg6, SvAMg63 and Sv1201 filler wires. FSW was carried out on a laboratory unit designed in the E.O. Paton Electric Welding Institute. Special tool with conical pin and 12 mm diameter shoulder was used for obtaining butt joints. Speed of the tool made 1420 rpm and linear speed of its movement along the butt was 8–14 m/h.

Samples for investigation of structure, determination of hardness and tensile strength at uniaxial tension were manufactured from obtained welded joints. TIG-welded standard samples were tested with the beads taken flush with the base metal as well as with additionally cleaned reinforcements.

The tests were carried out with the help of universal multipurpose servohydraulic system MTS 810. MIM-8M light microscope was used for investigation of structure of metal of welded joints. Transverse cross-sections of the welded joints were preliminary treated by means of the electrolytic polishing and additional etching in a solution of chloric, nitric and hydrofluoric acids.

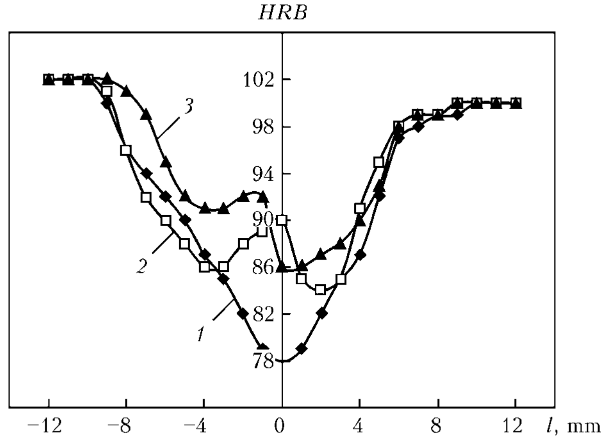


**Figure 1.** Distribution of metal hardness for TIG-welded joints on dissimilar aluminum alloys 1420 and 1201 made using SvAMg63 (*1*) and Sv1201 (*2*) filler wires, as well as for FS-welded joints (*3*): *l* — distance from weld axis

Hardness of metal of welded joints was measured on a weld face preliminary cleaning the reinforcement and bead flush with the base metal. At that, width of TIG-welds made on average 6.5 mm and for FS-welds it was 3.5 mm at 11 mm width of thermomechanical-affected zone (TMAZ). The degree of metal weakening in the welding zone was evaluated on the results of measuring of its hardness on ROSKWELL device under load $P = 600$ N.

Analysis of a hardness distribution showed that the degree of metal weakening in the weld as well as in the areas adjacent to it is always lower in FSW than in TIG welding. Thus, minimum hardness of the weld metal makes *HRB* 80 in TIG welding of 1201 alloy to AMg6 alloy using SvAMg6 filler wire and *HRB* 83 using Sv1201 filler wire. FSW method allows increasing this index up to *HRB* 86. The metal of fusion-welded weld made using SvAMg63 and Sv1201 filler wires has minimum hardness *HRB* 78 and 84, respectively, in welding together hardenable by heat treatment alloys 1420 and 1201. Application of FSW method provides weld metal hardness up to *HRB* 86 (Figure 1). Minimum hardness of the metal of TIG-welds on dissimilar alloys AMg6M and 1460 using SvAMg6 filler wire is also at the level of *HRB* 78.

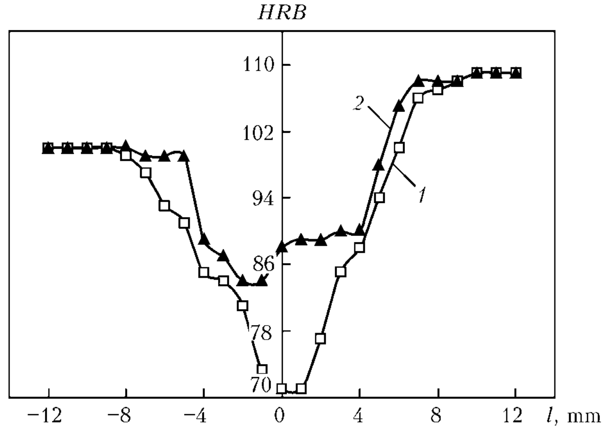


**Figure 2.** Distribution of metal hardness for TIG-welded joints on dissimilar copper-containing aluminum alloys 1201 and 1460 made using Sv1201 (*1*) filler wire, as well as for FS-welded joints (*2*)

Usage of Sv1201 filler wire allows increasing hardness of the weld metal up to *HRB* 84, but in this case it is significantly lower that in solid phase welding (*HRB* 89). In TIG joining of lithium-containing aluminum alloys 1420 and 1460 using SvAMg63 and Sv1201 filler wires the minimum hardness of metal in the weld is provided around *HRB* 78 and 86, respectively. This index during their solid phase welding makes not lower than *HRB* 87. TIG-welds on dissimilar hardenable by heat treatment copper-containing aluminum alloys 1201 and 1460 made using Sv1201 filler wire have minimum hardness *HRB* 71. It increases up to *HRB* 88 (Figure 2) in FSW.

Measuring of the temperature near the edge of tool shoulder, carried out with the help of chromel-alumel thermocouples, showed that lower degree of metal weakening of dissimilar aluminum alloys in FSW is conditioned by smaller heating of metal in the welding zone. Thus, the maximum temperature near the edge of shoulder makes 395 or 415 °C (Figure 3) and the metal heats up to 500 °C in a weld nugget depending on location of alloys 1460 and 1201 from the side of advancing or retreating of the tool.

Special thermomechanical conditions of joints generation in FSW promote formation of fine-grained crystalline structure of the weld metal and areas adjacent to it. The character areas — weld nugget, TMAZ and HAZ — can be outlined in the welded joints as in welding of similar aluminum alloys. But if the adjacent areas have virtually no differences in their structure from obtained in welding of corresponding alloys in similar combination, then the weld nugget contains microareas with completely and par-

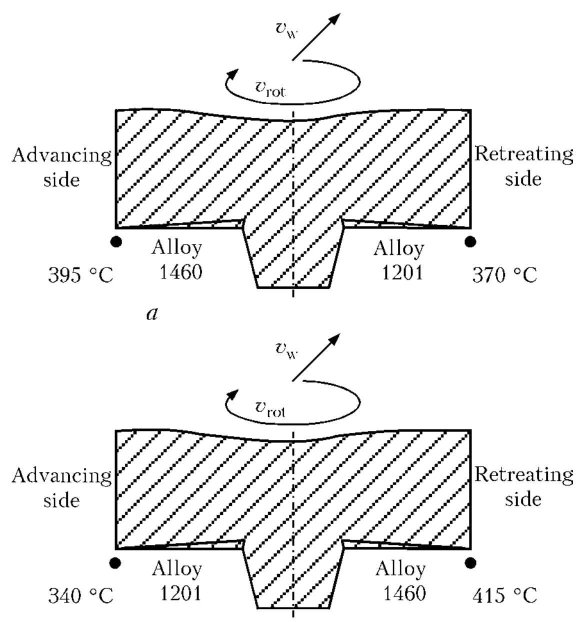


**Figure 3.** Dependence of maximum metal temperature near the edge of tool shoulder in FSW of dissimilar aluminum alloys 1460 and 1201 on their location relative to direction of tool rotation: *a* — alloy 1460 from the side of tool advancing, alloy 1201 from the side of retreating; *b* — conversely; $v_w$ — welding speed; $v_{rot}$ — speed of tool rotation

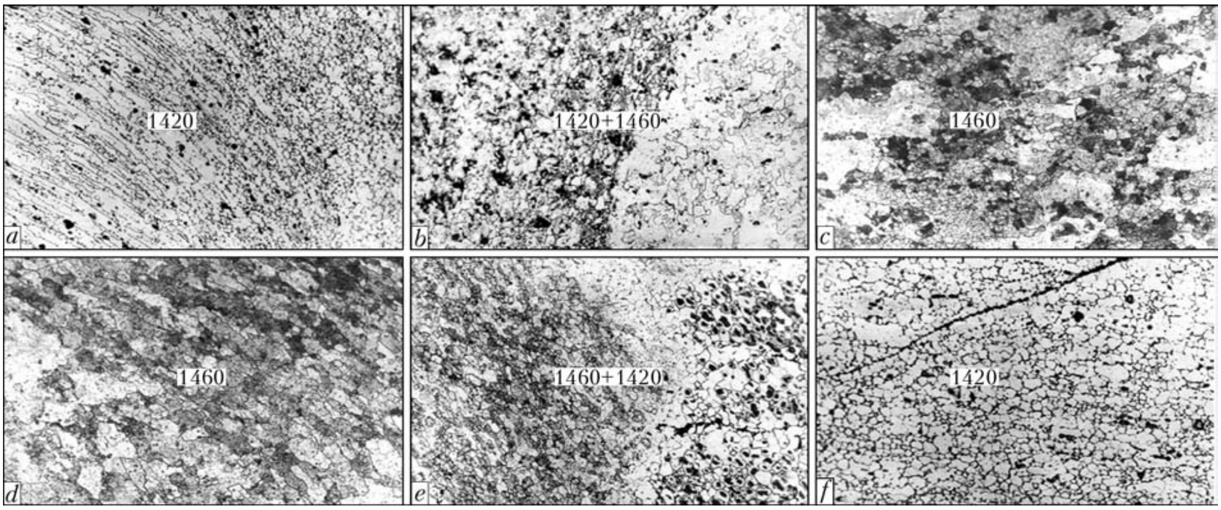


**Figure 4.** Microstructures (×400) of FS-welded joints on dissimilar aluminum alloys 1420 and 1460 at their different location relative to direction of tool rotation: *a, d* — TMAZ from the side of tool advancing; *b, e* — weld nugget; *c, f* — TMAZ from the side of tool retreating

tially mixed metal and microlayers with non-mixed metal (Figure 4). The lines of intermetallics and grains are oriented in parallel to sheet surface in HAZ metal and in the direction of the tool movement and plasticized metal traveling behind it in TMAZ metal. In this case, the grains are sufficiently coarse and elongated, however, they can be fine and equiaxial, apparently, recrystallized at increased temperature in a process of deformation, immediately on the weld boundary. Presence of equiaxial grains and chaotically distributed ground intermetallic inclusions is character for the weld metal. Their size is significantly smaller than in the base metal, TMAZ and HAZ metal as well as in any area of TIG-welded joint (Figure 5).

A permanent joint is formed in the solid phase without material melting during FSW process. Formed at that fine structure of the weld metal and areas immediately adjacent to it provides high strength of such joints. Thus, an ultimate strength of the samples, failing along the weld to base metal FZ from the side of 1201 alloy, is at the level of 304 MPa (Table) in alloy 1201 to alloy AMg6 welding. This index, respectively, makes 16 and 25 MPa below for TIG-welded samples with eliminated weld reinforcement made using Sv1201 and SvAMg6 filler wires. Samples of FS-welded joints on hardenable by heat treatment alloys 1201 and 1420 also failure along the weld to base metal FZ from the side of 1201 alloy. Their strength reaches 311 MPa and exceeds the results, obtained in fusion welding using filler wire SvAMg63 and Sv1201 by 39 and 71 MPa, respectively. The failure of FS-welded joint samples of AMg6 and 1460 alloys can take place along the TMAZ and HAZ from the side of AMg6 alloy. Their tensile strength is at the level of 329 MPa that exceeds this index for the samples of TIG-welded joints without weld reinforcement, made using SvAMg6 and Sv1201 filler wires, by 78 and 46 MPa, respectively. FS-welded joints of magnesium-doped alloys 1420 and AMg6 failure along the HAZ from the side of AMg6 alloy and have tensile

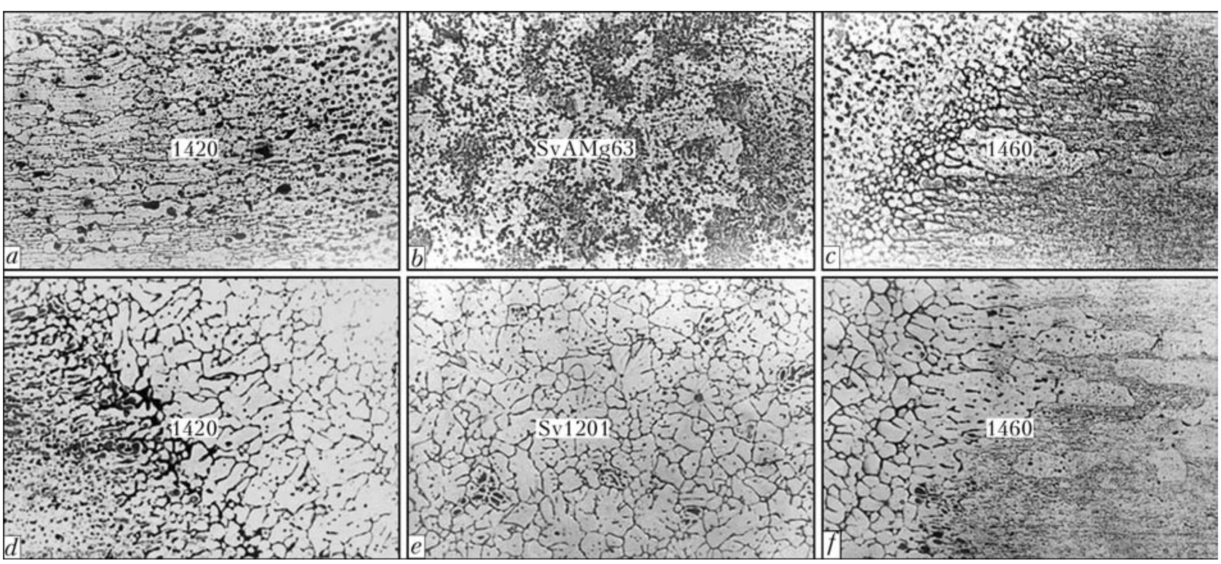


**Figure 5.** Microstructures (×400) of areas of joints on aluminum alloys 1420 and 1460, TIG-welded with filler wires: *a, c, d, f* — weld to base metal FZ; *b, e* — weld

Strength of FS- and TIG-welded joints on dissimilar aluminum alloys

| Alloys being welded | Welding method | Filler wire | $\sigma_t$ of the samples without weld reinforcement, MPa | Place of failure | $\sigma_t$ of the samples with weld reinforcement, MPa | Place of failure |
|---|---|---|---|---|---|---|
| 1201 + AMg6 | FSW | – | 304 | $FZ_{1201}$ | – | – |
| | TIG | Sv1201 | 288 | $FZ_{1201}$ | 302 | $FZ_{1201}$ |
| | | SvAMg6 | 279 | $FZ_{1201}$ | 312 | $FZ_{1201}$ |
| 1201 + 1420 | FSW | – | 311 | $FZ_{1201}$ | – | – |
| | TIG | Sv1201 | 240 | $FZ_{1420}$ | 287 | $FZ_{1201}$ |
| | | SvAMg63 | 272 | $FZ_{1420}$ | 301 | $FZ_{1201}$ |
| AMg6 + 1460 | FSW | – | 329 | $TMAZ_{AMg6}$ $HAZ_{AMg6}$ | – | – |
| | TIG | Sv1201 | 283 | $FZ_{AMg6}$ | 283 | $FZ_{1460}$ |
| | | SvAMg6 | 251 | Weld | 321 | $FZ_{AMg6}$ |
| 1420 + AMg6 | FSW | – | 340 | $HAZ_{AMg6}$ | – | – |
| | TIG | SvAMg63 | 314 | Weld/$FZ_{AMg6}$ | 343 | $FZ_{AMg6}$ |
| 1201 + 1460 | FSW | – | 285 | $FZ_{1201}$ | – | – |
| | TIG | Sv1201 | 257 | Weld | 294 | $FZ_{1201}$ |
| 1420 + 1460 | FSW | – | 286 | $FZ_{1420}$ | – | – |
| | TIG | Sv1201 | 281 | $FZ_{1420}$ | 335 | $FZ_{1420}$ |
| | | SvAMg63 | 288 | Weld/$FZ_{1420}$ | 358 | $FZ_{1420}$ |

*Note*. Average values of indices according to test results of 3–5 samples are given.

strength 340 MPa, whereas samples of TIG-welded joint without weld reinforcement have tensile strength only 314 MPa. The strength of the joint samples makes 285 MPa in FSW of copper-doped hardenable by heat treatment alloys 1201 and 1460. Their failure occurs on the weld to base metal FZ from the side of 1201 alloy as in TIG-welded samples with weld reinforcement made using Sv1201 filler wire. But joints without weld reinforcement failure along the weld metal and have strength below 275 MPa, i.e. lower than joints obtained in the solid phase. And even presence of the weld reinforcement in all samples of joints mentioned above just rarely allows achieving the same level of strength as in the solid phase welding. FS-welded joints on lithium-containing aluminum alloys 1420 and 1460 failure along the weld to base metal FZ from the side of alloy 1420 and have 286 MPa tensile strength. Approximately the same strength index is provided in the samples of joints without weld reinforcement in TIG welding using Sv1201 and SvAMg63 filler wires. However, strength of the samples with weld reinforcement made using Sv1201 and SvAMg63 wires increases up to 335 and 358 MPa, respectively.

Thus, the weld and areas adjacent to it are heated below the base metal melting temperature in FSW, due to which the possibility of formation of crystallization cracks is eliminated in obtaining of the permanent joints on single and dissimilar aluminum alloys.

Intensive mixing of plasticized metal in the limited area under excessive pressure promotes formation of subdendritic structure of the weld nugget, consisting of homogeneous and partially mixed layers of alloys being welded as well as TMAZ, containing simultaneously stretched elongated relative to the direction of tool movement grains and small recrystallized equiaxial grains.

Grain size refinement, increase of volume fraction of their boundaries and shattering of intermetallic phases in metal of FS-welded welds on dissimilar aluminum alloys allow obtaining higher values of tensile strength of welded joints than in fusion welding.


1. Lozovskaya, A.V., Chaika, A.A., Bondarev, A.A. et al. (2001) Softening of high-strength aluminium alloys in different fusion welding processes. *The Paton Welding J.*, **3**, 13–17.
2. Mashin, V.S., Poklyatsky, A.G., Fedorchuk, V.E. (2005) Mechanical properties of aluminium alloys in consumable and nonconsumable electrode arc welding. *Ibid.*, **9**, 39–45.
3. Ishchenko, A.Ya. (1985) Character of hot cracks in fusion welding of high-strength aluminium alloys. In: *Current problems of welding of nonferrous metals*. Kiev: Naukova Dumka.
4. Rabkin, D.M. (1986) *Metallurgy of fusion welding of aluminium and its alloys*. Kiev: Naukova Dumka.
5. Liptak, I.A., Baysinger, F.R. (1968) Welding dissimilar aluminium alloys. *Welding J.*, **4**, 173–180.
6. Ishchenko, A.Ya., Lozovskaya, A.V., Yavorskaya, M.R. et al. (1991) Properties of welded joints of AD0 aluminium with AMg6 alloy using different filler wires. *Avtomatich. Svarka*, **5**, 12–18.
7. Dawes, C.J., Thomas, W.M. (1996) Friction stir process welds aluminium alloys. *Welding J.*, **3**, 41–45.
8. Lambrakos, S.G., Fonda, R.W., Milewski, J.O. et al. (2003) Analysis of friction stir welds using thermocouple measurements. *Sci. and Techn. of Welding and Joining*, **5**, 385–390.
9. Lohwasser, D. (2001) Welding of airframes by friction stir. In: *Proc. of 3rd Int. Symp. on Friction Stir Welding* (Kobe, Japan, Sept. 27–28, 2001), 1–6.
10. Polovtsev, V.A., Makarov, N.V., Shillo, G.V. et al. (2008) Friction welding of aliminium liners of metal-composite high-pressure cylinders. *Tekhnologiya Mashinostroeniya*, **1**, 38–41.

# MECHANICAL PROPERTIES OF BRAZED JOINTS ON DISPERSION-STRENGTHENED COPPER ALLOY

**S.V. MAKSYMOVA, V.F. KHORUNOV** and **V.A. SHONIN**
E.O. Paton Electric Welding Institute, NASU, Kiev, Ukraine

The paper gives results of investigations of a set of properties of the brazed joints on a copper alloy strengthened by dispersed particles of $Al_2O_3$, produced by vacuum brazing using adhesion-active brazing filler metals. It is shown that application of heat treatment of the base metal in combination with filler metal of the Cu–Ti system ensures tensile strength of the brazed joints at a level of 81 % of that of the as-received base metal, and 92 % of that after preliminary heat treatment.

***Keywords:*** *vacuum brazing, dispersion-strengthened copper alloy, butt brazed joint, adhesion-active brazing filler metals, tensile mechanical properties*

Joints produced by high-temperature brazing are heterogeneous systems consisting of different materials characterised by different physical-mechanical properties. Strength of the brazed joints greatly depends on a proper choice of composition of a brazing filler metal, its mechanical properties and compatibility with the base material. The technological process of brazing allows avoiding high residual stresses in the joints, melting of the base metal and cracking. Hence, the process makes it possible to preserve properties of the base metal with no disturbance of its structural state. The brazing process involves physical-chemical interaction of the base metal with a molten filler metal, this affecting composition the brazed seam. At the same time, mechanical properties of the brazed joints differ from properties of the filler metal in the initial state [1], and are in direct dependence on the structural state of the seam metal and its width [2].

This study gives results of investigations of mechanical properties of the brazed joints on a dispersion-strengthened copper alloy (Glidcop Al-25) produced by using adhesion-active filler metal based on the Cu–Ti, Cu–Mn–Ni–Fe–Si and other systems (Table 1). Microstructural peculiarities of the brazed joints on heat-resistant copper alloy Glidcop Al-25 strengthened with dispersed oxide particles of $Al_2O_3$ were studied earlier by using different filler metals and heating methods [3, 4].

Dispersion-strengthened copper alloy Glidcop Al-25 in the as-received state and after annealing at a temperature of 950 °C for 1 h was used to investigate mechanical properties of the base metal and brazed joints. Cylindrical billets about 70 mm long with prepared edge surfaces were utilised for making butt brazed joints. To ensure alignment of the brazed pieces, before brazing they were put in a special fixture, the filler metal was introduced into the gap, and then they were placed in a furnace. Brazing was performed in vacuum at a liquidus temperature of the filler metal by using radiation and resistance heating. In case of resistance heating, compressive pressure of 10 g/cm$^2$ was applied to the brazed pieces. The time of holding at a brazing temperature was 3 min in both cases. However, in radiation heating the total brazing time (till unloading from the furnace) was longer — about 130–140 min, and in resistance heating it was approximately 20 min. Cylindrical specimens for static tensile tests were made from the produced butt brazed billets about 140 mm long. Sizes of the gauge zone of the specimens were as follows: length $l_0 = 50$ mm, and diameter $d_0 = 10$ mm. Thread M16 was made in the grip regions of the specimens.

Tensile tests were carried out according to GOST 6996–66 and GOST 1497–84. Electromechanical testing machine UME-10tm fitted with the required electronic equipment, strain gauge with a gauge length of 25 mm and $X$–$Y$ recorder N307/1 was used for the tests. Deviations of the measured load were not in excess of ±1 %. The test temperature was 20–24 °C.

Conditional values of tensile strength $\sigma_t$, yield strength $\sigma_{0.2}$ and elasticity limit $\sigma_{0.01}$, as well as elongation $\delta_{2.5}$, reduction in area $\psi$ and elasticity modulus $E$ were determined. Deformation diagram $F$ (load) and $\Delta l$ (elongation of a specimen) was recorded during the tests. To determine the $\sigma_{0.2}$, $\sigma_{0.01}$ and $E$ values, the speed of a grip was $8 \cdot 10^{-3}$ mm/s, while further tests to complete fracture were conducted at a speed of $8 \cdot 10^{-2}$ mm/s. Upon achieving the residual elongation value of $\varepsilon \geq 0.2$ %, the load was decreased to $F = 0$. After readjustment of the grip movement mode and scale of recording of the diagram, the tests were continued to complete fracture.

**Table 1.** Melting temperature of brazing filler metals, °C

| No. of filler metal | Base system | $T_S$ | $T_L$ |
|---|---|---|---|
| 1 | Cu–Ti | 950 | 990 |
| 2 | Cu–Mn–Ni–Fe–Si | 810 | 890 |
| 3 | Ti–Zr–Ni–Cu–V–Be | 748 | 857 |
| 4 | Ti–Zr–Ni–Cu | 830 | 955 |

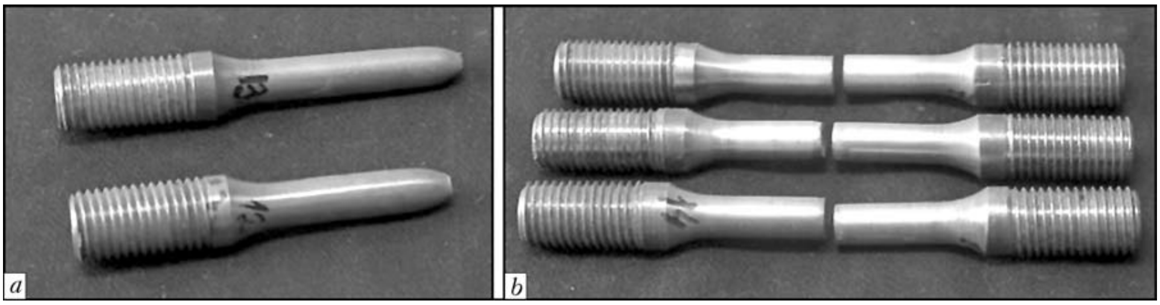


**Figure 1.** Appearance of specimens after mechanical tests: *a* — base metal; *b* — brazed joints

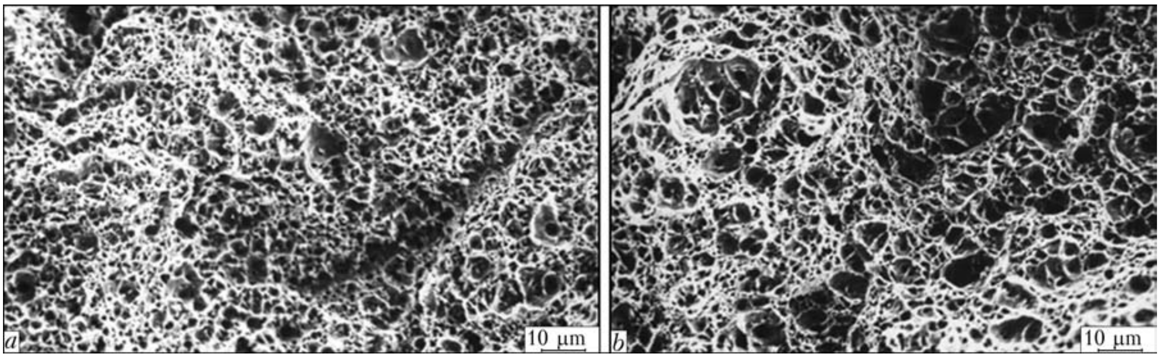


**Figure 2.** Fractographs of fracture surface of base metal in initial state (*a*) and after annealing (*b*)

Diameter of the gauge region of the specimens before the tests, $d_0$, and after the tests, $d_t$, was measured in three different sections and in two mutually perpendicular directions. Measurements of the brazed specimens were made in sections along the joining zone by using micrometer MKO-25 with a scale division value of 0.01 mm.

Elongation $\delta_{2.5}$ at fracture was determined from the deformation diagram for deformation meter gauge length $OL$ = 25 mm, and by measuring residual elongation between the base marks on a specimen, $\Delta l = l_U - l_O$. For this, light transverse marks were made on the specimen surfaces on two sides from the seam centre for a gauge length of 25 mm. To reveal the character of non-uniform deformation, additional

**Table 2.** Results of tensile tests of base metal and butt brazed joints on copper alloy Glidcop Al-25

| Specimen No. | Filler metal alloying system | $\sigma_t$, MPa | $\sigma_{0.2}$, MPa | $\sigma_{0.01}$, MPa | $E$, MPa | $\delta_{2.5}$, % | $\psi$, % |
|---|---|---|---|---|---|---|---|
| PM-1 | – | 491.5 | 440.6 | 245.1 | 108,606 | 10.40 | 68.80 |
| PM-2* | – | 430.1 | 351.9 | 243.6 | 101,365 | 7.20 | 75.80 |
| 1 | Cu–Ti | 353.2 | 337.4 | 230.8 | 94,594 | 0.561 | 2.70 |
| 2 | Cu–Ti | 353.4 | 333.1 | 219.5 | 99,925 | 0.79 | 2.31 |
| 3* | Cu–Ti | 397.2 | 322.7 | 217.2 | 96,970 | 1.42 | 5.99 |
| 4* | Cu–Ti | 382.4 | 320.3 | 218.6 | 94,365 | 3.89 | 5.41 |
| 5 | Cu–Mn–Ni–Fe–Si | 111.9 | >111.9 | 111.9 | 93,898 | 0.05 | 0.10 |
| 6 | Cu–Mn–Ni–Fe–Si | 253.9 | >253.9 | 191.2 | 98,727 | 0.07 | 0.50 |
| 7* | Cu–Mn–Ni–Fe–Si | 305.3 | 304.1 | 202.5 | 97,388 | 0.27 | 1.69 |
| 8* | Cu–Mn–Ni–Fe–Si | 282.6 | >282.6 | 215.2 | 95,785 | 0.09 | 1.00 |
| 9 | Ti–Zr–Ni–Cu–V–Be | 310.3 | >310.3 | 245.1 | 91,539 | 0.07 | 0.99 |
| 10 | Ti–Zr–Ni–Cu–V–Be | 234.3 | >234.4 | 234.3 | 99,917 | 0.01 | 0.20 |
| 11 | Ti–Zr–Ni–Cu | 136.8 | >136.8 | >136.8 | 108,823 | 0 | 0.60 |
| 13** * | Cu–Ti | 387.1 | 322.1 | 223.0 | 92,300 | 4.20 | 16.40 |
| 14** * | Cu–Ti | 376.6 | 322.2 | 197.1 | 99,160 | 2.50 | 8.40 |
| 15** | Cu–Mn–Ni–Fe–Si | 357.9 | 334.0 | 214.7 | 99,914 | 0.60 | 2.04 |
| 16** | Cu–Mn–Ni–Fe–Si | 305.0 | >305.0 | 214.9 | 100,833 | 0.12 | 0.56 |

*Preliminary annealing. **Brazing with resistance heating.

transverse marks were made within the gauge length on the specimen surfaces (PM-1, PM-2, Nos. 3, 4, 7, 8, 13 and 14) with the roughness removed by grinding: with an interval of 1 mm within the seam zone, and with an interval of 2 mm outside the seam. Toolmaker's microscope BIM-1 having micrometric screws and a scale division value of 0.005 mm was employed to make the transverse marks and measure the elongation value. The measurement data were used to determine residual local elongations between the neighbouring marks $\delta_{l_i = 1} = \frac{l_{U,\,i} - l_{O,\,i}}{l_{O,\,i}} \cdot 100$ %, where $l_{U,\,i}$ and $l_{O,\,i}$ are the distances between the marks before and after the tests, respectively.

Base metal specimens PM-1 and PM-2 subjected to tension fractured with a substantial plastic deformation within the gauge (proportional) part of a specimen to form a neck in the fracture zone (Figure 1, *a*). Structure of the fracture surface in the initial state was homogeneous, characterised by a pit-like tough relief (Figure 2, *a*).

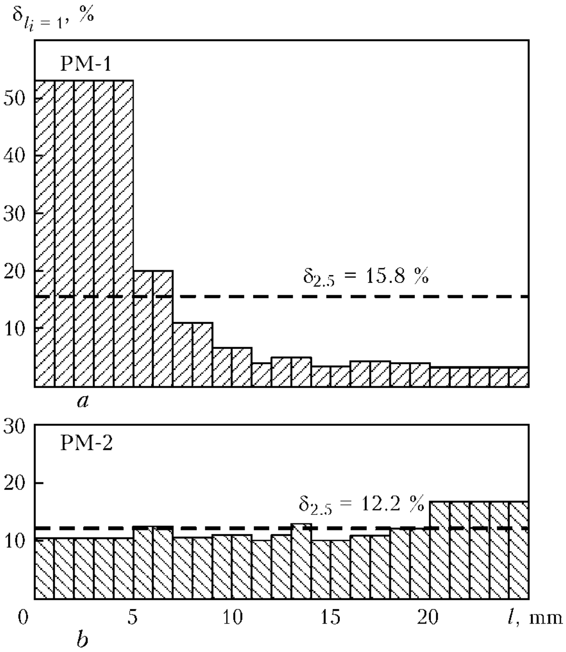


**Figure 3.** Character of distribution of residual elongation in tensile tests of cylindrical specimens of alloy Glidcop Al-25 in initial state (*a*) and after annealing (*b*)

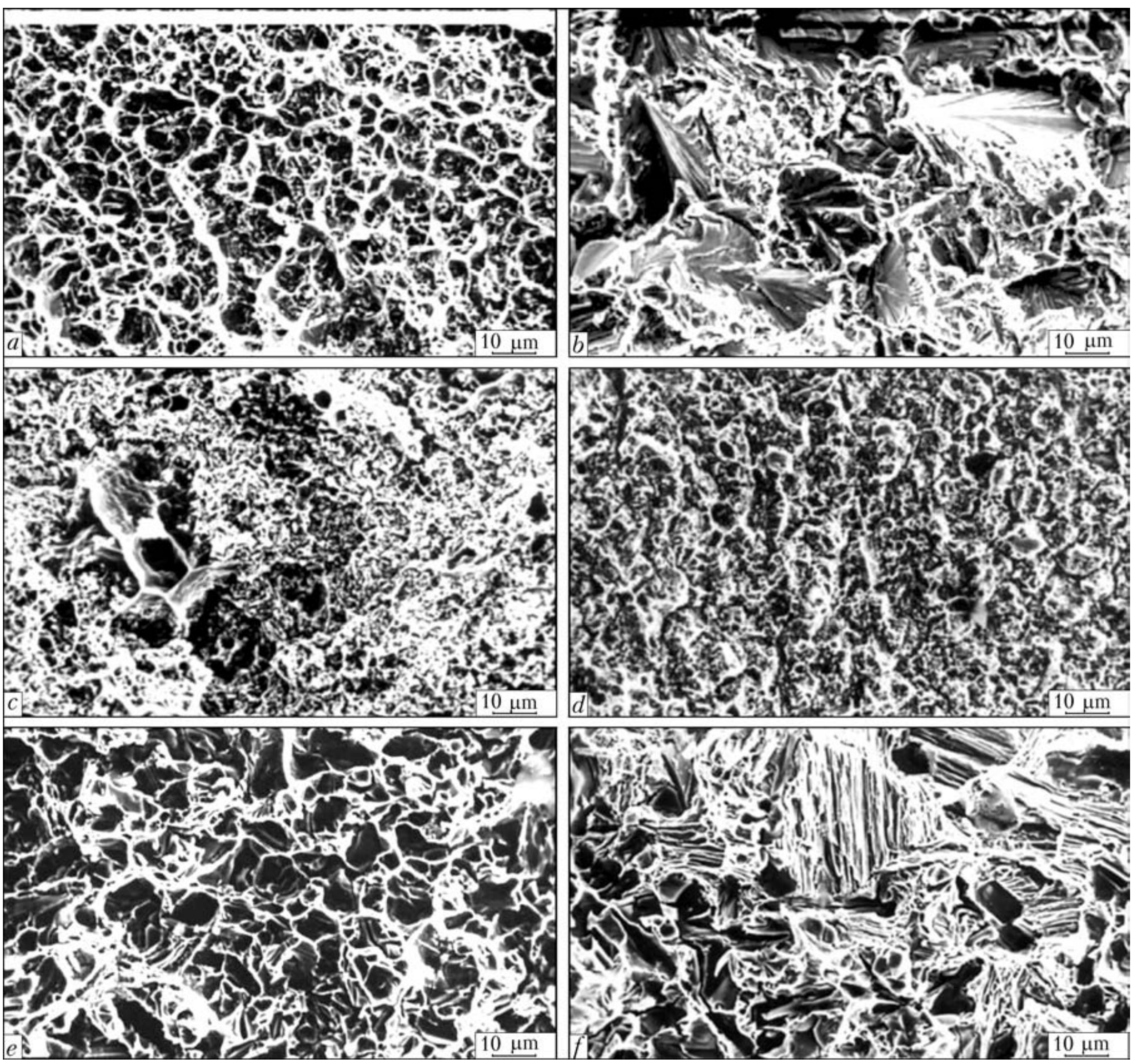


**Figure 4.** Fractographs of fractures of brazed joints on dispersion-strengthened copper alloy produced with filler metals Nos. 4 (*a*), 3 (*b*), 2 (*c*, *d*) and 1 (*e*, *f*)

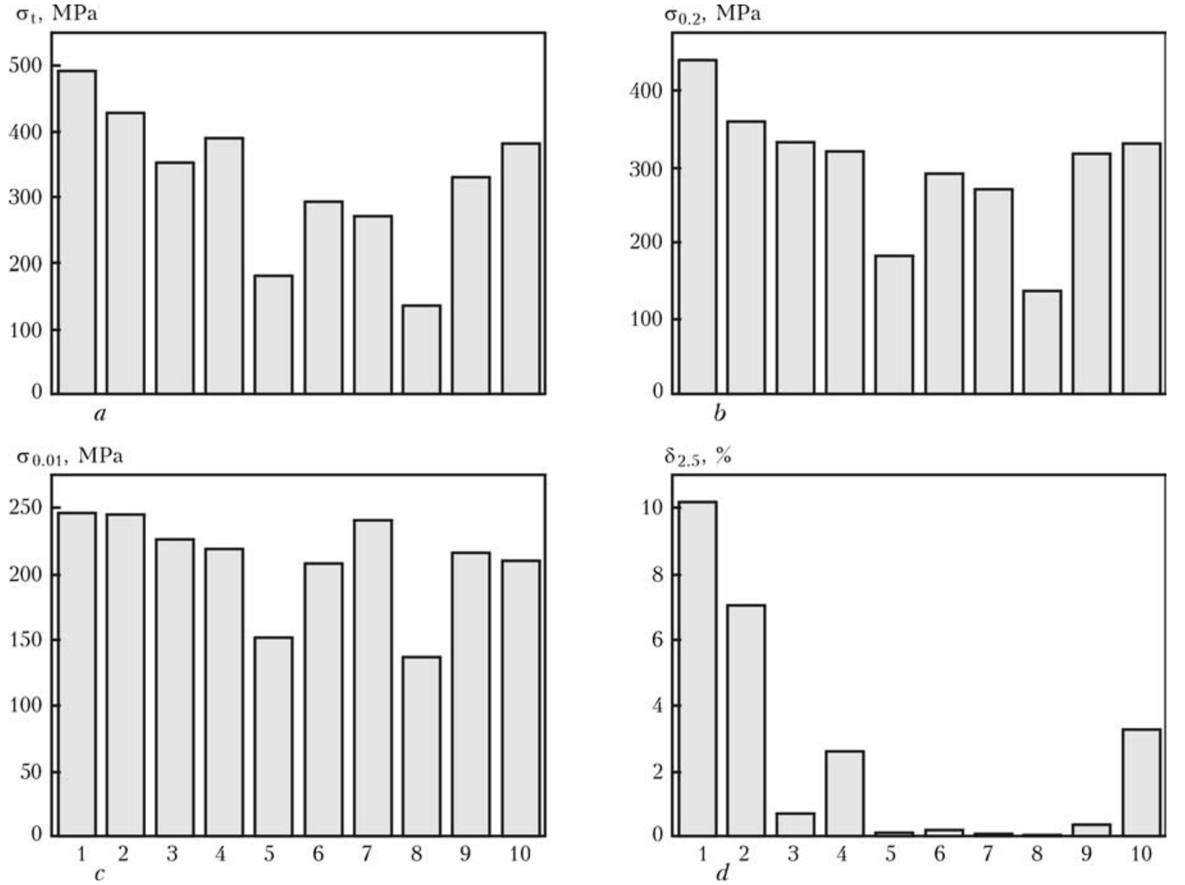


**Figure 5.** Diagrams of average values of mechanical properties of alloy Glidcop Al-25 in the initial (1) and annealed state (2), and of the brazed joints (3–10) produced with filler metals based on the Cu–Ti (3), Cu–Ti[1] (4), Cu–Mn–Ni–Fe–Si (5), Cu–Mn–Ni–Fe–Si[1] (6), Ti–Zr–Ni–Cu–V–Be (7), Ti–Zr–Ni–Cu (8), Cu–Mn–Ni–Fe–Si[2] (9) and Cu–Ti[1, 2] (10): [1] — preliminary heat treatment of base metal at 950 °C for 1 h; [2] — brazing by using flowing current

Annealing led to increase (two times) in the local value of residual elongation, compared with the non-annealed specimen (Table 2, Figure 3). However, because of fracture of the specimen in the annealed state outside the measurement part, it had a lower value of residual elongation $\delta_{2.5}$.

Strength of alloy Glidcop Al-25 decreased by 60 MPa after heat treatment (see Table 2), i.e. its strength corresponded to 430 MPa. Fracture was of a tough character, but pits had a larger size (about 10 μm) than in the previous specimen (see Figure 2, *b*), which may result from partial coarsening of the strengthening phase.

In tensile tests of the brazed specimens, fracture occurred in the seam with a minimal plastic deformation of the base metal in the near-seam zone (see Figure 1, *b*). It was determined that the lowest strength of the brazed joints, 137 and 234–310 MPa, was obtained with the brazing filler metals based on the Ti–Zr–Ni–Cu (see Table 2) and Ti–Zr–Ni–Cu–V–Be systems, respectively. The fracture surface contained a large number of regions with a brittle fracture (Figure 4, *a*, *b*).

The higher strength values were obtained with a filler metal of the Cu–Mn–Ni–Fe–Si system, although the spread of values was significant (of an order of 140 MPa). Preliminary heat treatment of the base metal in case of radiation heating allowed increasing the tensile strength value from 112–254 to 283–305 MPa. Further increase in strength ($\sigma_t$ = 305–358 MPa) can be achieved by using resistance heating (Table 2, specimens Nos. 15 and 16), which provides rapid heating and cooling, and a minimal brazing time. Moreover, application of a compressive force led to pressing out of part of a molten filler metal from the gap, which also had a positive effect on mechanical properties of the brazed joints. Analysis of the data obtained shows that the use of resistance heating allows reducing the brazing time (approximately 6–7 times) compared to radiation heating and, at the same time, increasing strength of the brazed joints by about 50 MPa in brazing with the filler metal based on the Cu–Mn–Ni–Fe–Si system.

As shown by fractography results on the character of fracture of the brazed joints, topography of the fracture surfaces is affected by composition of the brazed seam, i.e. microstructural components of the seam. For example, the fracture surface of specimen No.6 ($\sigma_t$ = 254 MPa, radiation heating) features a mixed character of fracture with a large number of tear ridges (Figure 4, *c*). Isolated particles containing up to 20 wt.% Al can be seen on the fracture surface.

The character of fracture of the specimens produced by brazing with the same filler metal (Cu–Mn–Ni–

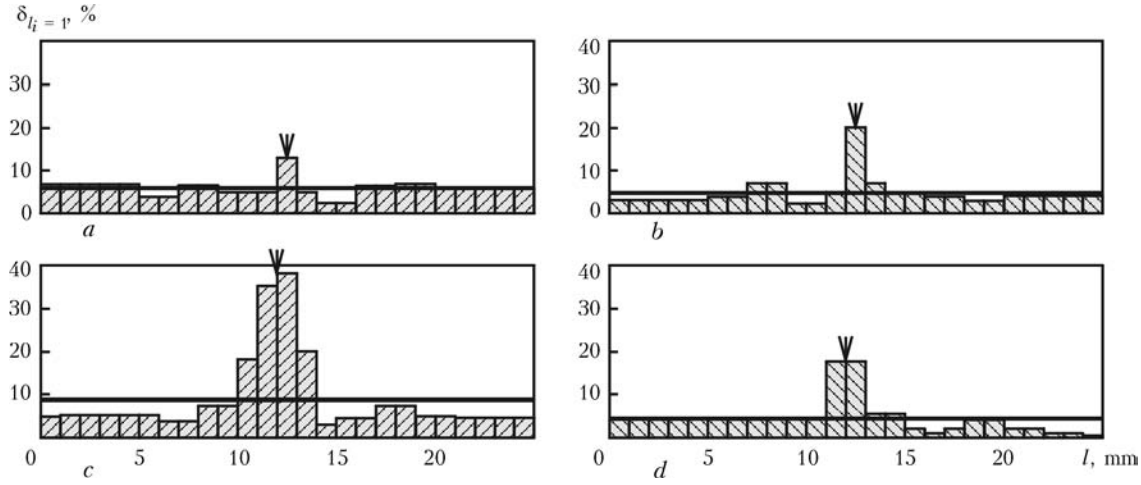

**Figure 6.** Character of distribution of residual elongation in tensile tests of butt joints brazed with the Cu–Ti system filler metal in vacuum furnace by using radiation heating (*a* — specimen No.3; *b* — No.4), and by the flowing current (*c* — No.13; *d* — No.14): $\delta_{2.5}$ = 5.90 (*a*), 4.76 (*b*), 8.86 (*c*) and 4.35 (*d*) %

Fe–Si) by using resistance heating ($\sigma_t$ = 305 MPa) featured a structure with finer grains. The content of aluminium decreased and equalled about 10 wt.% in some particles. Specimen No.15 exhibiting the highest strength for the given filler metal ($\sigma_t$ = 358 MPa) had a more fine-grained structure of the fracture surface (Figure 4, *d*). The content of aluminium in white particles continued decreasing, and was no more than 6 wt.%. Therefore, tensile strength of the brazed joints increased with decrease in the weight content of aluminium in the seam.

The best strength characteristics of the brazed joints (with good consistency) were obtained in brazing with the Cu–Ti filler metal by using both radiation heating ($\sigma_t$ = 353 MPa, Table 2) and flowing current ($\sigma_t$ = 377–387 MPa). The fracture had a fine-grained pit-like structure, the size of facets being relatively small and not in excess of 10 μm. The content of aluminium in the seam was no more than 1 wt.%.

Preliminary heat treatment of the base metal in case of radiation heating made it possible to increase tensile strength of the joints from 353 to 397 MPa, this being 81 % of strength of the base metal in the as-received state, and 92 % — after preliminary heat treatment. At the same time, brittle fracture of the transcrystalline type occurred at a maximal strength (Figure 4, *e*, *f*).

Advantages of this filler metal can be more clearly demonstrated by the diagrams that show the average results of tensile mechanical tests of the base metal, as well as of the brazed joints produced with different filler metals (Figure 5, *a*–*c*).

It should be noted that preliminary heat treatment in brazing (with radiation heating) leads to increase of elongation (Figure 5, *d*) in case of using the Cu–Ti filler metal. Short-time tensile strength $\sigma_t$ of the brazed joints is no more than proof yield stress $\sigma_{0.2}$ of the non-annealed base metal, and the values of elongation $\sigma_{0.2}$ are more than two times lower than the corresponding value for the base metal (Figure 5, *d*). The value of conditional elasticity limit decreases but insignificantly.

Heat in brazing with the flowing current is released mostly within the zone of the mating surfaces, this being proved by comparison of the character of distribution of residual elongation $\delta_{2.5}$ in the annealed butt joints produced with the Cu–Ti filler metal (Figure 6, *c*, *d*).

Tensile strength of the brazed joints produced with the Cu–Ti filler metal in case of resistance heating is sufficiently stable (3.76.6–387.1 MPa), but lower than in brazing using radiation heating by about 10 MPa. Radiation heating, which has a favourable effect on structuring of the brazed seams [3] and, hence, mechanical properties of the brazed joints, is more preferable for this filler metal.

## CONCLUSIONS

1. Strength of the brazed joints produced on dispersion-strengthened copper alloy Glidcop Al-25 by vacuum brazing with filler metals of the Ti–Zr–Ni–Cu–V–Be and Ti–Zr–Ni–Cu systems is at a low level, and does not exceed 310 and 137 MPa, respectively.

2. The use of the Cu–Ti filler metal (with radiation heating) combined with preliminary heat treatment of the base metal provides high tensile strength of the brazed joints, constituting 81–92 % of strength of the base metal. Resistance heating allows a considerable reduction of the brazing time (6–7 times) compared to radiation heating. However, in this case the brazed joints have a lower strength, which is 78–89 % of that of the base metal.

1. Kuznetsov, O.A., Pogalov, A.I. (1987) *Strength of brazed joints*. Moscow: Mashinostroenie.
2. (2003) *Reference book on brazing*. Ed. by I.E. Petrunin. Moscow: Mashinostroenie.
3. Maksymova, S.V., Khorunov, V.F. (2009) Structural peculiarities of brazed joints on dispersion-strengthened copper. *Zbirka Nauk. Prats NUK*, 428(**6**), 90–99.
4. Maksymova, S.V., Khorunov, V.F., Shonin, V.A. et al. (2002) Vacuum brazing of dispersion-strengthened copper alloy Glidcop Al-25. *The Paton Welding J.*, **10**, 13–17.

# THERMAL-BARRIER MULTILAYER PLASMA COATINGS $ZrO_2$–NiCrAlY

**A.L. BORISOVA, A.Yu. TUNIK, L.I. ADEEVA, A.V. GRISHCHENKO, T.V. TSYMBALISTAYA** and **M.V. KOLOMYTSEV**
E.O. Paton Electric Welding Institute, NASU, Kiev, Ukraine

Comparative characteristics of multilayer plasma coatings $ZrO_2$–NiCrAlY are given. It is established that phase composition of the external ceramic layer depends on thickness of the metallic interlayer, i.e. its thermal conductivity that affects the rate of cooling of the $ZrO_2$ particles deposited on it. Thickness of the metallic interlayer should not exceed 100 μm to ensure optimal heat resistance of the ceramic layer.

***Keywords:*** *zirconia, alloy NiCrAlY, powders, plasma spraying, multilayer coatings, phase composition, structure, heat resistance of coatings*

Many pressing problems of modern engineering, one of the most important among which is improving the efficiency and quality of power machines, can be successfully solved by applying thermal barrier coatings (TBC). The world-wide experience of using TBCs on parts of internal combustion engines allows optimising working conditions of the engines, increasing their efficiency, reducing consumption of fuel and lubricants, decreasing toxicity of exhaust gases, etc. Plasma coatings with an external ceramic layer of partially stabilised zirconia and metallic interlayer of NiCrAlY are recognised to be the most suitable TBCs for internal combustion engines [1]. Heat resistance and service life of coatings based on $ZrO_2$, which is characterised by polymorphic transformations and substantial volume changes taking place in heating and cooling, depend to a considerable degree upon the phase composition of the thermal barrier layer formed during spraying.

The optimal phase composition of the external ceramic layer is considered to be the maximal content of the so-called tetragonal T′-phase with a low degree of tetragonality, providing high heat resistance, as well as the presence of an insignificant (4–5 wt.%) content of the monoclinic phase. Martensitic transformation of the latter leads to formation of a network of fine cracks in the coating, thus preventing its fracture [2–5]. The T′-phase is structurally identical to the tetragonal T-phase, but it differs in an increased content of $Y_2O_3$ dissolved in it, this leading to growth of the volume of a tetragonal phase cell and simultaneous decrease of the degree of tetragonality down to one, i.e. to transformation into a structure of cubic modification.

Many issues related to formation of the optimal phase composition of the external ceramic layer of TBC (chemical composition and fraction of a spraying powder, technological parameters of the spraying process, coating thickness, etc.) are studied in sufficient detail. However, this process can also be affected by such unstudied factors as conditions of cooling of particles of the sprayed ceramic layer, including those that also depend upon the thickness of the metallic interlayer.

One of the ways of improving heat resistance of TBC is to form graded coatings, the composition of which gradually changes from the metallic interlayer to the external ceramic layer [6–8]. It is thought that transition cermet layers deteriorate thermal fatigue properties of the coatings at a temperature above 1170–1220 K, which is caused by intensive oxidation of the metallic component of a transition layer [3]. This leads to initiation of extra compressive stresses within the coating and premature exfoliation of the ceramic layer.

The purpose of this study was to address two problems: investigation of the effect of thickness of the metallic NiCrAlY layer on phase composition of the external ceramic $ZrO_2$ layer to determine its optimal value, and evaluation of peculiarities of formation and structure of multilayer coatings $ZrO_2$–NiCrAlY, involving comparative tests of aluminium parts of internal combustion engines with such coatings to heat resistance under thermal cycling conditions.

The $ZrO_2$ powder stabilised by 6.2 wt.% $Y_2O_3$ was used as a material for deposition of the external ceramic layer of TBC, and the NiCrAlY powder of alloy PKh16N77Yu6I produced by the calcium reduction method was used as a material of the metallic interlayer. Its chemical composition was as follows, wt.%: 73.64–75.44 Ni, 17.02–17.58 Cr, 5.78–5.86 Al, 0.88–1.07 Y, and 0.87–1.85 Ca.

Mixtures of the powders for deposition of multilayer coatings were prepared in air in the laboratory attritor at a minimal rotation speed of the impeller equal to 400 rpm for 30 min. The powder mixtures had the following chemical composition: $(100 - n)$NiCrAlY + $n$$ZrO_2$, where $n$ = 0, 50 and 100 (for three-layer coatings), or 0, 25, 50, 75 and 100 wt.% (for five-layer coatings).

The plasma coatings were deposited by using machine UPU-8M. Steel samples were used as a coating

**Table 1.** Spraying parameters for plasma coatings*

| Composition of spraying powder, wt.% | Fraction, μm | $U$, V | Plasma gas | | Spraying distance, mm |
|---|---|---|---|---|---|
| | | | Composition | Flow rate, l/min | |
| NiCrAlY | −100 − +40 | 40 | Ar + $N_2$ | 24 | 130 |
| $25ZrO_2$ + 75NiCrAlY | −60 − +40 | 40 | Ar + $N_2$ | 26 | 130 |
| $50ZrO_2$ + 50NiCrAlY | | 50 | Ar + $N_2$ | 28 | 120 |
| $75ZrO_2$ + 25NiCrAlY | | 55 | $N_2$ | 30 | 120 |
| $ZrO_2$ | | 60 | $N_2$ | 31 | 100 |

*Spraying current $I$ = 500 A.

substrate, and aluminium alloy samples were used to study heat-protecting properties. The deposition parameters were adjusted depending on the composition of a spraying material (Table 1).

Investigation of the powders and coatings was carried out by metallography using microscope «Neophot-32» with an attachment for digital photography, scanning electron microscopy (electron microscope JSM-840), durometric analysis (LECO hardness meter M-400 under a load of 0.25 N), and X-ray diffraction phase analysis (diffractometer DRON-UM1, Cu$K_\alpha$ radiation). Data of the diffractometry experiment were processed by using software PowerCell 2.4 for full-profile analysis of X-ray spectra of a mixture of polycrystalline phase components.

Heat-protective properties of the coatings were investigated by subjecting their surfaces to direct heating with a gas torch jet flame, and the $C_3H_8$ + $O_2$ gas mixture with a volume ratio of 1:3 was used as a fuel mixture. The torch was placed at a distance of 35–40 mm from the surface of a coated sample. The samples were heated for 3 s to a temperature of 400 °C and cooled with air flow approximately for 20 s, and then with water approximately for 6 s to a temperature of 70–80 °C. The temperature of the samples was determined by using digital multimeter UT-70B. Thermal cycling was carried out up to violation of integrity of a coating or its separation from the substrate to no more than 15 %.

**Characteristics of initial powders.** The $ZrO_2$ powder stabilised with 6.2 wt.% $Y_2O_3$ (Figure 1, *a, b*) consisted of particles of an irregular fragmented shape with sharp edges, 40–60 μm in size. According to the results of X-ray diffraction phase analysis, it contained 89.8 wt.% of the tetragonal phase (T-$ZrO_2$) and 10.2 wt.% of the monoclinic (M-$ZrO_2$) phase (Figure 1, *c*).

The powder of alloy NiCrAlY consisted of irregular particles in the form of conglomerates with a size of 40–100 μm (Figure 1, *d, e*). According to the data of X-ray diffraction phase analysis, it contained the following phases: γ-nickel solid solution and γ′-$Ni_3Al$ in-

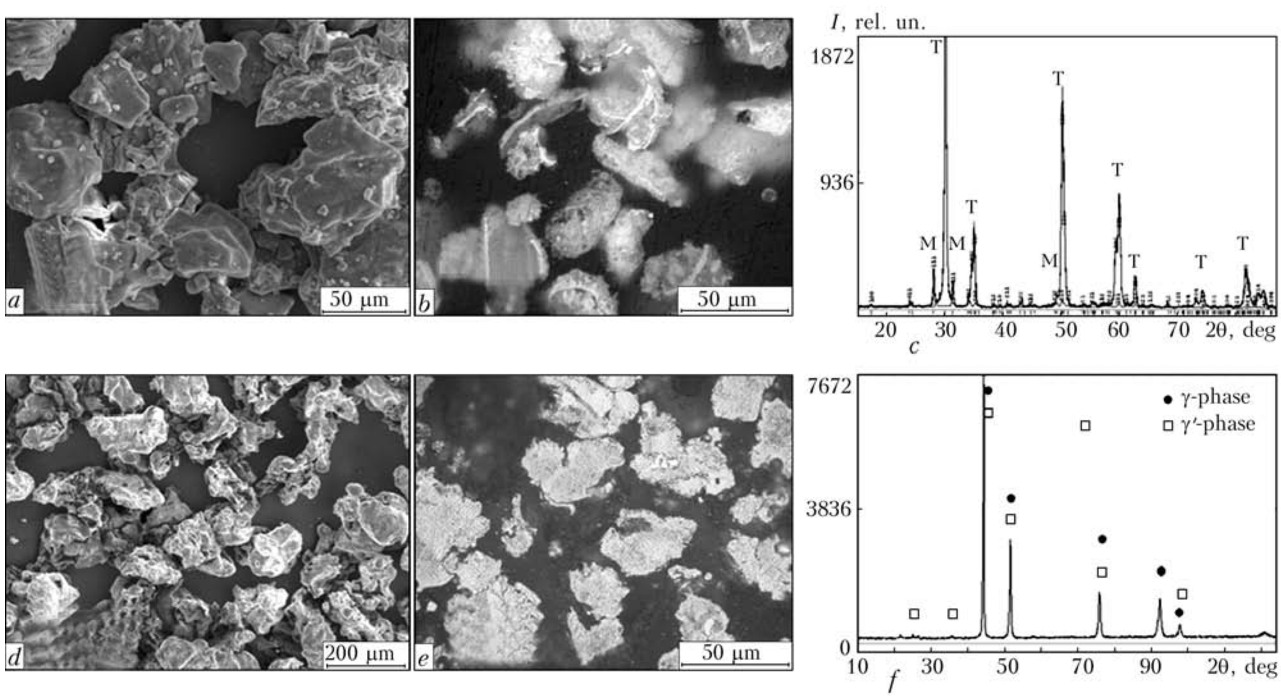


**Figure 1.** Appearance (*a, d*), microstructure (*b, e*) and X-ray patterns (*c, f*) of powders $ZrO_2$ + 6.2 wt.% $Y_2O_3$ (*a–c*) and NiCrAlY (*d–f*)

**Table 2.** Characteristics of two-layer $ZrO_2$–NiCrAlY coatings with different thickness of metallic interlayer

| Thickness of metallic interlayer, μm | | Phase composition of ceramic layer | *HV*, MPa | |
|---|---|---|---|---|
| NiCrAlY | $ZrO_2$ | | NiCrAlY | $ZrO_2$ |
| ~50 | 200–230 | T-$ZrO_2$, traces of M-$ZrO_2$ | 2630 ± 540 | 11,990 ± 1420 |
| ~100 | 200–250 | T-$ZrO_2$, traces of M-$ZrO_2$ | 3110 ± 560 | 11,230 ± 2130 |
| ~150 | 200–210 | T-$ZrO_2$, C-$ZrO_2$ (12 wt.%), traces of M-$ZrO_2$ | 3130 ± 500 | 11,020 ± 1110 |

*Note*. C — cubic modification of $ZrO_2$.

termetallic (Figure 1, *f*). Structure of the particles was a nickel-based solid solution (γ-phase) reinforced with dispersed particles of $Ni_3Al$ (γ′-phase).

**Two-layer plasma coatings.** Investigation of the effect of thickness of the NiCrAlY interlayer on phase composition and properties of the ceramic layer of TBC showed that thickness of the ceramic layer was approximately identical in all the samples and equal to about 200 μm, while thickness of the metallic interlayer varied from 50 to 150 μm. Characteristics of the two-layer $ZrO_2$–NiCrAlY coatings are given in Table 2.

It was found that in all the cases the formed two-layer coating was dense, having no cracks and delaminations at both interfaces between the ceramics and interlayer and between the binding layer and substrate (Figure 2). The metallic interlayer had a clearly defined lamellar structure with thin oxide intermediate layers along the lamellar boundaries. Microhardness of the interlayer grew from 2630 to 3130 MPa with

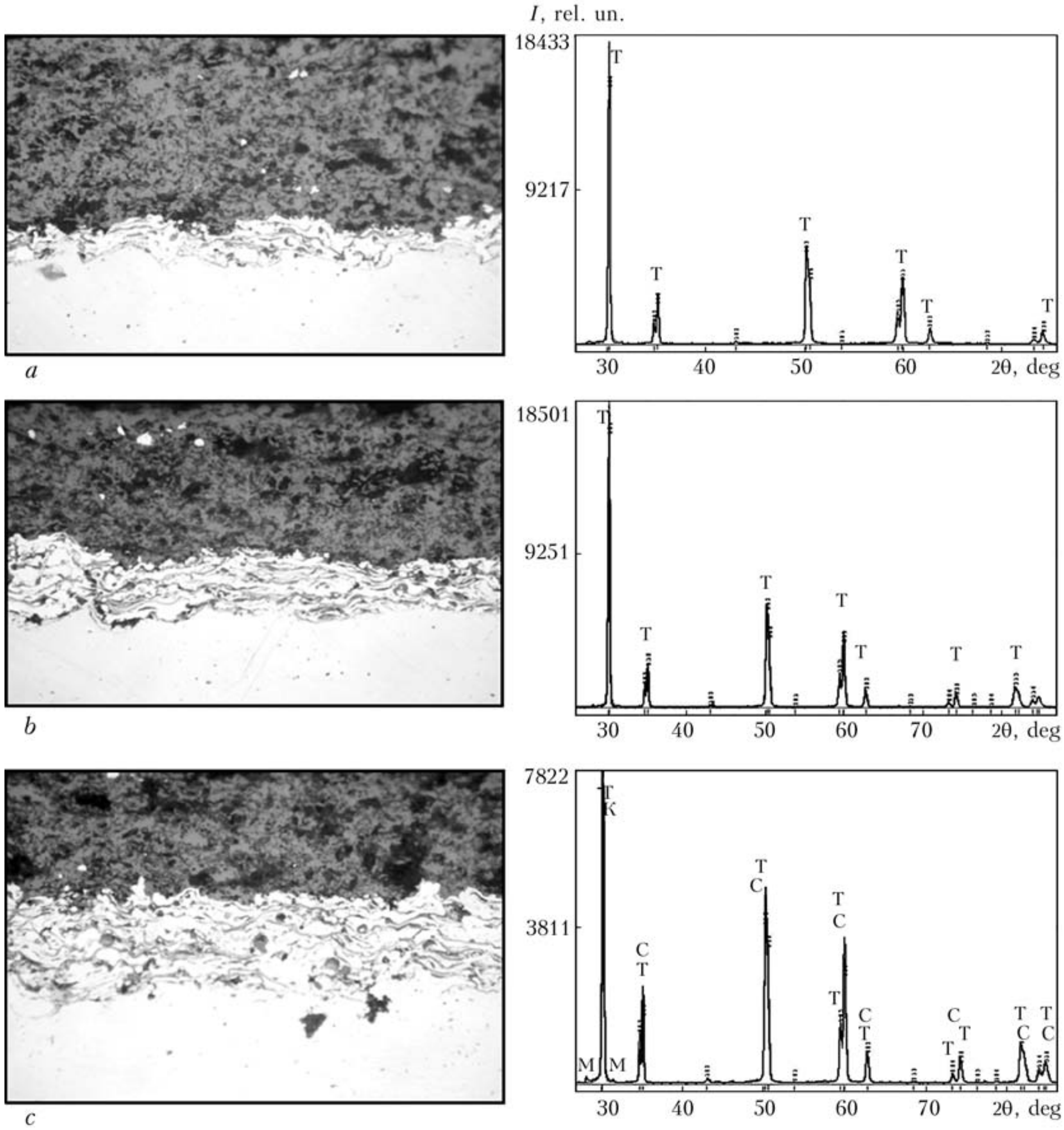


**Figure 2.** Microstructure (×200) (*left*) and X-ray patterns (*right*) of two-layer plasma coatings with metallic interlayer 50 (*a*), 100 (*b*) and 150 (*c*) μm thick

**Table 3.** Effect of thickness of metallic interlayer on phase composition and crystalline lattice parameters (*a, c, b*) of phases of $ZrO_2$ ceramic layer

| Investigation object | Thickness of NiCrAlY interlayer, μm | Phase composition of ceramic layer | | | | | | | |
|---|---|---|---|---|---|---|---|---|---|
| | | T-$ZrO_2$ | | | | M-$ZrO_2$ | | | |
| | | *a*, nm | *c*, nm | *c/a* | $V\cdot10^3$, $nm^3$ | *a*, nm | *b*, nm | *c*, nm | β, deg |
| Powder $ZrO_2$ | – | 0.51047 | 0.51672 | 1.0122 | 134.6469 | 0.51439 | 0.52081 | 0.53230 | 99.16 |
| Powder $ZrO_2^*$ | 50 | 0.51078 | 0.51623 | 1.0107 | 134.6823 | 0.51460 | 0.52120 | 0.53130 | 99.20 |
| | 100 | 0.51079 | 0.51629 | 1.0108 | 134.7030 | 0.51668 | 0.52044 | 0.53237 | 99.20 |
| | 150 | 0.51054 | 0.51632 | 1.0113 | 134.5793 | 0.51713 | 0.52714 | 0.52771 | 99.20 |

*$a$ = 0.51147 nm for C-$ZrO_2$ modification.

increase in its thickness (see Table 2). According to the data of X-ray diffraction phase analysis, phase composition of the interlayer was as follows: nickel-based solid solution, γ′-$Ni_3Al$, β-NiAl, and solid solution of nickel in chromium α-Cr. Unlike the composition of the spraying powder, new phases β-NiAl, NiO and α-Cr appeared in the coating, which formed as a result of flowing of the particles through the plasma jet.

The ceramic layer of all the coatings had no lamellar structure, and microhardness of the coatings was approximately the same (about *HV* 11,000 MPa). Thickness of the metallic interlayer had almost no effect on structure and microhardness of the $ZrO_2$ layer. However, it changed its phase composition. With a coating deposited on the metallic interlayer 50 and 100 μm thick, the main phase of the ceramic layer was the tetragonal phase, while the weight content of the monoclinic phase decreased to 2 % compared with the initial powder, where its content was 10.2 wt.%. In the case of the 150 μm thick interlayer, the ceramic layer also contained about 12 wt.% of cubic modification of $ZrO_2$, in addition to the above phases (see Figure 2). At a depth of 100 μm from the surface, phase composition of the ceramic layer of all the coatings was practically identical. It was a mixture of the tetragonal phase with 4 wt.% of the monoclinic phase.

Evaluation of the degree of tetragonality and volume of an elementary cell of the tetragonal $ZrO_2$ phase showed that at an interlayer thickness of 150 μm the degree of tetragonality of $ZrO_2$, $c/a$, was 1.0113, and volume of the elementary cell was $V = 134.5793\cdot10^{-3}$ $nm^3$. At an interlayer thickness of 50 and 100 μm, the phase formed had a lower degree of tetragonality ($c/a$ = = 1.0107 and 1.0108) and an increased volume of the elementary cell, $V = 134.6823\cdot10^{-3}$ and $134.7030\cdot10^{-3}$ $nm^3$, respectively (Table 3). These phases are close in their structure to the T′-$ZrO_2$ quench phase, which, according to literature data [9], is characterised by resistance to both low and high temperatures, and by an increased stability at cyclic temperature changes. Therefore, the preferable thickness of the NiCrAlY interlayer is no more than 100 μm.

**Multilayer coatings.** Spraying of multilayer coatings was preceded by making and investigation of samples with one-layer coatings of powder mixtures with 25, 50 and 75 wt.% $ZrO_2$.

It was found that all the coatings of the powder mixtures were uniform in thickness, had no cracks, and tightly adhered to the substrate (Figure 3). Increasing the NiCrAlY content of the spraying powder was accompanied by growth of the quantity of metallic particles with a round or lamellar shape in the structure. The coating with a minimal content of the ceramic component (25 wt.%) was characterised by the highest lamellar content (see Figure 3, *c*). Microhardness of the coatings dramatically grew with increase of the zirconia content of the layer: *HV* 4760 ± 1810, 5150 ± 1190 and 7310 ± 2250 MPa at 25, 50 and 75 wt.% $ZrO_2$ (Table 4). According to the data of X-ray diffraction phase analysis, the composition of the cermet layers was almost constant and included different combinations of phases: γ-nickel-based solid solution, γ′-$Ni_3Al$, T-$ZrO_2$, M-$ZrO_2$, NiO and α-Cr

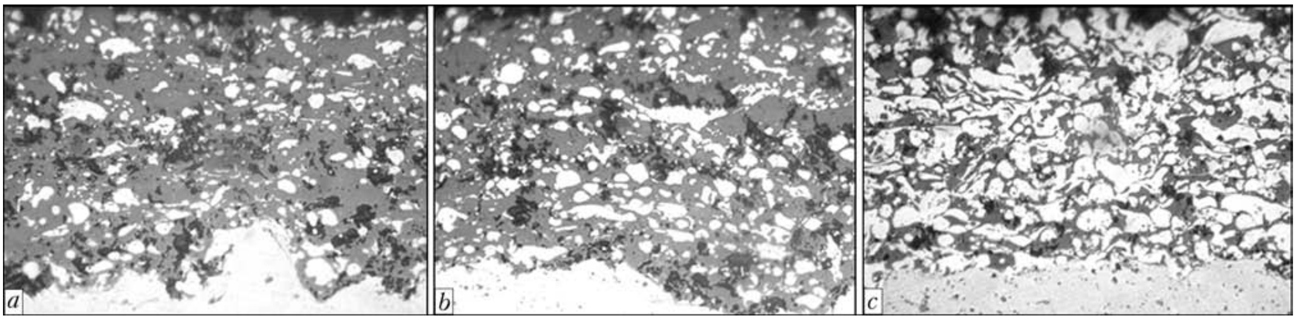


**Figure 3.** Microstructure (×400) of plasma coatings produced from different powder mixtures, wt.%: *a* — $75ZrO_2$ + 25NiCrAlY; *b* — $50ZrO_2$ + 50NiCrAlY; *c* — $25ZrO_2$ + 75NiCrAlY

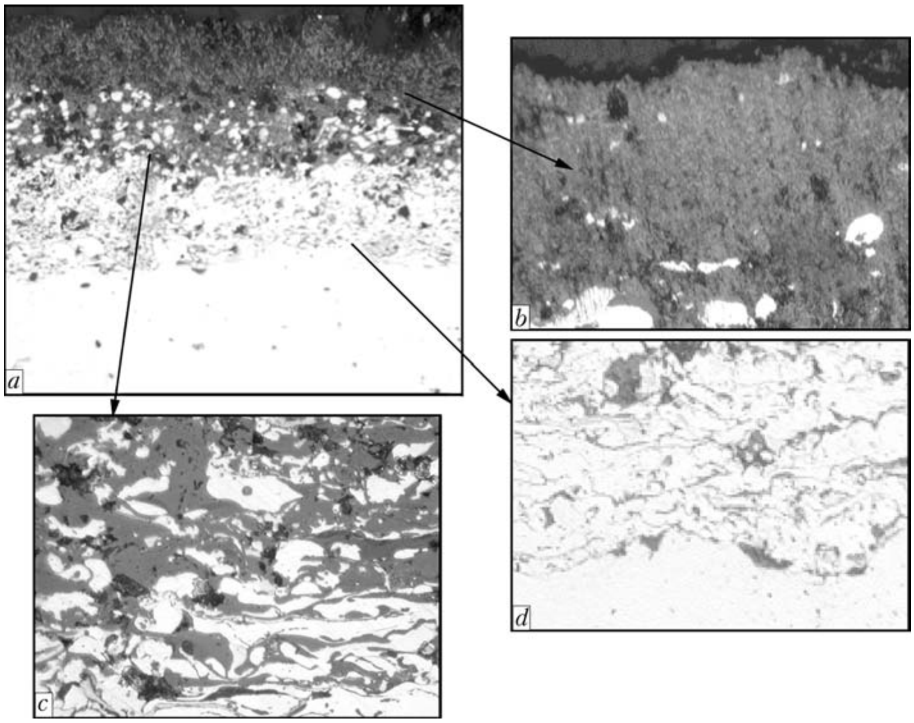

**Figure 4.** Microstructure of three-layer plasma coating: *a* — general view (×200); *b* — external $ZrO_2$ layer; *c* — intermediate layer, 50 wt.% NiCrAlY + 50 wt.% $ZrO_2$; *d* — internal NiCrAlY layer (*b*–*d* — ×500)

(see Table 4). In contrast to the initial powders, two new phases β-NiAl and NiO, as well as α-Cr, formed as a result of thermal and physical-chemical interaction of the spraying material with the plasma jet.

Structure, phase composition and microhardness of intermediate cermet layers of the three- (Figure 4) and five-layer (Figure 5) coatings almost coincided with corresponding characteristics of the coatings from mechanical mixtures of the same composition (see Figure 3, Table 4). Evaluation of the degree of tetragonality of the protective layer of the three- and five-layer coatings showed that it was 1.0103 and 1.0108, respectively. Therefore, in this case the tetragonal phase was also close to the T′-$ZrO_2$ quench phase.

When tested to heat resistance, the samples with the two- and five-layer coatings (Table 5) withstood 1500 thermal cycles, exhibiting no external changes. The traces of fracture on the surfaces of both two- and multilayer coatings formed not earlier than after 2000 thermal cycles.

Microhardness of the two-layer $ZrO_2$–NiCrAlY coating (with total thickness of about 570 μm), having a lamellar structure of the nickel interlayer and a layer of $ZrO_2$ formed from the round particles (Figure 6, *a*), hardly changed (see Table 5, variant 1) compared with the initial state (see Table 2). After 2000 thermal cycles of the tests, a longitudinal crack propagating into the $ZrO_2$ layer initiated within the zone of interface with the interlayer. Moreover, the surface layer of the $ZrO_2$ coating exhibited a negligible fracture (Figure 6, *b*). Only two phases, i.e. the tetragonal $ZrO_2$ phase (dominant) and an insignificant amount of the monoclinic $ZrO_2$ phase (about 1 wt.%), were fixed in the X-ray pattern, this corresponding to phase composition of the surface layer of the coating before the tests (see Table 2).

Multilayer coatings of the $ZrO_2$–NiCrAlY system, approximately 500 μm thick, had no cracks, delaminations and exfoliations from the substrate after the tests. However, the surface ceramic layer exhibited a heavy fracture (Figure 6, *c, d*). The X-ray pattern in Figure 7 shows, in addition to the two zirconia phases (tetragonal and monoclinic), also the presence of phases γ′-$Ni_3Al$ and β-NiAl, oxides NiO, as well as α-$Al_2O_3$, which is a product of oxidation of NiCrAlY, this being indicative of violation of integrity of the external layer after 2000 thermal cycles. Microhardness of the multilayer coating, which grew in the initial sample with increase in the content of the ce-

**Table 4.** Characteristics of plasma coatings produced from NiCrAlY and $ZrO_2$ powders and their mixtures

| Powder composition, wt.% | Coating thickness, μm | Phase composition | *HV*, MPa |
|---|---|---|---|
| 100NiCrAlY | 90 ± 15 | γ-Ni, γ′-$Ni_3Al$, β-NiAl, α-Cr | 3110 ± 560 |
| 25$ZrO_2$ + 75NiCrAlY | 100 ± 20 | γ-Ni, T-$ZrO_2$, γ′-$Ni_3Al$, β-NiAl, NiO, α-Cr, M-$ZrO_2$ | 4760 ± 1810 |
| 50$ZrO_2$ + 50NiCrAlY | 90 ± 20 | γ-Ni, T-$ZrO_2$, γ′-$Ni_3Al$, β-NiAl, NiO, M-$ZrO_2$, α-Cr | 5150 ± 1190 |
| 75$ZrO_2$ + 25NiCrAlY | 100 ± 20 | T-$ZrO_2$, γ-Ni, γ′-$Ni_3Al$, β-NiAl, NiO, M-$ZrO_2$, α-Cr | 7310 ± 2250 |
| 100$ZrO_2$ | 200 ± 20 | T-$ZrO_2$, M-$ZrO_2$ (traces) | 11,450 ± 1350 |

**Table 5.** Characteristics of TBC after heat resistance tests*

| Variant No. | Composition of spraying powder (layer-by-layer), wt.% | Thickness of layers, μm | $HV$, MPa | Fracture region |
|---|---|---|---|---|
| 1 | 100NiCrAlY | 120 | 2950 ± 500 | Longitudinal crack in $ZrO_2$ layer within the interlayer interface zone |
| | $100ZrO_2$ | 450 | 11,000 ± 1200 | |
| 2 | 100NiCrAlY | 100 | 2820 ± 560 | Fracture to 75 % of $ZrO_2$ layer; underlying layers are crack- and exfoliation-free |
| | $25ZrO_2$ + 75NiCrAlY | 80 | 4630 ± 590 | |
| | $50ZrO_2$ + 50NiCrAlY | 120 | 5030 ± 860 | |
| | $75ZrO_2$ + 25NiCrAlY | 100 | 6850 ± 1000 | |
| | 100 $ZrO_2$ | 100 | 9560 ± 1100 | |

*Quantity of thermal cycles to fracture was 2000.

ramic component from the interlayer to the $ZrO_2$ layer (see Table 4), hardly changed in value (see Table 5, variant 2).

A thermocouple was calked on the opposite side of a sample to a depth of 2 mm to reveal dynamics of heating of the coatings. It fixed growth of temperature of the uncoated substrate, as well as of the two- and five-layer coatings. Up to 10 heating and cooling cycles were carried out. Analysis of cyclograms of the samples showed that maximal heating temperature of the samples with TBC decreased from 415 (without coating) to 365 and 345 °C (for two- and five-layer coatings, respectively).

Therefore, phase composition of the external ceramic layer (content of the monoclinic $ZrO_2$ phase and tetragonal T′-phase with a low degree of tetragonality) depends upon the thickness of the metallic interlayer. Thickness of the metallic interlayer

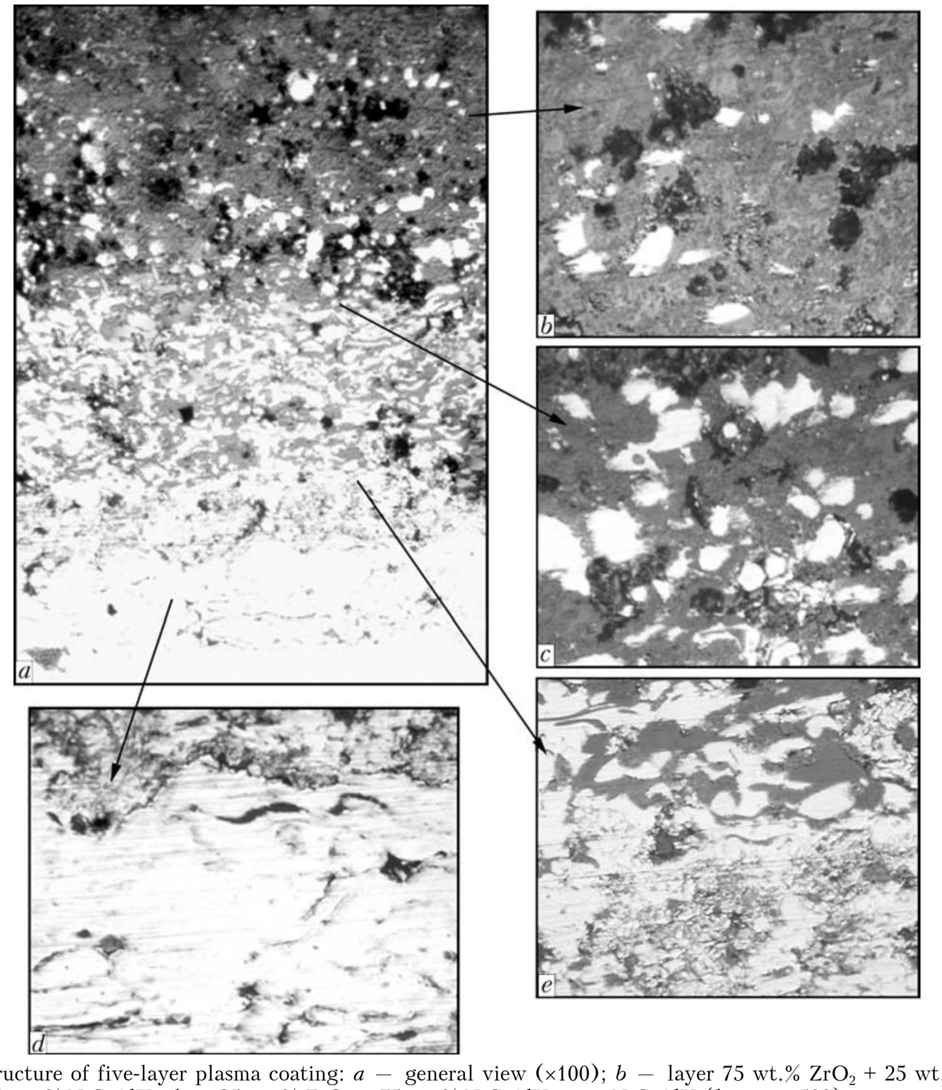


**Figure 5.** Microstructure of five-layer plasma coating: *a* — general view (×100); *b* — layer 75 wt.% $ZrO_2$ + 25 wt.% NiCrAlY; *c* — 50 wt.% $ZrO_2$ + 50 wt.% NiCrAlY; *d* — 25 wt.% $ZrO_2$ + 75 wt.% NiCrAlY; *e* — NiCrAlY (*b*–*e* — ×500)

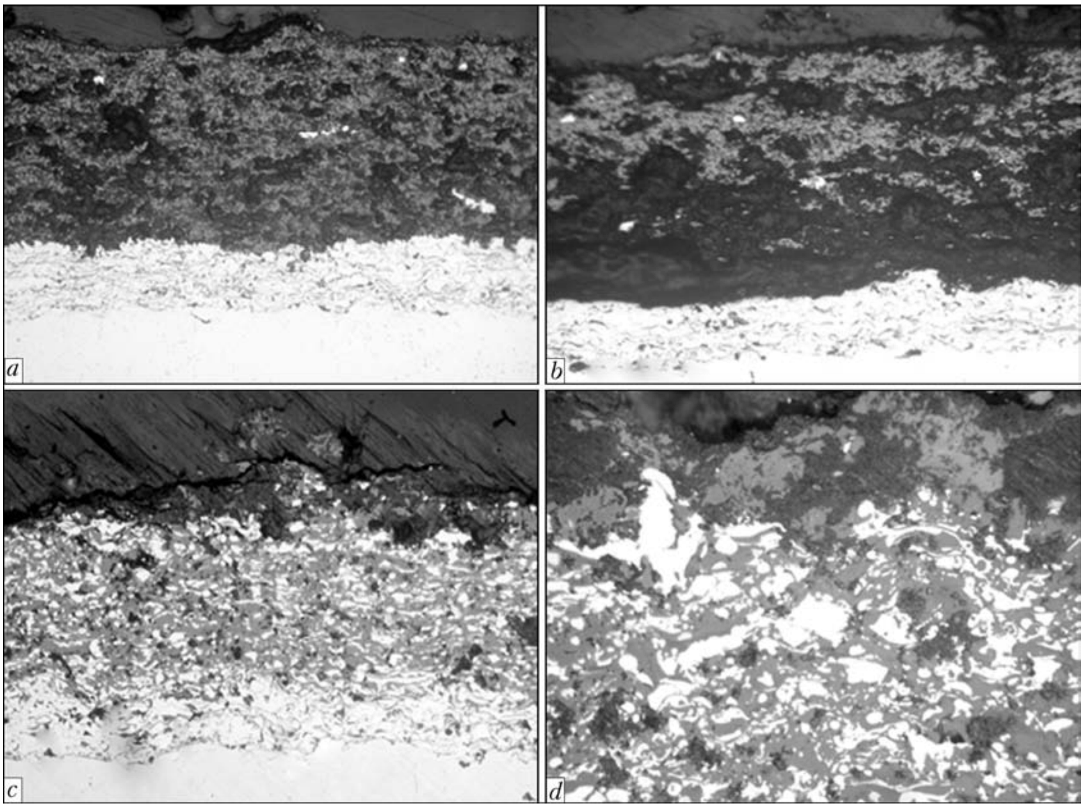


**Figure 6.** Microstructure of two- (×200) (*a, b* — see the text) and five-layer (*c* — ×100; *d* — ×400) coatings $ZrO_2$–NiCrAlY after heat resistance tests

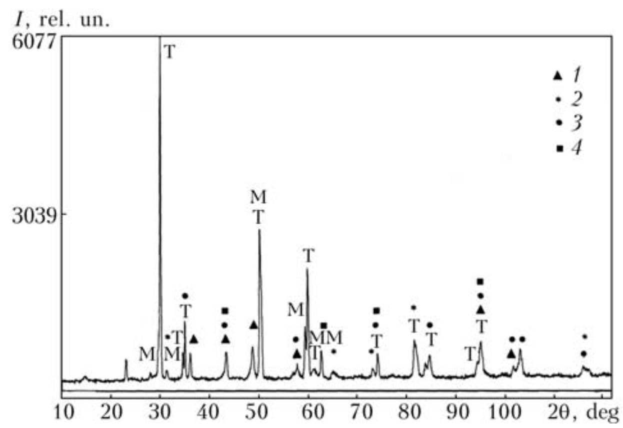


**Figure 7.** X-ray pattern of multilayer $ZrO_2$–NiCrAlY coating after heat resistance tests: *1* — $\gamma'$-$Ni_3Al$; *2* — β-NiAl; *3* — $\alpha$-$Al_2O_3$; *4* — NiO

should not exceed 100 μm to provide the optimal phase composition of the ceramic layer, i.e. the monoclinic phase content of no more than 4 wt.% and maximal content of the T′-phase, which is responsible for heat resistance under thermal cycling conditions.

It was established as a result of investigation of three- and five-layer coatings produced by using heat-resistant alloy–ceramics mechanical mixtures that their phase composition, microhardness and structure gradually changed in a direction from the substrate to external ceramic layer. Metallographic analysis revealed no cracks, exfoliations from the substrate and delaminations in the coatings.

The thermal barrier coatings withstood not less than 2000 thermal cycles in investigation of heat resistance of the two- and five-layer metal–ceramic coatings under thermal cycling conditions (heating with a gas flame jet to 400 °C for 3 s with subsequent cooling to 20 °C). Analysis of cyclograms of samples with the two- and five-layer coatings showed that these coatings allow decreasing temperature of the aluminium substrate by 50 and 70 °C, respectively.

1. Nikitin, M.D., Kuliya, A.Ya., Zakharov, N.I. (1977) *Thermal-barrier and wear-resistant coatings on engine parts*. Leningrad: Mashinostroenie.
2. Iliushenko, A.F., Okovity, V.A., Kundas, S.P. et al. (2002) *Formation of thermal coatings: theory and practice*. Ed. by A.F. Iliushenko. Minsk: NIIPMeOP.
3. Iliushenko, A.F., Ivashko, V.S., Okovity, V.A. et al. (1998) *Thermal-barrier $ZrO_2$-base coatings*. Minsk: NIIPMeOP.
4. Rutman, D.S., Toropov, Yu.S., Pliner, S.Yu. et al. (1985) *High-refractory zirconia materials*. Moscow: Metallurgiya.
5. Pliner, S.Yu., Dabizha, A.A. (1987) Hardening of zirconia ceramics through tetragonal-monoclinic transformations. *Ogneupory*, **3**, 58–62.
6. Khor, K.A., Gu, Y.W. (1997) Plasma spraying of functionally graded NiCrAlY/yttria stabilized zirconia coating using pre-alloyed powders. In: *Proc. of United Forum for Sci. and Technol. Advances on Thermal Spray* (Ohio, USA). Ohio: ASM Int., Materials Park, 259–265.
7. (1995) *Superalloys: Heat-resistant materials for aerospace and industrial power units*. Ed. by Ch.T. Sims, N.S. Stoloff, U.K. Hagel. Book 2. Ed. by R.E. Shalin. Moscow: Metallurgiya.
8. Frolov, Z.A., Poklad, V.A., Ryabenko, B.V. et al. (2004) Technological peculiarities of deposition of thermal-barrier coatings in production of gas turbine blades. *Svarochn. Proizvodstvo*, **11**, 39–41.
9. Kolomytsev, P.T. (1991) *High-temperature protective coatings for nickel alloys*. Moscow: Metallurgiya.

# PROSPECTS OF APPLICATION OF LASER AND HYBRID TECHNOLOGIES OF WELDING STEELS TO INCREASE SERVICE LIFE OF PIPELINES

**V.D. SHELYAGIN, V.Yu. KHASKIN, A.V. BERNATSKY** and **A.V. SIORA**
E.O. Paton Electric Welding Institute, NASU, Kiev, Ukraine

The experiments on development of techniques of multipass hybrid laser and laser-arc welding of pipe steels are described. Structure of produced joints, as well as their impact toughness and corrosion resistance were investigated. Rationality of further developments of appropriate technological processes for application of mentioned methods of welding to extend the service life of pipeline transport is shown.

***Keywords:*** *multipass laser welding, hybrid laser-arc welding, impact toughness, corrosion resistance*

The growth of service life of main pipelines is directly connected with further increase of quality of welded joints at high welding efficiency [1, 2]. This is especially actual for large pipeline systems, including intercontinental and transnational, those of high pressure (approximately 10–15 MPa for land and 20–25 MPa for off-shore pipelines). A need in increase of welding quality was stipulated also by application of steels of increased strength (X70, X80 and X100) for pipelines.

One of the ways to solve specified tasks is the application of laser radiation [3]. Owing to small sizes of weld pool and angle of convergence of focused radiation the laser welding enables significant decrease of angle of preparation of edges to be welded. Due to high speed of laser welding the comparatively low input energy allows minimizing heat influence on the parts being welded, and consequently, reducing the size of HAZ and residual deformations. Fine-grain structure of cast metal of weld and HAZ contributes to increase of corrosion resistance of welded joints.

Over the last decade a number of scientific research works was carried out, as a result of which technical solutions allowing use of laser and hybrid laser-arc welding for assembly of main pipelines were appeared. Thus, VITS company (Langenseld, Germany) together with BIAS Research Institute (Bremen, Germany) developed the method of a single-pass welding of position butt welds on main pipelines with thickness of wall $\delta \leq 20$ mm using radiation of powerful (about 20 kW) fiber laser. At the Institute of Welding (Halle, Germany) a machine for two-pass hybrid laser-arc welding of position butt welds on main pipelines was developed and successfully tested. Moreover, the second pass was performed using arc welding, i.e. the laser radiation was used only to form a root weld. The «Fronius» company (Austria) offered a hybrid tandem method of welding steels where two-arc tandem with consumable electrodes is combined with laser radiation located ahead [4].

The investigations of laser and hybrid laser-arc welding of pipe steels are carried out also at the E.O. Paton Electric Welding Institute. The experiments on hybrid laser-arc welding were initially performed in accordance with technological scheme presented in Figure 1 [5], which shows that laser radiation is positioned ahead of welding process, and the arc of consumable electrode is at the tail part. The main task of laser radiation is reaching of required penetration depth, and that of the arc is the formation of upper reinforcement and providing of such thermal cycle of welding at which the undesirable bainite and martensite structures are not formed.

The investigations carried out by the mentioned scheme showed that in a single-pass welding of steels of more than 5 mm thickness the 1.0 kW of arc power can substitute 0.5 kW of laser radiation power. It means that hybrid welding allows decreasing the cost of applied equipment and one running meter of a weld

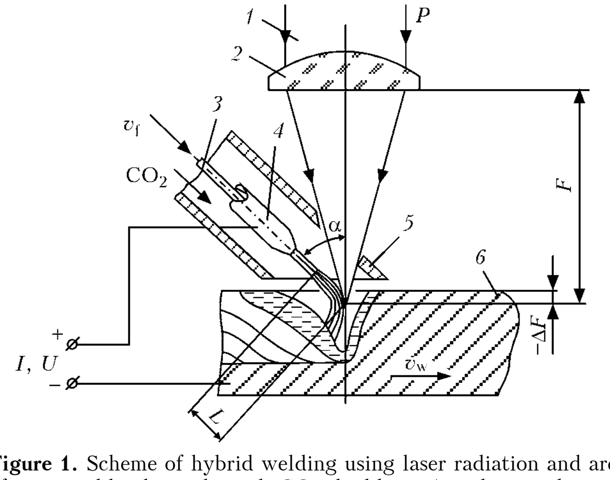


**Figure 1.** Scheme of hybrid welding using laser radiation and arc of consumable electrode with $CO_2$ shielding: *1* — laser radiation of power $P$, kW; *2* — focusing lens with focal distance $F$, mm; *3* — filler wire; *4* — shielding nozzle; *5* — copper current-carrying nozzle; *6* — specimen; $v_w$ — welding speed, m/h; $v_f$ — filler wire feed rate, m/h; $\Delta F$ — embedding of mouth of caustic of radiation relatively to the surface of specimen, mm; α — angle of electrode inclination to the axis of laser beam, deg.; $L$ — length of arc, mm; $I$ — welding current, A; $U$ — arc voltage, V

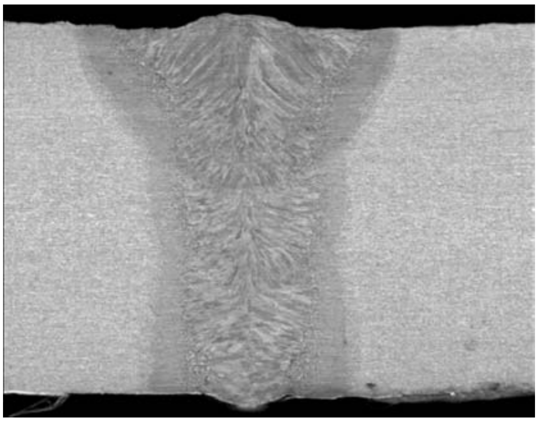

**Figure 2.** Macrosection of butt joint of steel 10G2FB (δ = 19 mm) produced using hybrid welding for 4 passes at the condition: $P$ = = 2.7 kW; $v_w$ = 2.5 m/h; $v_f$ = 400 m/h (diameter of electrode wire of 1.2 mm); $I_w$ = 200 A; $U_a$ = 25 V; shielding gas — $CO_2$, consumption $Q$ = 20 l/min

as compared with a laser welding. However, it was revealed that at the fixed power of laser radiation the maximal depth of penetration is also a fixed parameter, i.e. at decrease of welding speed the value of this parameter stops its growth at a certain moment (the width of a weld grows). In our case at the power of $CO_2$ laser radiation of up to 3 kW and close value of arc power the depth of penetration reaches 10 mm at the speed of welding of 30 m/h. Consequently, in welding of pipe steels of larger thickness it is possible either to increase the power of laser radiation or to use the multipass welding. Both these approaches have disadvantages: the first one needs considerable costs and reduces duration of thermal welding cycle, therefore, facilitates formation of undesirable hardened structures; the use of the second one leads to decrease in efficiency.

We have carried out investigations of multipass laser-arc welding of pipe steels of thickness of up to 20 mm into narrow groove. The examples of macrosections of butt joints produced during experiments are presented in Figures 2–4. Along with the selection of parameters of technological condition the metallographic peculiarities of specimens of butt joints, their corrosion resistance and impact toughness were studied.

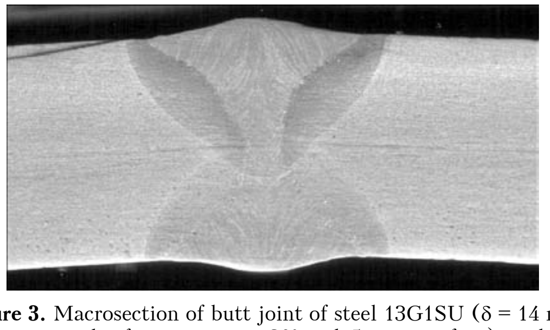

**Figure 3.** Macrosection of butt joint of steel 13G1SU (δ = 14 mm, X-groove, angle of preparation is 30° with 5 mm root face) produced for 2 passes using hybrid welding by arc with consumable electrode Sv-08G2S of 1.2 mm diameter and radiation of Nd:YAG laser at the condition: $P$ = 4.0 kW; $I_w$ = 260 A; $U_a$ = 27 V; $v_w$ = 30 m/h; $v_f$ = 510 m/h; shielding gas — mixture Ar + 18 % $CO_2$, $Q$ = = 14 l/min

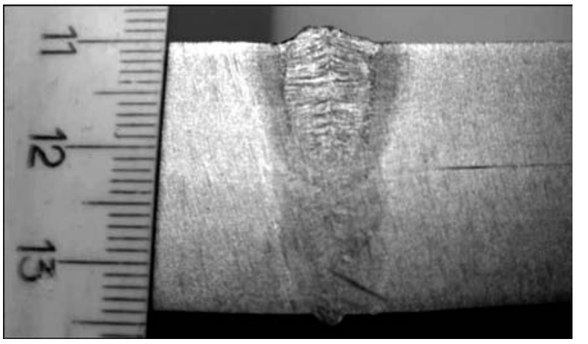


**Figure 4.** Macrosection of butt joint of steel 09G2S (δ = 25 mm) produced by narrow-groove hybrid welding for 6 passes using arc with consumable electrode Sv-08G2S of 1.2 mm diameter and radiation of Nd:YAG laser at the condition: $P$ = 4.4 kW; $I_w$ = 300 A; $U_a$ = 30 V; $v_w$ = 60 m/h; $v_f$ = 700 m/h; shielding gas — $CO_2$, $Q$ = 30 l/min

Except of welding of butts, the task of performance of a root weld using laser and hybrid welding was investigated. It was established that to produce the quality bead of reverse reinforcement of a weld on the side of a groove, the latter should have U-shape or rectangular shape. In case of Y-groove the shrinkage of weld metal occurs, i.e. defective formation of a joint. The task is significantly simplified in welding on the side of root face (opposite groove). To produce quality reverse reinforcement, we offer to perform laser welding in accordance with the scheme shown in Figure 5. In accordance with this scheme the root face of 5–7 mm is welded by radiation of $CO_2$ laser (or laser of another kind) of the power of up to 5 kW without use of a filler wire. Such technological method allows obtaining of reinforcement of the height of about 0.5–1.0 mm due to increase of volume of remelted metal. In this case the structure of weld metal and HAZ is fine-grained and characterized by increased resistance to corrosion, which is an important moment, as far as such weld is produced inside a pipe, i.e. at the place of contact with aggressive environment. Using the offered technological procedure the admissible gap between edges to be welded should not exceed 0.1–0.3 mm.

To evaluate electrochemical heterogeneity of steel 13G1SU welded joints performed using laser, hybrid laser-arc and arc methods of welding, the measurements of distribution of potential of electrochemical corrosion under the drop were carried out. As an electrolyte, the 3 % solution of sodium chloride in water

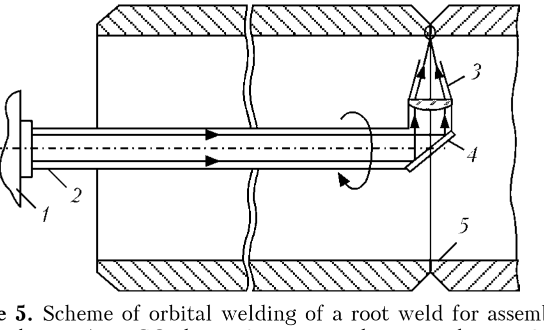


**Figure 5.** Scheme of orbital welding of a root weld for assembly of pipe butts: *1* — $CO_2$ laser; *2* — rotary beam conductor; *3* — laser welding head; *4* — rotary mirror; *5* — position butt joint

Potentials of electrochemical corrosion of butt joints of steel 13G1SU (δ = 14 mm) produced by different welding methods using 1.2 mm diameter wire Sv-08G2S

| Welding method | Potential in base metal $E_{BM}$, V | Potential in weld $E_w$, V | | Potential in HAZ $E_{HAZ}$, V* | | Difference of potentials of base metal–weld $\Delta E$, V |
|---|---|---|---|---|---|---|
| | | Top | Root | Top | Root | |
| Laser | −0.58 | −0.51 | −0.53 | −0.53 | −0.58 | −0.07 |
| Hybrid laser-arc | −0.58 | −0.52 | −0.52 | −0.52 | −0.54 | −0.07 |
| Arc | −0.58 | −0.48 | −0.49 | −0.49 | −0.54 | −0.10 |

*Values of $E_{HAZ}$ for HAZ positioned on the both sides of a weld are the same.

was used. The results of these investigations are given in the Table. It was established that a joint produced using welding arc with consumable electrode is distinguished by a higher heterogeneity. The joints produced using laser and hybrid welding are characterized by lower values of potential of electrochemical corrosion, they are more electrochemically homogeneous. Basing on this fact one can conclude that for the same steels using the same filler (electrode) wire and same gas shielding of weld pool, the laser and hybrid methods of welding are capable to provide higher corrosion resistance as compared with the arc welding.

The measurements of impact toughness *KCV* carried out by the Charpy method on the specimens with a sharp notch at −20 °C gave the following results (Figure 6). In two-pass laser-arc welding the weld metal is characterized by much higher impact toughness as compared with the base metal than in four-pass welding. Unlikely, the HAZ metal in four-pass welding has somewhat higher ductility than in two-pass welding (as compared with base metal). This can be explained by the fact that in four-pass welding each next pass influences the previous one and in two-pass welding performed on both sides of a specimen, such influence is practically excluded. Thus, in four-pass welding the recrystallization of weld metal and normalization of HAZ occurs and in two-pass welding mainly those structures are preserved which were formed initially. It is also proved by results of metallographic investigations. Thus, in four-pass welding in weld metal and HAZ the ferrite-pearlite structures are prevailed (see Figure 2). The similar structures are available in weld metal performed for two passes (see Figure 3). However, in HAZ metal of the latter the areas of upper bainite and martensite are formed that promotes the increase in hardness of these areas above the limiting values (*HB* 260–280).

In HAZ metal the highest hardness is observed in the place of transition of zone of coarse grain to the zone of fine grain (Figure 7), being the most critical to impact and cyclic loadings. Therefore, the specimens for measuring impact toughness, the values of which are given in Figure 6, were tried to be made so that the sharp notch was at this zone. The obtained results prove that, in spite of the sufficiently high values of impact toughness, the further investigations, directed to decrease of HAZ hardness in laser-arc welding, are required. However it should be taken into account that using this method of welding, as well as laser welding, there is a risk of formation of hardened structures in HAZ metal and in cast weld metal. Nowadays, the question on whether such structures are admissible (in connection with their fine dispersity and ductility) or they should be removed by post heat

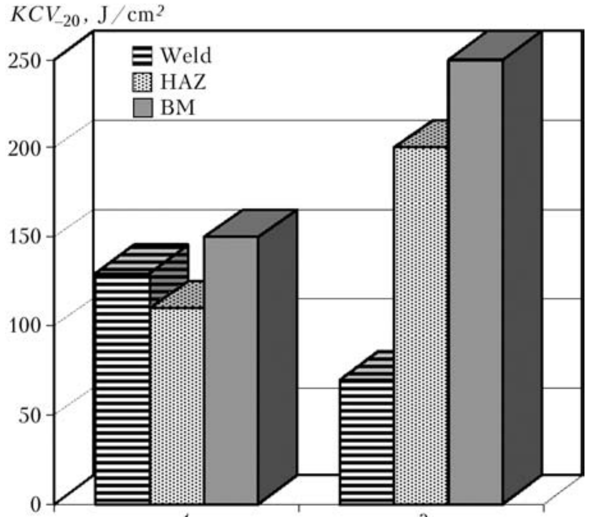


**Figure 6.** Results of measurement of impact toughness $KCV_{-20}$ of weld and HAZ metal of specimens of steel 13G1SU (δ = 14 mm) produced using hybrid method of welding for 2 passes (*1*) and of steel 10G2FB (δ = 19 mm) produced for 4 passes (*2*)

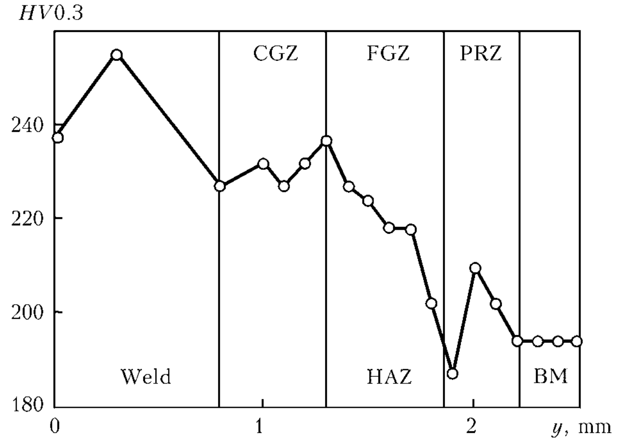


**Figure 7.** Distribution of hardness $HV0.3$ in a cross section $y$ of welded joint of steel 13G1SU (δ = 14 mm) produced using four-pass hybrid welding ($v_w$ = 60 m/h): CGZ — coarse grain zone; FGZ — fine grain zone; PRZ — partial recrystallization zone

treatment or application of additional technological procedures, is at the stage of investigations.

Therefore, the results of investigations of structure of pipe steel welded joints produced using multipass laser and laser-arc welding, and also their impact toughness and corrosion resistance allows considering the above-mentioned methods of welding to be challenging for increase of service life of pipeline transport. The hybrid laser-arc welding of pipe steels ($\delta >$ $> 5$ mm) allows the decrease in the power of laser radiation and partially its replacement by a less expensive power of electric arc, coming from the calculation of 1.0 kW of an arc instead of 0.5 kW of laser radiation power. At the power of laser radiation of up to 3 kW the application of hybrid welding process of steels is rational at the thickness of sheet of up to 10 mm, above this value the depth of penetration does not increase even at decrease of welding speed. To weld sheets of large thickness it is rational to use radiation of a higher power. With this purpose it is offered to use multipass laser and hybrid welding. In hybrid welding the width of a weld and HAZ is larger as compared with that of a laser one. The increase of welding speed and carbon content in base metal leads to formation of undesirable martensite structures in HAZ. The methods of elimination of this disadvantage require further study.


1. Semyonov, S.E., Rybakov, A.A., Goncharenko, L.V. et al. (2003) Evaluation of condition of metal of welded pipes of long-operated gas pipelines. *The Paton Welding J.*, **4**, 2–6.
2. Rybakov, A.O., Semenov, S.E., Goncharenko, L.V. (2006) Evaluation of condition and effects of strain ageing of gas pipeline metal in use of controlled rolling steel. In: *Problems of service life and safety of structures, constructions and machines*: Coll. on results obtained in 2004–2006. Kyiv: PWI.
3. Grigoriants, A.G., Grezev, N.V., Romantsov, I.A. et al. (2006) Development of technology of two-beam laser welding and full-scale tests of gas and oil pipes. *Svarochn. Proizvodstvo*, **5**, 3–37, 63, 64.
4. Staufer, H., Ruehrnoessl, M. (2006) Fuer grosse Blechdicken und hohe Schweissgeschwindigkeiten: Laserhybrid- + Tandemschweissen. *Praktiker*, **10**, 300–302.
5. Shelyagin, V.D., Khaskin, V.Yu., Garashchuk, V.P. et al. (2002) Hybrid $CO_2$-laser and $CO_2$ consumable-arc welding. *The Paton Welding J.*, **10**, 35–37.


# NEW BOOK

(2010) **Paton school:** Scientific-informational edition. — Kyiv: Naukova Dumka. — 440 p. Il., ISBN 978-966-00-0953-1.


The book contains information about the world recognized Paton scientific-engineering school in the field of welding and related technologies. The course of life of famous scientist Prof. Evgeny O. Paton, founder of the Electric Welding Institute, is described. The purposeful fundamental research works, started by him and his school, became a theoretical basis of welding science, transformed it into powerful tool of technical progress, providing revolutionary achievements in many branches of industry.

Under the leadership of Prof. E.O. Paton, the Paton school experienced the further rapid development, significantly expanded the topicality of investigations and developments, founded new scientific-technical directions, gained high authority and wide recognition in the world.

This school brought up a generation of famous scientists, members of the National Academy of Sciences of Ukraine, doctors and candidates of sciences, talented engineers who follow the ideas and methods of work of their teachers, basic principles and traditions of school, bring up new generations of pupils and successors multiplying a good fame of their alma mater.

The book is useful for scientific and engineering-technical personnel, post-graduate students, students, and also those who are interested in history of development of science and technology.

The book is available in the V.I. Vernandsky National Library of Ukraine, V. Stefanik Lviv Scientific Library, Library of the E.O. Paton Electric Welding Institute.

# IMPROVEMENT OF CYCLIC FATIGUE LIFE OF WELDED JOINTS WITH ACCUMULATED FATIGUE DAMAGE BY HIGH-FREQUENCY PEENING

**V.V. KNYSH, S.A. SOLOVEJ** and **A.Z. KUZMENKO**
E.O. Paton Electric Welding Institute, NASU, Kiev, Ukraine

The paper gives the results of investigation of the effectiveness of application of high-frequency mechanical peening (HFMP) with multistep and block loading to improve residual fatigue life of welded joints of low-alloyed steels with 50 % level of accumulated fatigue damages. It is established that application of HFMP technology allows 9–12 times improvement of cyclic fatigue life of such joints.

***Keywords:*** *welded structures, fatigue damage accumulation, high-frequency mechanical peening, cyclic fatigue life, effectiveness*

Intensification of economic activity necessitates extension of service life of diverse engineering structures. An important role is given to organizing effective measures on restoration of load-carrying capacity of welded metal structures. In repair-reconditioning operations a lot of attention should be paid to improvement of fatigue strength characteristics of welded components and elements. The most effective extension of fatigue life of welded joints with accumulated fatigue damage can be achieved by treatment of weld zones in welded joints by high-frequency mechanical peening (HFMP). Studies [1–3] give the data of experimental studies on improvement of fatigue resistance characteristics by HFMP technology of full-scale tubular nodes and samples of welded joints after accumulation of the set level of fatigue damage right up to formation of a surface crack. Investigations in this direction were mainly conducted at regular loading. Engineering structures are exposed to complex loading modes in service, when the sequence of amplitude values and average cycle stresses varies in a random fashion, so that it is important to assess the residual fatigue life of the joints at irregular loading in the laboratory [4].

The purpose of this study was to establish the effectiveness of application of HFMP technology for improvement of cyclic fatigue life of welded joints with 50 % accumulated fatigue damage under the action of multistep and block loading with identical parameters before and after strengthening.

Experimental studies were conducted on samples of welded joints of 09G2S steel ($\sigma_y$ = 370 MPa, $\sigma_t$ = = 540 MPa) which consisted of a plate with transverse stiffeners welded to it from each side. Blanks for samples were cut out of rolled sheets so that the long side were oriented along the rolled stock. Transverse stiffeners were welded by fillet welds from two sides by manual electric arc welding by UONI-13/55 electrodes. Sample shape and geometrical dimensions are given in Figure 1. Sample thickness is in agreement with the wide applicability of 12 mm rolled stock in welded structures, and the width of sample working part was selected proceeding from testing equipment capacity. At joint strengthening by HFMP technology a narrow zone of weld to base metal transition was subjected to surface plastic deformation. Fatigue testing of samples was conducted in URS 20 testing machine at uniaxial alternating loading with cycle asymmetry $R_\sigma$ = 0. All samples were tested to complete fracture.

Fatigue testing of welded joints of 09G2S steel strengthened at 50 % damage accumulation, was conducted on 18 samples, 9 samples in each case, respectively, under the conditions of multistep and block loading with increasing, decreasing and quasi-random order of load application. Thus, for each order of load application 3 samples were tested under the conditions of multistep and block loading.

At multistep and block loading the order of load application was assigned by the same five levels (steps) of applied maximum cycle stresses, but with different degrees of damage (number of stress reversal cycles) in each level (Figures 2 and 3).

So, increasing order of load application in the block was assigned by maximum cycle stresses equal to 180 MPa in the first loading step, with its subsequent

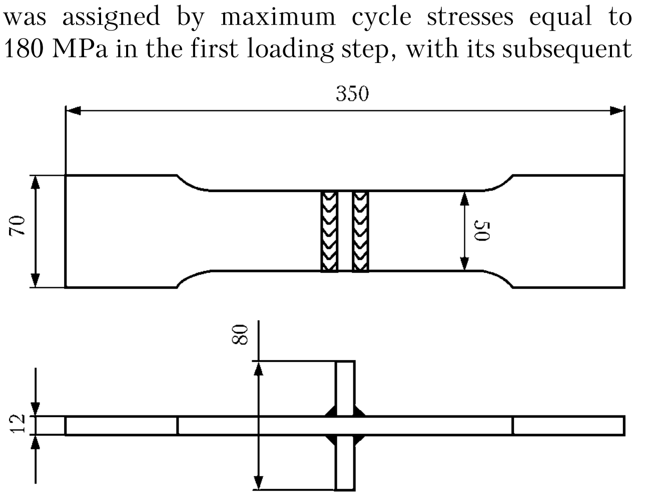


**Figure 1.** Schematic of a sample of 09G2S steel welded joint

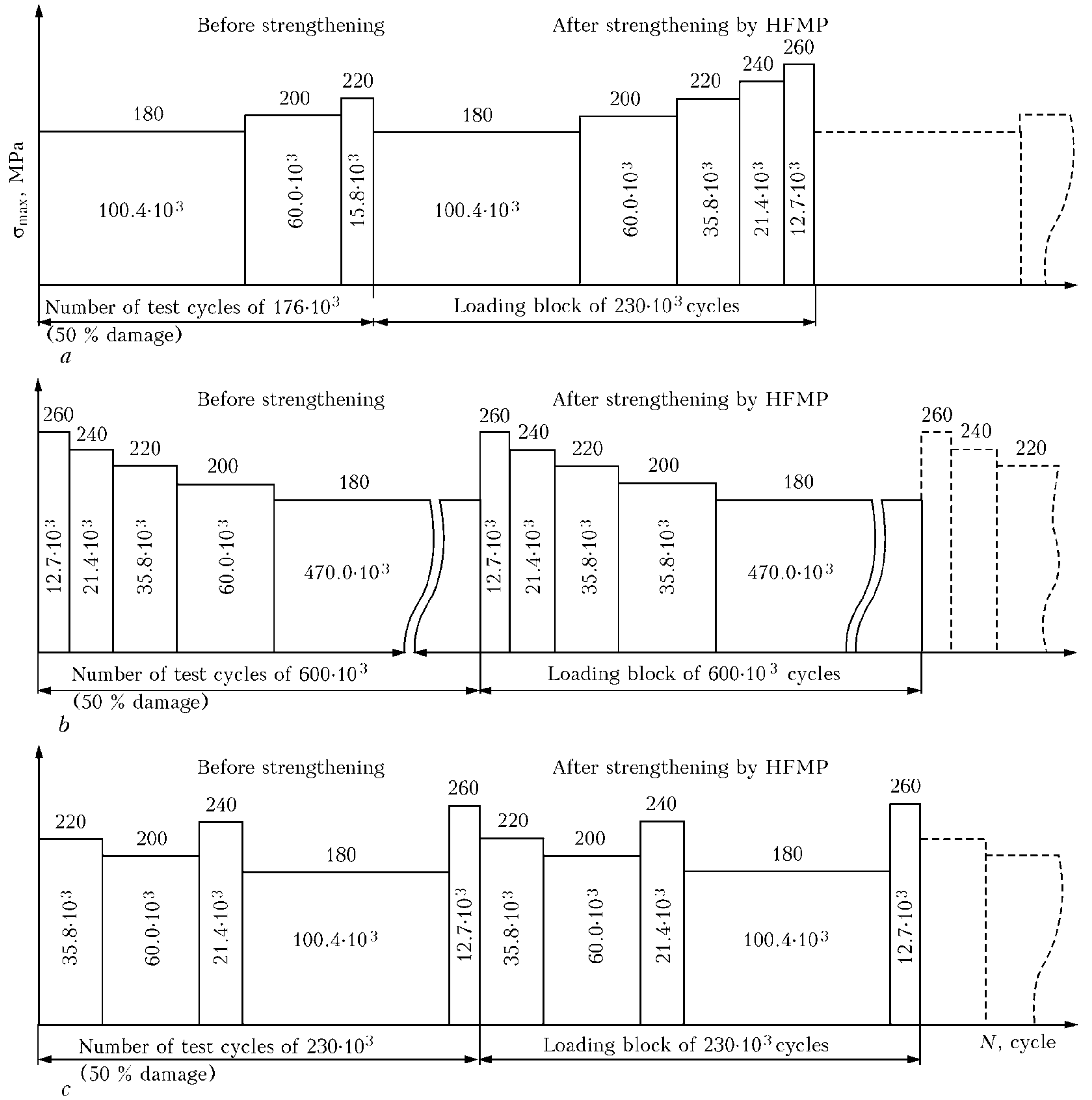


**Figure 2.** Schematic of multistep loading of samples of welded joint of 09G2S steel with increasing (*a*), decreasing (*b*) and quasi-random (*c*) sequence of load application in each block

increase to 260 MPa (fifth loading step) with 20 MPa step. Decreasing order of load application in the block was assigned by initial level of maximum cycle stresses of 260 MPa with subsequent decrease to 180 MPa, also with 20 MPa step. Quasi-random order of load application was assigned by the following five successive levels of maximum cycle stresses in the block: 220, 200, 240, 180, 260 MPa.

Strengthening of welded joints by HFMP technology was conducted after the joints have reached 50 % of their fatigue life. Number of stress reversal cycles before strengthening at each degree of loading under the conditions of multistep and block loading was assigned, proceeding from the earlier established in [5, 6] criteria of fracture of such samples of welded joints of 09G2S steel in an unstrengthened condition at similar loading. At multistep alternating loading for all the orders of load application the total damage level of the joints equal to 50 %, was assigned by reducing 2 times the values of the number of test cycles in each loading step, given in [5]. At block loading for all the orders of load application in the block 50 % damage was assigned by reducing 2 times the number of loading blocks to welded joint failure, derived earlier [6], while keeping unchanged the number of cycles in the block. After joint strengthening, the loads at multistep and block loading remained the same as before strengthening, except for multistep loading with increasing order of load application. With this type of loading, fracture of welded joint samples in an unstrengthened state occurred already in the second or third loading step [5]. As welded joint strengthening by HFMP technology greatly improves the fatigue resistance characteristics, all the five loading steps were applied to the sample after strengthening (Figure 2, *a*).

A criterion of completion of testing under the conditions of multistep and block loading was complete fracture of the samples. If under the conditions of multistep loading, the welded sample strengthened at

50 % damage accumulation did not fail after the assigned five loading stages (in one loading block), this loading block was repeated. Thus, after strengthening the welded samples instead of multistep loading, were practically brought to complete fracture under the conditions of block loading. Here the block length (number of stress reversal cycles in one block) for joints strengthened by HFMP was equal to a sum of cycles corresponding to 50 % damage of welded joints in as-welded condition (see Figure 2). An exception was multistep loading with increasing order of load application, in which after strengthening the block length was increased from 176 up to 230 thou cycles of stress reversal (see Figure 2, *a*).

At multistep loading of welded joints after 50 % damage accumulation and subsequent strengthening all the three sample series were subjected to nine loading blocks in the strengthened state. Welded joint samples which were tested in a decreasing order of load application, after nine loading blocks withstood approximately $5.5\cdot10^6$ cycles of stress reversal. No fatigue cracks were detected in any of the welded samples. As strengthening by HFMP technology guaranteed 9 times extension of the joint residual fatigue life, it was decided to conduct further testing of samples to fracture at higher levels of maximum cycle stresses (310 MPa) under the conditions of regular loading. Fatigue life of samples which were tested earlier at multistep loading with increasing sequence of load application, at regular loading was equal to 97.8–301.2 thou cycles, with decreasing sequence it was 109.8–276.4 thou cycles and with quasi-random sequence it was 156.1–377.8 thou cycles of stress reversal. Thus, cyclic fatigue life of all the three sample series at increased maximum cycle stress of 310 MPa was in the range of 97.8–377.8 thou cycles of stress reversal, which was equal to 21–83 % of fatigue life of welded joints strengthened by HFMP technology in as-welded condition. The difference of approximately $3.5\cdot10^6$ stress reversal cycles in the number of test cycles at maximum cycle stress level of 180 MPa under the conditions of multistep loading in these three sample series did not have any influence on scatter of cyclic fatigue life at increased regular loading. Thus, after HFMP of a welded joint even with 50 % damage, the levels of maximum cycle stresses (180 MPa) which are much lower than the endurance limit of a strengthened joint (260 MPa) do not have

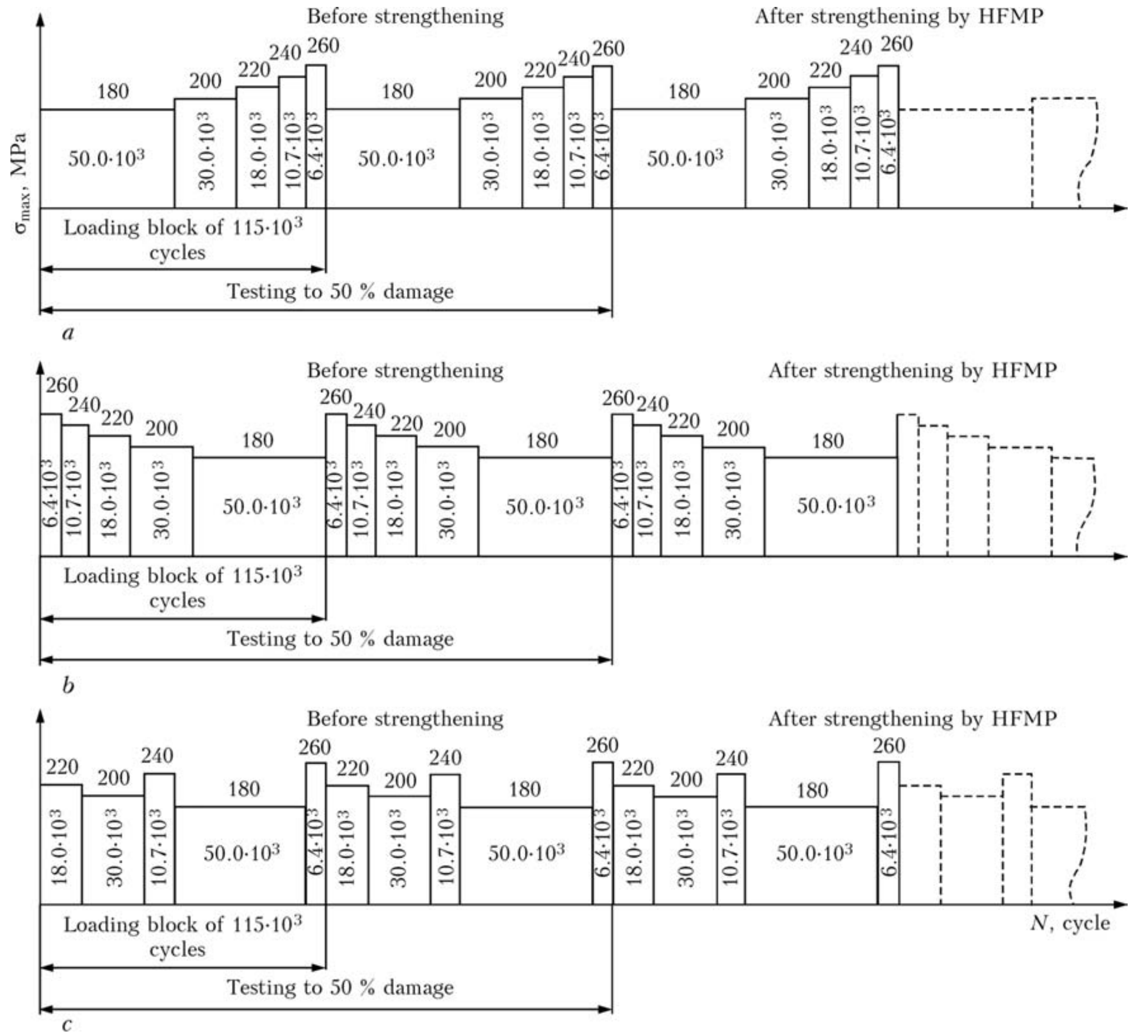


**Figure 3.** Schematic of block loading of samples of welded joint of 09G2S steel with increasing (*a*), decreasing (*b*) and quasi-random (*c*) sequence of load application in each block

any damaging effect. This is also confirmed by experimental data obtained in [2].

At block loading, after 2 loading blocks in unstrengthened condition (accumulation of 50 % damage) and subsequent strengthening all three sample series were subjected to 25 loading blocks in the strengthened state. No fatigue cracks were found in any of the welded samples. Considering that HFMP strengthening of welded joints with 50 % damage guarantees extension of their residual fatigue life by more than 12 times at unchanged parameters of block loading, it was decided to conduct further fatigue testing of samples to fracture at the level of maximum cycle stresses increased up to 310 MPa under the conditions of regular loading. Scatter of fatigue life values for nine samples tested at increased load was in the range of 115–284 thou cycles, which was equal to 25–62 % of fatigue life of welded joints, strengthened by HFMP technology in as-welded condition.

## CONCLUSIONS

1. It is established that strengthening by HFMP technology of welded joints after accumulation of 50 % damage guarantees extension (without crack formation) of their residual fatigue life by 9–12 times under the conditions of application of multistep and block loading before and after strengthening. Fatigue life of tested samples of welded joints was equal from $2\cdot10^6$ up to $5\cdot10^6$ stress reversal cycles.

2. After HFMP of welded joints with 50 % fatigue damage accumulation the levels of applied maximum cycle stresses in the loading block that are much lower than the endurance limit of a strengthened welded joint, do not have any damaging effect.

1. Knysh, V.V., Kuzmenko, A.Z., Vojtenko, O.V. (2006) Increasing fatigue resistance of welded joints by high-frequency mechanical peening. *The Paton Welding J.*, **1**, 30–33.
2. Garf, E.F., Litvinenko, A.E., Smirnov, A.Kh. (2001) Assessment of fatigue life of tubular connections subjected to ultrasonic peening treatment. *Ibid.*, **2**, 12–15.
3. Knysh, V.V., Kuzmenko, A.Z., Solovej, S.A. (2009) Increase of cyclic fatigue life of tee welded joints with surface cracks. *Ibid.*, **1**, 29–33.
4. Troshchenko, V.T., Sosnovsky, L.A. (1987) *Fatigue resistance of metals and alloys*: Refer. Book. Pt 1. Kiev: Naukova Dumka.
5. Knysh, V.V., Kuzmenko, A.Z., Solovej, S.A., (2008) Accumulation of fatigue damage in tee welded joints of 09G2S steel in the initial condition and after strengthening by high-frequency mechanical peening. *The Paton Welding J.*, **10**, 10–15.
6. Knysh, V.V., Kuzmenko, O.Z., Solovej, S.O. (2009) Accumulation of fatigue damage in tee welded joints in the initial condition and after strengthening by high-frequency mechanical peening under block loading. *Mashynoznavstvo*, **9**, 27–31.

# TENDENCIES IN DEVELOPMENT OF MECHANIZED WELDING WITH CONTROLLED TRANSFER OF ELECTRODE METAL (Review)

**V.A. LEBEDEV**
E.O. Paton Electric Welding Institute, NASU, Kiev, Ukraine

Assessment of modern developments of mechanized equipment for consumable electrode welding and surfacing was performed. It is shown that modern engineering solutions involve control of electrode metal transfer as the main means of improvement of mechanized arc processes. Examples of realization of electrode metal transfer control are given.

***Keywords:*** *welding, surfacing, pulse, source, inverter, transfer, control, feed mechanism*

Developed and commercially available semi-automatic welding and surfacing machines are being continuously improved to produce welds and deposited beads with optimum ratio of geometrical parameters and metal quality, including the near-weld zone; reducing the cost of post-weld treatment; reducing consumption of material and energy resources, lowering the influence of welding operator on welding and surfacing processes.

All the above directions were combined by the main topic of ESAB concern «Increase of efficiency» in «Welding and Cutting» Exhibition held in Essen, Germany, from September 14 to 19, 2009. In this work illustrative material from promotional brochures of leading companies-exhibitors in the exhibition was used.

The tasks of improvement of welding equipment were solved by various methods in different periods, also by developing new welding consumables, application of multicomponent mixtures of shielding gases, improvement of the main and auxiliary components and equipment as a whole.

In 1960s pulsed-arc welding process became rather widely accepted. Its essence consisted in application of pulsed algorithms for welding current source control of electrode metal transfer [1].

At present improvement of welding processes and equipment for mechanized welding proceeds, mainly, allowing for the capabilities offered by application of inverter sources of welding current and various algorithms of control of electrode metal transfer and welding cycle. This was demonstrated in the Exhibition by the majority of the participating companies-manufacturers of the respective equipment for welding steels, titanium and aluminium alloys. This equipment mainly belongs to semi-automatic machines for consumable electrode welding.

One of the first developments in the field of controllable electrode metal transfer using inverter sources of welding current were engineering solutions, proposed by KEMPPI, Finland, in the form of synergic control. The essence of this control process is known and described in [2]. KEMPPI technologies and equipment are being continuously developed and improved. As an example of such an improvement a new MIG/MAG process — FastROOT — was proposed, which is welding by a modified short arc based on digital control of arc parameters (welding current and voltage). It is applied for welding low-carbon and alloyed steels and makes the welder's work easier and faster. Welding can be performed in all positions, with good penetration and at practically complete absence of spatter. FastROOT technology ensures better weld quality, than in TIG welding at a higher efficiency. The principle of FastROOT operation is based on separation of the welding cycle into two periods: short-circuiting period and arcing period, which alternate (Figure 1). During the short-circuiting period the wire is shorted into the weld pool, the current rises abruptly and remains on the set level. At the start of the short-circuiting period, there is a short jump of welding current. During the short-circuiting period at an abrupt jump of current up to the specified

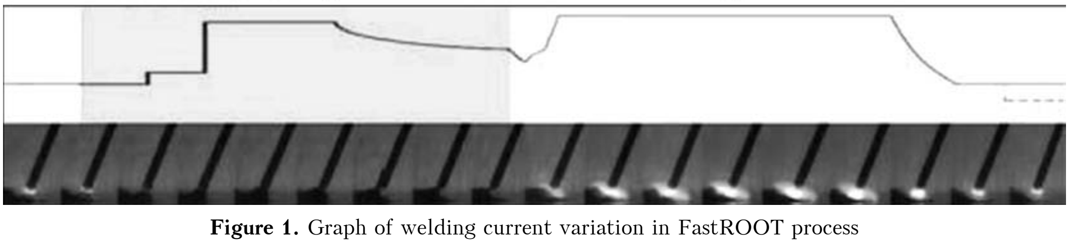


**Figure 1.** Graph of welding current variation in FastROOT process

**Figure 2.** FastMIG Synergic semi-automatic machine

level, the electrodynamic force grows, ensuring separation of the metal drop from the welding wire tip. At a slow lowering of welding current a smooth separation of the drop takes place. At the moment of drop transfer into the weld pool the second period of current rise begins and the arc is struck. Accurate control of the time of current rise and decrease guarantees an absence of spatter at transition from short-circuiting to arcing.

During arcing period the weld pool forms and the required penetration of weld root is ensured. These two periods of current rise follow each other, and at the end of each of them the current is set and maintained at the specified level. Accurately set base current guarantees transfer of each subsequent drop during the short-circuiting period, creating the conditions for continuous separation of drops and their transfer into the weld pool practically without spatter with a guarantee of arcing stability and simplicity of welding process control.

Semi-automatic machine with realization of the considered FastMIG Synergic process is shown in Figure 2.

A direction in which attention is focused on development of systems and means of electrode metal transfer control, providing an effective solution of the problems of ensuring process quality, as well as energy- and resource-saving, continues to be intensively developed now. A confirmation of the rationality of this path of development of mechanized welding and surfacing is provided both by the entire wide range of semi-automatic machines for welding and surfacing demonstrated by numerous companies in «Welding and Cutting 2009» International Exhibition in Essen, and the package of work currently performed by PWI.

Most of the semi-automatic machines of modern design incorporate welding current sources with various algorithms of output parameter variation, allowing control of electrode metal transfer. Here SST technologies, «cold welding» technologies, their different variants and combinations of actions on the arc process (controlled formation and transfer of electrode metal drop) are used.

The widest spectrum of technological innovations was presented by known CLOSS Company, Germany. They include «cold process» (CP) realized using a semi-automatic welding machine of this company of GLC 353 QUINTO CP type, which has essential advantages compared with the usual technology, particularly in welding of thin-walled parts. Owing to a new shape of welding current pulses a lowering of thermal load on the base material (reduction of energy input) is achieved and power of welding wire melting, and, therefore, welding speed, are increased simultaneously. The cycle of electrode metal transfer occurs by the following algorithm (Figure 3):

- in the phase of positive main current base material cleaning (oxide layer breaking up) occurs, and an accurately calculated amount of thermal energy is applied to the material;
- in the pulsation phase drop separation without spatter occurs;
- in the phase of negative base current (drop formation) the arc covers the wire tip. Transfer of a certain amount of thermal energy to the welding wire takes place, the weld pool cooling down.

This provides an excellent filling of gaps between the parts being welded, accuracy and repeatability of welding result.

CP welding is optimum and effective for joining high-strength, stainless steels, coated materials, aluminium alloys, as well as for MIG brazing.

The following should be named as advantages of CP welding with the above-mentioned other algorithms of forming welding current pulses: high welding speed; increased efficiency; high welding quality;

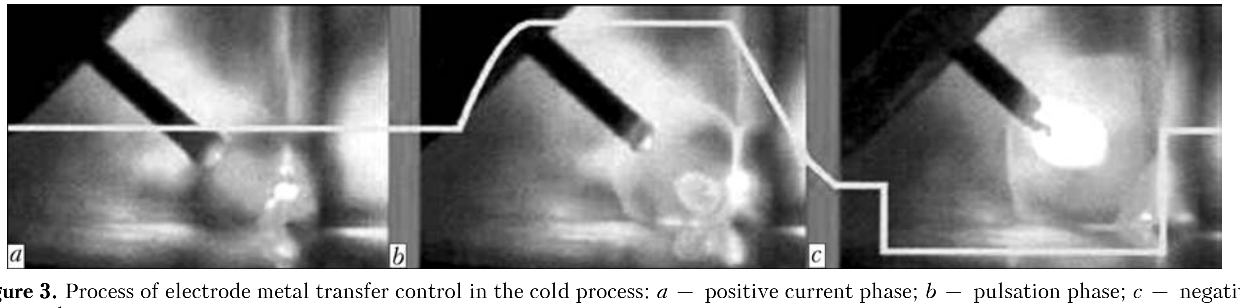


**Figure 3.** Process of electrode metal transfer control in the cold process: *a* — positive current phase; *b* — pulsation phase; *c* — negative current phase

lowering of thermal energy transfer into the material; reduction of thermal deformations; lowering of the risk of cracking in the weld zone because of temperature gradients; minimized molten metal spatter; no need for subsequent treatment; possibility of application of large diameter electrode wire; lowering of electrode wire costs; possibility of creating a new process — inert gas brazing (MIG brazing).

Technology and equipment for welding using STT-process developed at Lincoln Electric Company, USA, was extensively displayed in the exhibition. High-quality semi-automatic welding of root welds with back formation of the joint, welding of sheet material, and lower spatter of electrode metal, are achieved in this case.

Shapes of welding current and voltage curves in semi-automatic welding by STT method are shown in Figure 4. Considered process was realized in INVERTEC STT2 welding source which is shown in Figure 5.

The following developments of Lincoln Electric should be noted: welding current sources of Power Wave 355M type — all-purpose inverter arc power sources, also for gas-shielded pulsed-arc semi-automatic welding with synergic control of welding parameters and program control of current pulse shape. The source incorporated the latest achievements in power inverter equipment and microporcessor control with optimized software, developed at Lincoln Electric, ensuring wide capabilities of welding in combination with ease of operation. The welder just has to select one of more than 60 welding programs, depending on material type, wire diameter and shielding gas and set the welding wire feed rate. The source automatically provides the optimum shape and parameters of current pulses, maintaining control of each drop of the metal being deposited. The range of welded materials is very wide: steels, stainless steels, aluminuim, nickel alloys, etc. Equipment allows lowering the requirements to welder professional level and at the same time ensures an improved quality and efficiency of welding operations; technology of control of the shape and parameters of welding current pulses Wave Control ensures an optimum running of welding process, i.e. for each type and size of wire and material the optimum welding properties of the source are set to achieve the best welding results. The main advantages of the new technology of controlling the welding current shape are accurate control of welding process parameters, their interaction, instant response to possible deviations of arc parameters, and ease of operation.

New modes, proposed and demonstrated in the exhibition by Lincoln Electric are:

• Power mode — provides a stable smooth process in short-arc welding of thin materials;

• Pulse-in-Pulse — improves cleaning in semi-automatic welding of aluminium and forms the weld of the same appearance as in tungsten electrode welding;

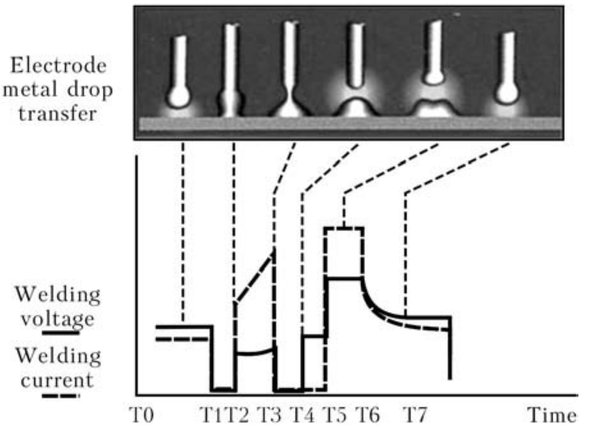


**Figure 4.** Diagrams of transfer of electrode metal drop at SST control

• Rapid Arc — designed for high-speed (up to 2.5 m/min — according to developer materials) semi-automatic welding of carbon steels up to 4 mm thick.

All the new developments of Lincoln Electric are based on adaptive synergic programs, i.e. have program feedbacks for correlation of arising deviations of the welding process, distinguishing the source from most of the analogs with rigidly set pulse parameters. Welding programs are constantly complemented by new ones developed by the manufacturer. Note that the user of this equipment is able to develop his own welding programs, using the acquired Wave Designer software. This, in our opinion, accounts for very broad acceptable of STT-process and its various modifications, differing from each other by some features of the pulse shape, and in some cases containing additional impacts due to the software and capabilities of modern power sources. So, STEL Company, Italy, has developed and uses in the semi-automatic machines combined control, which includes both pulsed synergic algorithms, and modulation, ensuring good labour conditions for welders, also in other positions than the horizontal one, when making short and spot welds at high and repeatable quality.


**Figure 5.** Welding current source INVERTEC STT2

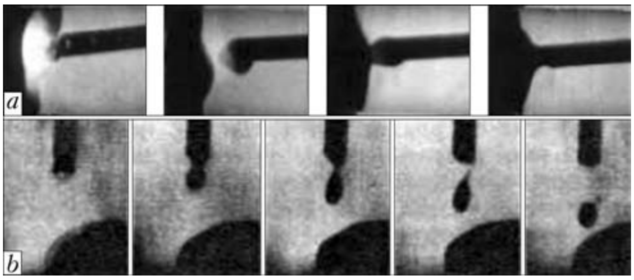

**Figure 6.** Filmograms of electrode metal transfer process: *a* — process with FSC; *b* — pulsed-arc process

For comparison let us consider the developments of SPA SELMA-ITS, Russia–Ukraine [3]. A new welding process was proposed, which is also a variant of semi-automatic welding with periodical short-circuiting and which was called the process of welding with forced short-circuiting — FSC. The development was based on analysis of short-comings of STT process — high cost of complex inverter welding equipment; expensive programming of welding mode parameters, if it is necessary to perform welding in a mode non-standard for this welding machine and complex maintenance; welding machine is controlled by changing the cyclogram of welding arc current, which makes it impossible to use pulsed modes, and low reliability in case of long connecting cables (more than 25 m from the power source to feed mechanism), which, in its turn, imposes serious technological limitations; lowering of welding process efficiency by at least 25 % because of shortening of free arcing time of welding arc and presence of a considerable number of short-circuits.

FSC process is based on application of welding current sources with combined external volt-ampere characteristics. The essence of the use of such characteristics consists in that, depending on the size of electrode metal drop and phase of drop transition into the weld pool (drop growth, formation of a bridge between the drop and electrode, drop transition into the pool, bridge rupture), the volt-ampere characteristic can be rigid or drooping. The power of the arc discharge at the moment of bridge rupture is limited, and open-circuit voltage after bridge rupture and drop transition into the weld pool is increased for welding process stabilization. Transfer control is performed not by current, but by arc voltage. Application of other thyristor or inverter sources (without special control algorithms) does not provide a high quality of the welded joint in mechanized welding, because of scatter of electrode metal drop sizes, chaotic transition from the process of long-arc welding to short-arc welding, considerable spatter, low welding properties at the change of electrode wire diameter and position in space.



**Figure 7.** Welding current source Origo Mig C3000i

During FSC process, compared to the traditional process of $CO_2$ welding (Figure 6) with short-circuiting of the arc gap, the time of electrode metal drop contact with the arc is considerably reduced, arcing time is shortened (by the value of short-circuiting duration) and weld pool dimensions are reduced, respectively, the process becomes more flexible and controllable in terms of technology.

Let us consider a few more engineering solutions, used by a number of leading companies-manufacturers of mechanized equipment.

QSet function is the most recent development of Swedish concern ESAB in the field of intellectual digital welding. Modern electronics allows development of software, helping welders to control MIG/MAG welding process. One-time pushing of QSet button and several seconds of trial welding are enough to automatically set all the short-arc parameters, namely an optimum ratio of arcing duration and short-cricuiting duration, at which a more efficient use of the arc is achieved at the same short-circuiting frequency. The same procedure is repeated when wire grade or diameter and/or shielding gas type are changed. The system can itself find the optimum settings. Wire feed rate can be changed at any time during the welding process or between the welding operations. If the different butt geometry, material thickness or welding positions require different feed rates, then the established optimum welding parameters guarantee a stable short arc, which provides a high welding quality. QSet function is used to set a stable process of short-arc welding at different wire extensions at the change of welded item geometry, which helps the welders. For instance, in narrow-gap welding time is also saved on scraping the welds, as ideal adjustment of the arc minimizes spattering. Figure 7 shows a source of welding current of Origo Mig C3000i type with a built-in QSet function.

A very interesting solution realized in ESAB equipment, is pulsed control algorithm, which allows controlling in a broad range the «arcing–short-circuiting» time at the same transfer frequency (Figure 8). It is also possible to change the frequency of short-circuiting of the arc gap by changing the choke inductance. Here, short-circuiting frequency decreases with increase of choke inductance. All this is achieved by

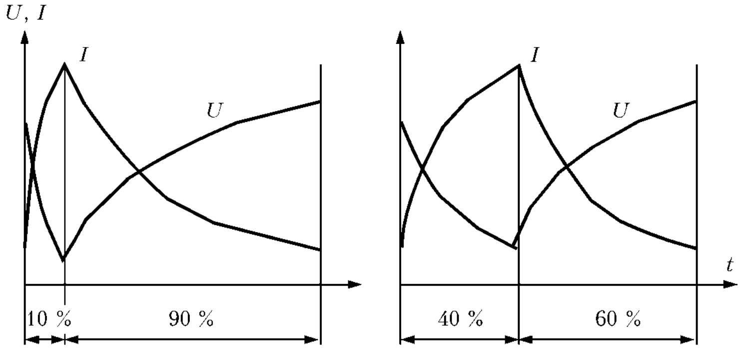


**Figure 8.** Capabilities of control of short-circuit and arcing time

QSet function. Settings of choke inductance, welding voltage and electrode wire feed rate, in addition to ensuring the process stability, also essentially influence the heat input. At greater inductance arcing time is increased, short-circuiting frequency is decreased and heat input is increased.

Let us consider the method of control of forceArc process developed by EWM, Germany. In mechanized gas-shielded welding (inert gas or mixture of gases with high argon content) jet process of electrode metal transfer by fine drops without short-circuiting is often used. This is possible at relatively long arc with high value of welding voltage, which is not always effective in practice, as the arc can be deflected because of magnetic blow, and, in addition, undercuts or pores can occur, as well as loss of alloying elements. At arc shortening as a result of welding voltage lowering, duration of short-circuiting phases is increased and spatter is enhanced.

Appearance of inverter machines and modern digital control systems enabled at a very short arc with long short-circuiting phases to quickly «intervene» into the adjustment process. At arc excitation current is lowered until programmed arc voltage has been reached. As a result, short-circuiting duration is markedly reduced, and spattering is minimum. Electrode metal transition into the weld is of a jet nature with finest drops and practically without short-circuiting. At further lowering of voltage the arc length will decrease. The arc runs in molten metal depression, forming under the pressure of plasma flow. Size of metal drops moving into the pool, changes from fine to medium drops. Frequency of the drops following each other increases to such a state when their sequence forms a short-time contact with the melt, leading to short-circuiting with increased metal spatter. Such a transfer is influenced by control algorithm of inverter current sources. In this case the inductance is adjusted using an electronic system. At short-circuiting it can be completely switched off (just the welding wire inductance remains). Therefore, current increase and lowering in the short-circuiting phase and at arc excitation can be adjusted very quickly. Spattering is very low.

Voltage drop and rise are used as setting parameters for the adjustment process. Voltage is measured continuously and each voltage change is recorded appropriately (highly dynamic adjustment of instantaneous values).

Such a type of control ensuring jet transfer during welding is called EWM-forceArc. Current and voltage change can be ensured without any significant spatter.

Fast adjustment of the process allows welding to be performed with a long wire extension, which is favourable for the weld at limited access to it (difficult access to the welding site). In this case, however, sufficient flow rate of shielding gas must be ensured.

High-speed filming frames in Figure 9 demonstrate arcing and electrode metal transfer during the EWM-forceArc process.

PHOENIX 500 EXPERT PULS semi-automatic machine, in which control of MIG/MAG process of forceArc welding is realized, is shown in Figure 10.

Application of forceArc process can lead to the following results: increased penetration due to high pressure of plasma in the arc; absence of undercuts

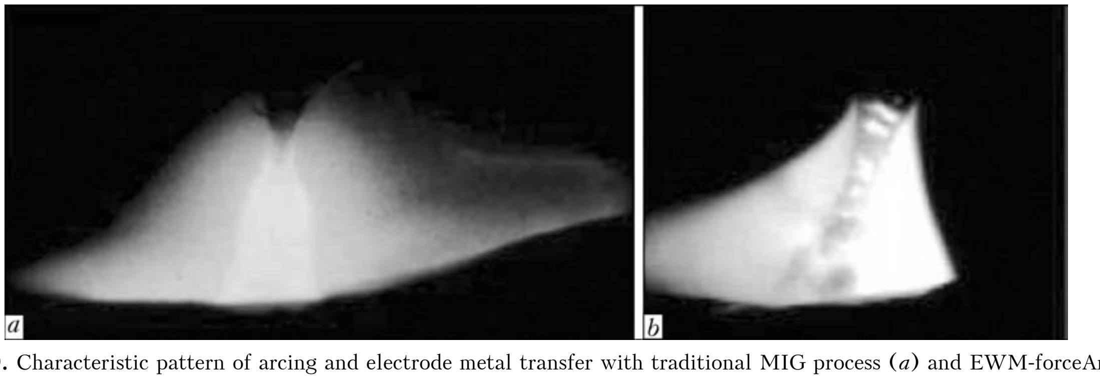


**Figure 9.** Characteristic pattern of arcing and electrode metal transfer with traditional MIG process (*a*) and EWM-forceArc (*b*)

**Figure 10.** Semi-automatic machine PHOENIX 500 EXPERT PLUS

due to a very short arc; high cost-effectiveness owing to a high welding speed; better weld quality as regards the heating zone and distortion due to slight heating.

The well-known Fronius Company, Austria, has essentially widened the capabilities of CP-process, developing CMT — cold metal transfer. The novelty of this control process consists in the method of drop separation, in which, in addition to other features, metal transfer is relatively cold compared to conventional processes. Not only wire feeding in weld pool direction is used, but also a reverse motion, i.e. electrode wire is fed forward and in a certain phase of drop transfer it is reversed, promoting electrode metal transition into the weld pool. An inverter welding current source is used, the control algorithm of which is conjugated with electrode wire motion. The main moments of electrode metal transfer cycle provided by reverse motion of electrode wire, are shown in Figure 11.

Achieving CMT with programmable operation of feed mechanism leads to a process with new characteristics. Performance of welds and braze seams practically without spatter becomes possible, which allows avoiding subsequent expensive and time-consuming machining. The feature of CMT process compared to traditional arc welding processes consists in that metal transfer occurs at almost zero current. At regular submerged-arc welding the current rises considerably in the short-circuiting phase, and in CMT process current value remains low in this phase. Here, despite a very low current value in the short-circuiting phase, drop separation is still possible, as this is promoted by reverse motion of the wire, which is attributable to surface tension of liquid metal by analogy with SST-process, obtained through control of welding current source parameters.

Weld formation quality (appearance, possibility of gravity welding without backing, small heat-affected zone, etc.) in sheet metal welding in CMT-process is given in Figure 12.

The process allows controlling heat input, which, in its turn, influences weld geometry. A combination of CMT process and pulsed arc is applied, if it is necessary to eliminate the lack-of-penetration in the weld, or increase welding speed. CMT-process also has advantages at arc excitation.

It should be noted that a number of companies use pulsed movement of wire at sufficiently high frequencies (for instance, MEGATRONIC, Denmark) — frequency of tens of Hertz. This, however, is true only for cases of application of filler wires.

Use of pulsed feed of electrode wire in welding and surfacing equipment displayed in the Essen exhibition, was limited to the above-described developments of Fronius, the essence of which consists in that the usual algorithm of electrode wire motion with a specified speed, providing an integral value of its melting speed, is interrupted at the required time by reverse motion of the electrode away from the item.

Having analyzed the considered algorithms of electrode metal transfer control by the type of SST and CMT one can come to the conclusion that such technologies practically do not actively control the transfer, as, for instance, this is done in the pulsed-arc process [1], but just create optimum (soft) transfer conditions. They, however, cannot be widely accepted, for instance in flux-cored electrode wire welding and surfacing.

A number of algorithms of control of electrode metal transfer with specified parameters were pro-

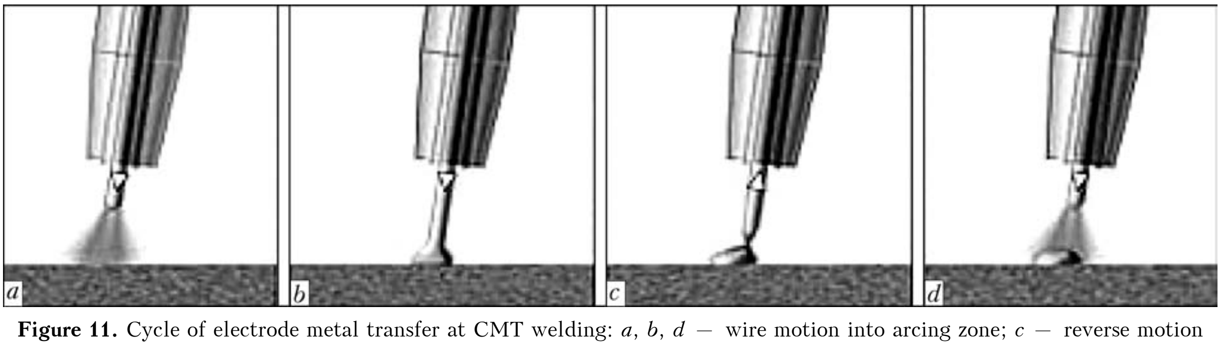


**Figure 11.** Cycle of electrode metal transfer at CMT welding: *a*, *b*, *d* — wire motion into arcing zone; *c* — reverse motion

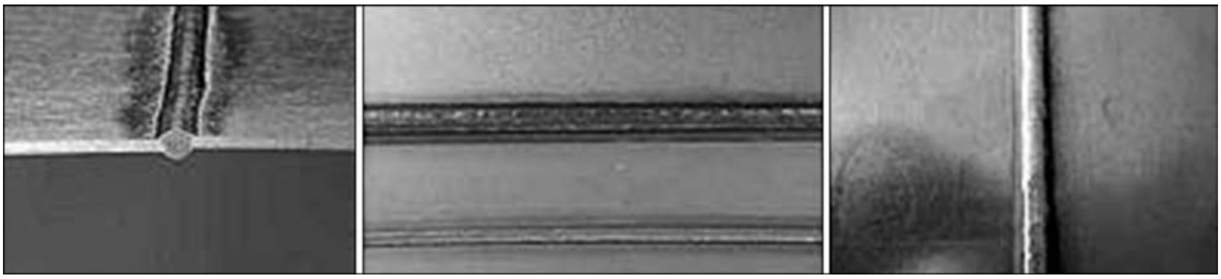

**Figure 12.** Appearance of welds when CMT process is used

posed by Russian researchers [4]. Technical realization of such algorithms is quite complicated and no real solutions were proposed, which could be the basis for commercial equipment in this direction, although quite interesting and promising results on real control of electrode metal transfer were indeed obtained during investigations. An exception is the feed mechanism with electromagnetic drive and drivers — one-sided grips. Such a feed system is difficult to adjust and is limited both as to operation period (unreliable designs of one-sided grips), and as to electrode wire types (flux-cored wire cannot be fed).

Adjustment of pulsed feed parameters can be regarded as the main objective, which is considered in [5] in all its aspects.

PWI of the NAS of Ukraine also pays a lot of attention to pulsed feed systems with one-sided grips with electric motors and electric magnets. Certain results have been achieved. A number of experimental semi-automatic machines have been developed, however, the work has not yet been taken to the stage of commercial introduction. At present, having a sufficiently large scope of the required theoretical studies on the possibilities of pulsed feed of electrode wire [6], a concept has been developed of design of pulsed feed mechanisms, which is based on application of electric motors in the two main directions:

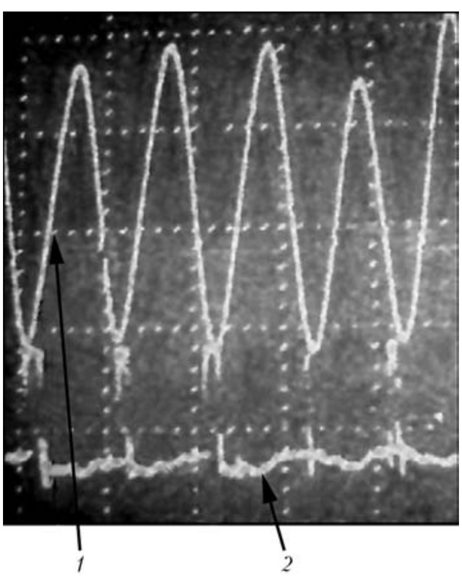


**Figure 13.** Oscillograms of wire feed rate *1* and voltage *2* in steel welding (1.2 mm Sv-08G2 wire, welding voltage of 21–22 V, welding current of 120 A)

- with application of special converters of rotary motion of electric motor shaft into pulsed motion of feed rollers and electrode wire;
- with application of special high-speed electric motors and feed roller mounting directly on the electric motor shaft.

Both these directions are effective for adjustment of feed pulse parameters, although in the first case the system has certain gaps, but it is sufficiently inexpensive (less expensive than the regular reduction gear feed systems). The system in the second direction is perfect, controllable (up to 70 Hz now, more than 100 Hz in the near-term). Such systems can indeed provide a controllable electrode metal transfer when using wires of various designs and in a rather broad range of processes and modes of arc welding and surfacing. PWI developed an arc welding process with pulsed feed, realization of which practically guarantees control of transfer with a short-circuiting phase, at which the level of electrode metal losses and power costs are lowered with production of welds of a good shape and appearance.

Figure 13 shows characteristic oscillograms of electrode wire pulsed feed rate and voltage for steel welding. Each drop transfer corresponds to a feed pulse at correctly selected parameters of pulsed motion of electrode wire, and the above transfer is performed in different pulse phases for the processes of welding steels and aluminium.

Figure 14 shows deposited beads of metal of aluminium alloys produced by the conventional mechanized process and process with pulsed feed of electrode wire. Absence of undercuts, regular bead formation at visual absence of inclusions, when pulsed feed process is used, are obvious. Possibility of obtaining a

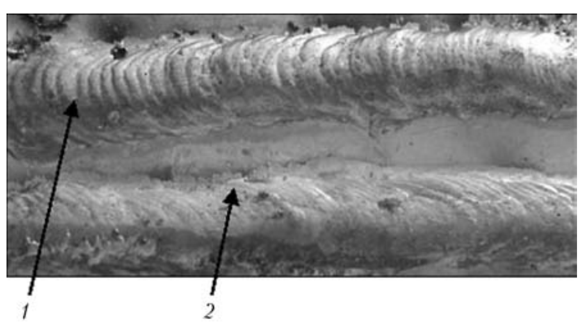


**Figure 14.** Deposition on plates from aluminium alloys with pulsed *1* and regular *2* electrode wire feed

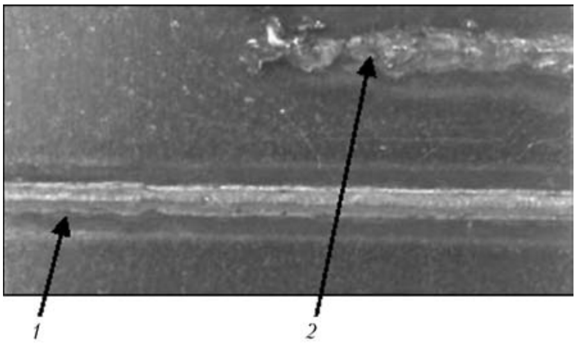

**Figure 15.** Bead deposition on steel sheet 1.2 mm thick with pulsed *1* and regular *2* electrode wire feed

sound metal bead at deposition on sheet metal is shown in Figure 15.

Revealing the features of electrode metal transfer in welding with pulsed feed allows defining the requirements to one more controlled transfer process, namely that with simultaneous use of pulsed feed mechanism and pulsed source of welding current. This direction was implemented in practice at PWI [7]. Such a method of forced control of transfer yields very good results at small energy consumption for pulse formation from a pulsed source (3–5 times lower than in pulsed-arc process in aluminium welding). However, up to now this process was difficult to implement because of a number of special requirements to the pulsed feed mechanism. PWI development of a new type of completely controllable pulsed feed mechanisms based on special designs of computerized valve electric motors enables commercial implementation of transfer control with action on the drop of two pulsed impact sources operating by a certain algorithm.

In conclusion it can be stated that one of the main directions in improvement of equipment for mechanized welding and surfacing processes is ensuring the possibility of effective controllable transfer of electrode metal. The highest effect can be achieved using advanced inverter-type welding current sources with computerized control and adjustment systems (Lincoln Electric, Fronius, CLOOS, etc.), as well as results of theoretical investigations and developments of systems of pulsed feed of electrode wire, conducted in Ukraine and Russia.


1. Potapievsky, A.G. (1974) *Shielded-gas consumable electrode arc welding*. Moscow: Mashinostroenie.
2. Voropaj, N.M., Ilyushenko, V.M., Lankin, Yu.N. (1999) Specifics of pulsed arc welding with synergic control of parameters (Review). *Avtomatich. Svarka*, **6**, 26–32.
3. Karasyov, M.V., Vyshemirsky, E.M., Bespalov, V.I. et al. (2004) Characteristics of modern units for mechanized GMA welding. *The Paton Welding J.*, **12**, 36–39.
4. Brunov, O.G., Fedko, V.T., Slistin, A.P. (2002) Varieties of methods of welding wire pulse feed for $CO_2$ consumable electrode welding. *Svarochn. Proizvodstvo*, **11**, 58.
5. Lebedev, V.A., Pichak, V.G., Smolyarko, V.B. (2001) Pulsed wire feed mechanisms with pulse parameter control. *The Paton Welding J.*, **5**, 27–33.
6. Lebedev, V.A., Pichak, V.G. (1998) Mechanised $CO_2$ arc welding with controlled pulse feed of electrode wire. *Svarochn. Proizvodstvo*, **5**, 30–33.
7. Paton, B.E., Lebedev, V.A., Mikitin, Ya.I. (2006) Method of combined control of electrode metal transfer process in mechanized arc welding. *Ibid.*, **8**, 27–32.

# PROPERTIES OF $Al_2O_3$ + Cr + TiN COATINGS AFTER ELECTRON BEAM TREATMENT

**A.A. BONDAREV**[1], **Yu.N. TYURIN**[1], **I.M. DUDA**[1] and **A.D. POGREBNYAK**[2]
[1]E.O. Paton Electric Welding Institute, NASU, Kiev, Ukraine
[2]Sumy Institute of Surface Modification, Sumy, Ukraine

Morphology of surface, element and phase composition of the $Al_2O_3$ + Cr + TiN composite coatings deposited by the combined methods using the pulse-plasma and vacuum-arc technologies with subsequent electron beam treatment were examined by scanning electron microscopy with microanalysis, back-scattered protons and X-ray diffraction analysis. It is shown that exposure to the high-power flow of electrons causes a change in structure, composition and properties of the composite coatings.

***Keywords:*** *composite coating, pulse-plasma, vacuum-arc and electron beam treatment, electron exposure, structure and phase composition, X-ray diffraction analysis, surface modification*

Formation of protective coatings on thin (0.2–0.5 mm) walls of components of atomic, electrochemical and chemical industries is of interest at present time. These components are manufactures as a rule from stainless steels of 18-10 type or special alloys. For example, operation of such components as blades of acid pumps requires a high adhesion of coating with the component surface, insignificant closed porosity and presence on the surface of passivating elements such as chromium, aluminum, titanium etc. A pulse-plasma coating technology [1, 2] fulfils these requirements.

Protective composite coatings were made on thin (0.3 mm) samples from stainless steel in the following way. A base coating from aluminum oxide of around 45–60 μm thickness was deposited on Impuls-5 unit with the help of high-velocity plasma jet. $\alpha$-$Al_2O_3$ powder of 27–56 μm in size was used as an initial powder.

The following modes were used for coating deposition: consumption of combustible mixture components 2 $m^3/h$ at frequency of detonation initiation 4 Hz; consumption of electric energy per each pulse of plasma — 2500–3500 J; length of powder jet limited by barrel — 0.35 m, distance 0.04 m; diameter of a coating spot deposited per one pulse — 0.033 m.

It is shown in study [1] that the coating consisted of up to 8 % of $Al_2O_3$ $\gamma$-phase, amorphous phases and the rest was $\alpha$-phase. Microhardness of the layer made up to 13000 MPa. Adhesion of the $Al_2O_3$ powder coating with a steel substrate, determined by glue procedure and scribing methods, made 40–60 MPa.

A layer of chromium of around 0.5 μm thickness and the following layer of coating from titanium nitride of 1.2–2.0 μm thickness were deposited on $Al_2O_3$ coating for improving corrosion properties. The coating was deposited using vacuum-arc source Bulat-5M. After that the surface was treated by a high-current electron beam (HEB) on U-212 unit [3]. Energy density of the HEB was sufficient for full fusion of the composite coating and partial fusion of the substrate layer (accelerating voltage was 30 kV, beam current — 20 mA, amplitude of beam oscillation — 15 mm, rate of surface scanning — 50 m/h (series No.1), 30 (series No.2), 3–15 (series No.3).

The peculiarities of HEB treatment lied in that the beam diameter made 0.3 mm at scanning pitch 0.9 mm. This provided formation of a streaky macrostructure on the surface, when strips with melted coating alternated with strips of non-melted coating.

Surface investigation was performed on the scanning electron microscope REM-MA-102. Analysis of obtained results (Figure 1) is evidence of surface roughness. Sufficiently low roughness of $Al_2O_3$ initial surface (Figure 1, *a*) is indicated. The roughness increases (Figure 1, *b*) after HEB treatment of composite coating, particularly, in the area of melted coating. HEB-treated zone contained an area of titanium drop, deposited in the vacuum-arc source Bulat-5M (Figure 1, *b*). It is to be a crater of 0.5 mm diameter at the bottom of which presence of round shape melted inclusions is observed.

Element analysis was carried out on an X-ray spectrometer made on the basis of semi-conducting Li–Si detector. The spectra, obtained on round shape inclusions of the crater bottom, contain such elements as titanium, chromium and iron, among which the titanium is dominant. It is also determined that the concentration of these elements in different points of the crater bottom is not constant, i.e. the thickness of drop fractions is also different. A presence of small aluminum concentrations was found on the clean areas of crater surface. The results obtained in areas of the coating non-melted by HEB, were the following, wt.%: 13.9 Al, 48.2 Ti, 0.03 Cr and 0.42 Fe. The coating areas after HEB fusion contain, wt.%: 55.18 Al, 0.519 Ti, 0.2 Cr and 0.83 Fe.

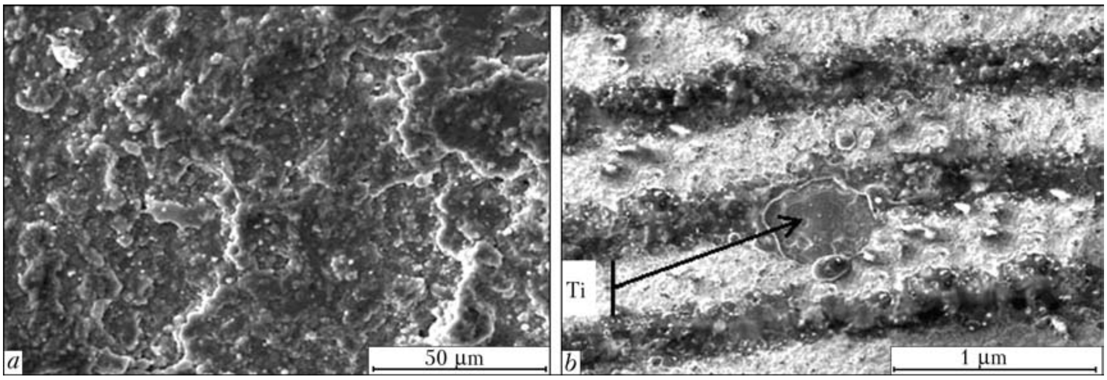


**Figure 1.** Microstructure of surface of the composite coatings: *a* — $Al_2O_3$ coating after pulse-plasma deposition; *b* — $Al_2O_3$ + Cr + + TiN coating after HEB treatment (series No.2)

Additional element analysis of the composite coatings was carried out by back-scattered (BS) protons method on the accelerator «Sokol» of the National Science Center «Kharkov Institute of Physics and Technology». Identification of the spectrum showed the presence of aluminum, titanium, oxygen and nitrogen on the surface of coatings in the samples subjected to fusion. BS-analysis showed an increase of oxygen concentration along whole thickness of the composite coating after HEB treatment. The concentration of oxygen is significantly lower without HEB treatment in near-surface layers of the coating. Reduction in depth of titanium content and simultaneous widening of distribution profiles are observed in the composite coatings after electron beam melting according to obtained results. An effective coefficient of titanium diffusion around $2.4\cdot10^{-8}$ $cm^2/s$ was obtained taking into account diffusion theory and good matching of form of distribution of titanium concentration with the Gaussian curve.

Study of phase composition of the substrate for $Al_2O_3$ coating and surface of composite coatings $Al_2O_3$ + Cr + TiN were made on X-ray diffractometer DRON-2.0 in $CuK_\alpha$-irradiation. Obtained results indicate the fact that the main element of substrate matrix is γ-Fe (fcc) with lattice parameter 0.3592 nm. It was determined with the help of X-ray diffraction analysis that the coating surface is to be a multiphase combination. Presence of such phases as γ-$Al_2O_3$, β-$Al_2O_3$, TiN and Cr is observed simultaneously with the main phase of corundum powder.

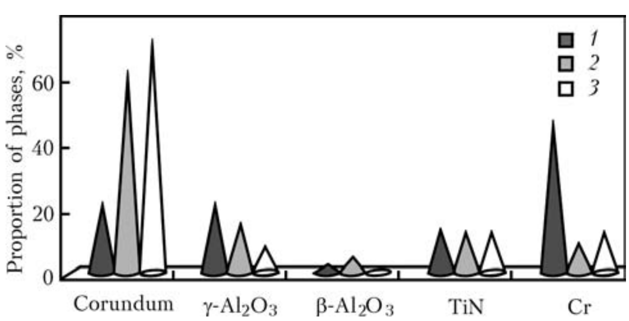


**Figure 2.** Calculation results of percent proportion of phases of the composite coatings of series Nos. 1–3 (*1–3*)

Evaluation of percent proportion of phases in the coatings with somewhat changed modes of modification (Figure 2) was carried out. Analysis of data is evidence of the fact that modes of coating and energy of HEB treatment have significant influence on the phase composition of coating material. Most probably that, in particular, the high-energy pulse-plasma deposition of coatings and electron beam treatment are the reason of occurrence of polymorphic transformations of $\gamma \rightarrow \alpha$ and $\beta \rightarrow \alpha$ type in $Al_2O_3$. Increase of concentration of the initial composition of α-$Al_2O_3$ depositing powder is observed at increase of time of electron beam treatment.

Hardening of $Al_2O_3$ particles with a speed not more than $10^7$ K/s in air [4] is required for preserving γ-phase, nucleuses of which were formed in a melt. α-phase can be obtained in air if the particles are cooled with the speed of less than $5\cdot10^4$ K/s.

Based on calculations carried out a conclusion was made about significant influence of HEB modification of surface on a change of parameters of lattice of surface constituent elements (series No.1: $a$ = = 0.447 nm, $c$ = 0.136 nm, $c/a$ = 2.87; series No.2: $a$ = 0.477 nm, $c$ = 0.129 nm, $c/a$ = 2.72; series No.3: $a$ = 0.477 nm, $c$ = 0.129 nm, $c/a$ = 2.71).

The parameter of nitride titanium lattice equals 0.426 nm in the surface initial state. It makes 0.422 nm after surface treatment with low dose of HEB. Size of titanium nitride lattice makes 0.425 nm in the composite coatings after surface treatment with high dose of HEB. The results obtained for lattice parameters of chromium sublayer were the following: for series Nos 1–3 $a$ = 0.288, 0.287 and 0.288 nm, respectively.

Thus, aluminum, titanium, chromium, nitrogen and oxygen are the main constituents of the surface. Initial material of the coating from aluminum oxide powder undergoes a series of phase transformations [4, 5] after composite coating. The X-ray diffraction analysis showed the presence of aluminum oxide in the form of three modifications (α-, β-, γ-$Al_2O_3$) in the coating: chromium and titanium nitride.

Modification of the composite coating with the help of HEB results in recovery of corundum phase and increases the coefficient of titanium diffusion. The material of composite coating after HEB melting has higher density and consists of high temperature phases of aluminum oxide alloyed by titanium and chromium. It is expected that this coating will have increased corrosion properties under operation in active high temperature media.


1. Tyurin, Yu.N. (1999) Improvement of equipment and technologies of detonation coatings. *Avtomatich. Svarka*, **5**, 13–18.
2. Tyurin, Yu.N., Zhadkevich, M.L. (2008) *Plasma strengthening technologies*. Kiev: Naukova Dumka.
3. Lankin, Yu.N., Bondarev, A.A., Bondarev Andr. A. (2001) Computer control of processes in weld pool during electron beam welding. In: *Surface engineering and renovation of products*. Kiev: ATM of Ukraine.
4. Pogrebnjak, A.D., Tyurin, Y.N., Kobzev, A.A. et al. (2001) Structure and properties of $Al_2O_3 + Cr_2O_3$ coatings deposited to steel 3 (0.3 wt.% C) substrate using pulsed detonation technology. *Vacuum Surf. Eng.*, **62**, 21–26.
5. Uglov, V.V., Cherend, I.I., Khodasevich, V.V. (1998) Modification of aluminium by implantation of nitrogen ions. *Fizika i Khimiya Obrab. Materialov*, **2**, 37–40.


## *NEWS*

## *THREE IN ONE*

A welding multisystem (chopper) providing three welding processes (MIG/MAG, TIG and MMA) is proposed by SELMA company.

VD-320 KS welding multisystem is designed:

• for semi-automatic gas-shielded welding (MIG/MAG-DC mode) by 1.0–1.6 mm diameter steel wire using wire feed mechanism manufactured by OJSC SELMA Company as well as for semi-automatic welding of aluminum and its alloys in argon atmosphere by 1.2 mm diameter OK 18.01, OK 18.04, AMg-5 wires in 130–180 A current range at arc voltage of 19–24 V;

• for non-consumable electrode argon arc welding at direct current (TIG-DC mode) at completing with BU-TIG control unit;

• for consumable covered electrode arc welding of products from carbon and alloyed steels (MMA-DC mode).

Main advantages:

• low consumption of energy in comparison with traditional welding sources for 300 A;

• rectifier has a built-in block for reduction of open-circuit voltage increasing safety during performance of welding operations in MMA mode;

• possibility of carrying out of three welding processes: MIG/MAG-DC, TIG-DC, MMA-DC;

• smooth adjustment of welding current;

• digital display of welding current and voltage;

• adjustment of short-circuit current in MMA mode;

• adjustment of time of «Hot start» for providing stable arc initiation in MMA mode;


• possibility of connection of a remote-control station for adjustment of welding current in MMA mode;

• availability of thermal protection from overloading;

• availability of socket (36 V) for a gas heater connection;

• state-of-the-art element base;

• small weight and overall dimensions in comparison with traditional welding sources for 300 A.

# UKRAINIAN-GERMAN WORKSHOP «PLASMA AND ELECTRON BEAM TECHNOLOGIES FOR PROTECTIVE COATINGS»

The Ukrainian-German Workshop «Plasma and Electron Beam Technologies for Protective Coatings» was held in Kiev on 16–17 June 2010. Organisers of the Workshop from Germany were the European Joint Committee on Plasma and Ion Surface Engineering and European Society of Thin Films, and from Ukraine — the E.O. Paton Electric Welding Institute. The relevance of holding this Workshop was determined by the necessity to activate the efforts in addressing the problem of wear of tools and machine parts, which leads to a loss of about 5 % of the national product in the scopes of the world economy. Development of new innovation solutions in the field of multilayer wear-resistant coatings by vapour and gas phase deposition technologies allows reducing friction losses and extending service life of tools and machine parts. The key customers of such coatings are cutting tool industry and motor car construction.

Another high-end area of development of the surface engineering technologies includes new thermal barrier and corrosion-resistant coatings, which also contribute to extension of service life of machine parts and mechanisms and allow decreasing materials and power expenditures in various sectors of the world economy.

The program of the Workshop consisted of four groups of presentations covering the following key subjects:

- wear-resistant protective coatings;
- hard material coatings;
- thermal protection coatings;
- corrosion protection coatings.

20 papers were presented and discussed at 6 sessions. Papers were presented by three institutions of Germany — leaders in the field (Munich Technical University, Fraunhofer Institute for Electron Beam and Plasma Technology, German Aerospace Centre), by the University of West Bohemia (Czechia), Company «Hauzer Techno Coating BV» (The Netherlands), Sheffield Hallam University (Great Britain), by Russian institutions (CRISM «Prometey», St.-Petersburg, and National University of Science and Technology, Moscow), National Academy of Sciences of Ukraine (E.O. Paton Electric Welding Institute, Institute for Problems of Materials Science, Institute for Superhard Materials, Physico-Mechanical Institute, and Kharkov Institute of Physics and Technology). In addition, from Ukraine the papers were presented by associates of the Kharkov and Sumy Universities. 9 papers were presented at the poster session, including from the E.O. Paton Electric Welding Institute, Institute for Superhard Materials, Institute for Problems of Materials Science, Kharkov Institute of Physics and Technology, and National Aviation University.

The sessions of the Workshop were attended by about 100 people — Workshop participants, associates of the institutes of the National Academy of Sciences of Ukraine, students and lecturers of the Kiev Polytechnic Institute, and representatives of industrial enterprises.

The exhibition of products of the engineering centres of the E.O. Paton Electric Welding Institute was arranged.

Of high interest to those present at the Workshop were presentations made by the leaders in the area of hard nanocomposite coatings Prof. J. Musil (Czechia) and Prof. S. Veprek (Germany). They gave analysis of state-of-the-art in this area and prospects for its further development. The possibility was shown of producing such coatings with a hardness that exceeds that of diamonds, and with a high thermal stability, allowing their application at temperatures of up to 140 °C, as well as coatings that combine the high hardness and impact toughness values.

The paper presented by Prof. B.A. Movchan described achievements of the E.O. Paton Electric Welding Institute in the field of development of new nanostructural coatings by the hybrid electron beam process. New results in the field of protective EB and other vapour-phase coatings were reported in presentations by J.P. Heinss (Germany), E. Dabizha (Institute for Superhard Materials) and A. Ustinov (E.O. Paton Electric Welding Institute). Results of development of new nanocomposite coatings produced by magnetron sputtering were covered in presentations made by Yu. Borisov (E.O. Paton Electric Welding Institute), V. Ivashchenko (Institute for Problems in Materials Science), N. Azarenkov (Kharkov Institute of Physics and Technology) and V. Kiryukhantsev-Korneev (National University of Science and Technology, Moscow). R. Braun (German Aerospace Centre) in his presentation told about development of new thermal barrier coatings for parts of γ-titanium–aluminium alloys, and Yu. Borisov (E.O. Paton Electric Welding Institute) described the thermal barrier coatings with quasi-crystalline and approximant structure.

The papers presented at the Workshop were published on the site of the European Society of Thin Films.

The joint memorandum on collaboration between research organisation of Ukraine and Germany in the field of surface engineering, including preparation of the collaborative research program, and arrangement of joint workshops on various issues of surface engineering was prepared and signed on the basis of the Workshop results. An important outcome of the Workshop was that during it the scientists from Ukraine and Western Europe involved in surface engineering could establish personal contacts, which should lead to activation of international cooperation. In particular, a contributory event was communication of the Workshop participants during the evening boat trip along the Dnieper River.

*Prof. Yu.S. Borisov, PWI*

# SUBSCRIPTION
# FOR «THE PATON WELDING JOURNAL»

If You are interested in making subscription directly via Editorial Board, fill, please, the coupon and send application by fax or e-mail.

The cost of annual subscription via Editorial Board is $324.

Telephones and faxes of Editorial Board of «The Paton Welding Journal»:
Tel.: (38044) 287 6302, 271 2403, 529 2623
Fax: (38044) 528 3484, 528 0486, 529 2623.

«The Paton Welding Journal» can be also subscribed worldwide from catalogues of subscription agency EBSCO.

**SUBSCRIPTION COUPON**
**Address for journal delivery**

**Term of subscription since** ____________ **200** ____ **till** ____________ **200** ____
**Name, initials** ____________________________
**Affiliation** ____________________________
**Position** ____________________________
**Tel., Fax, E-mail** ____________________________